Neurobiology and modeling
of cuticular hair sensilla of scorpions

Response characteristics and implications for biomimetic design

Dissertation

zur

Erlangung des Doktorgrades (Dr. rer. nat.)

der

Mathematisch-Naturwissenschaftlichen Fakultät

der

Rheinischen Friedrich-Wilhelms-Universität Bonn

vorgelegt von

Nikolay Kladt

aus

Bonn

August 2007

This dissertation is dedicated to Silke and to my parents, Barbara and Rüdiger. Thank you for your love and support.

Abstract

In this thesis, the neurobiology of mechanoreceptive sensilla on the pectines of the scorpion *Pandinus cavimanus* was examined. The morphology of the pectines, the innervation and morphology of the sensilla as well as their response characteristics were analyzed. Based on the neurobiological results, mechanoreceptive bristles of arthropods were characterized from a technical point of view. A biomimetic, physical model of the mechanoreceptive hairs was developed that exhibited several important characteristics of the biological examples.

Following main results were achieved:

1. On the pectines of scorpions, several types of cuticular receptors are located. Of these receptors, only the chemo- and mechanosensory peg sensilla have been studied in detail so far. This thesis extends the knowledge of the pectines by an analysis of the mechanoreceptive long hair sensilla (pectinal hair sensilla, PHS). A detailed description of their morphology, innervation and response characteristics is given.

   - The morphological studies showed that the hairs are robust sensilla with lengths of 300-1400 μm and diameters of 30 μm at the base, tapering to about 10 μm at the tip. The sockets allow wide range of movements, certainly within the range of 20-30 degrees.

   - Each sensillum is associated with a cluster of 4-6 bipolar sensory cells, approximately 70-100 μm below the hair socket.

   - It was possible to record up to three different action potential classes (units) which could be distinguished by size, response characteristics and conduction velocity. Two of these units were analyzed in more detail. The response characteristics showed two phasic units, one large (L) and one small (S), coding the velocity of a stimulus. One medium-sized unit (M) showed phasic-tonic characteristics, also coding the duration of a stimulus. The deflection threshold for all units was determined to be approximately 1°. The velocity response curves showed that the M-unit responded best to angular velocities

between 2 °/s and 500 °/s while the L-unit responded best to velocities of
50-2500 °/s. The velocity responses were confirmed by the frequency response
curves. An analysis of the directional characteristics of the M- and L-units
revealed cardioid response curves, suggesting a broad directional tuning.

Taking together the morphological and electrophysiological results, it is suggested
that these sensilla belong to the group of long hair sensilla distributed all over the
scorpion body. A possible role as obstacle detectors involved in reflexive body-
height adjustments is supported by the position of the sensilla on the pectines,
their response characteristics and the timing between sensory and motor activity
within the pectine nerves after stimulation of single hairs.

This suggests a revised and more elaborated function of the pectines, where the
pectinal hair sensilla are needed to control the height of the pectines, and also the
body (in addition to the chemo- and mechanosensory functions of the peg sensilla).

2. In the scope of this thesis, a biomimetic, physical model of the previously inves-
tigated sensory hairs of scorpions was developed. The model was designed with
regard to the functional structure of the biological examples. The dimensions were
similar, with socket diameters <100 μm and hairshaft lengths <1-2 mm. The
mechano-electrical transducer employed fiber optics with regard to the biological
transduction process. This model was able to mimic important response properties
of the biological sensors such as amplitude-, temporal- and directional character-
istics. Furthermore, a modular design enabled the use of biological structures as
parts of the models, e.g. torn out hairshafts of biological sensilla. Overall, the
constructed sensors represent a first step toward a universal model that allows in-
ference about biological systems by variation of single biomechanical parameters.

Contents

III Discussion

8 Conclusions and Outlook

Chapter 1

General introduction and overview of the thesis

Highly complex behaviors can even be observed in presumably 'simple' animals. Their capability to perform such behaviors results from their complex sensory-motor systems which show intricate interactions between sensors, nervous structures and motor systems. One of the key components of sensory-motor systems are sensors. These are *matched filters*, extracting specific information from the environment and providing this (filtered) information to the nervous system for further processing (Wehner, 1987).

Arthropods are well suited and commonly used for the study of such sensory-motor systems. Although they show sufficiently complex behaviors, they are simple enough to promise insights into the underlying processes. Furthermore, they are easily accessible to all kinds of experimental approaches, ranging from genetics (e.g. research of acoustic communication in *Drosophila*, Tauber and Eberl, 2003) to experiments with simultaneous manipulation of sensory input and intracellular measurements of nervous activity in animals still showing *fictive* behavior (e.g. study of locust flight, Wolf and Pearson, 1989).

In addition to these experimental approaches, mathematical and physical modeling have become more common in recent years (e.g. the promising area of biorobotics research). One reason for this increase in modeling studies is the availability of powerful, low-cost computers and professional software tools. Furthermore, an increasing variety of high-end technical devices is industrially produced for mass-markets and adaptable for technical models (e.g. lasers, micro-motors or image sensors). However, physical modeling and especially biorobotics are yet not common tools for neuroethology.

Motivation

The rationale behind this thesis was to investigate mechanical senses of arthropods, in particular sensory hairs which are often distributed all over the body of an animal.

A basic question was addressed: What is the information content, a 'simple' type of cuticular hair sensillum conveys? Does it only provide information about the time and place of a stimulus or is more information obtained? These questions can be addressed with several approaches and on different levels of analysis. With physical modeling, and in particular biorobotics, as a tool for the analysis of sensory-motor systems in mind, this thesis aims to (1) investigate a basic type of mechanoreceptive hair sensillum with classical neurobiological methods and (2) use the results of the neurobiological analysis to design a biomimetic model of arthropod hairs that may allow inference about the biological system.

In the following, these two main topics are shortly outlined:

1. As a model system, mechanoreceptive hair sensilla on the pectines (pectinal hair sensilla, PHS) of scorpions were chosen (see Fig. 1.1). A previous study has shown that these hairs probably represent 'simple' mechanoreceptors (Kladt, 2003). Furthermore, these hairs are suggested to be involved in simple obstacle-detection behaviors (Schneider, 2002; Kowalski, 2006). The neurobiological examinations included the morphology and innervation of the hairs as well as their electrophysiological response characteristics.

2. The investigated hair sensilla were taken as models for the construction of physical, biomimetic hair sensilla models. The constructed models were analyzed and compared to their biological counterparts. It was examined, whether important characteristics of the biological hair sensilla could be mimicked by a physical model and whether these kinds of models could be used to generate new hypotheses for the study of biological hair sensilla.

Overview of the thesis

Both topics focus on cuticular mechanoreceptors of arthropods. As they differed in their points of view, methods and main objectives, they are presented as separate parts. Each part contains an introduction, methods and results. After a presentation of the two topics, the final part of this thesis discusses the results of both topics and examines their relation. Overall, this thesis is divided into three parts:

Part I, Cuticular mechanoreceptors on the pectines of scorpions

This part is concerned with a neurobiological examination of cuticular hair sensilla on the pectines of scorpions. These studies include a description of pectine morphology, an examination of the morphology and innervation of the hair sensilla as well as a detailed electrophysiological analysis of their response characteristics:

Fig. 1.1: The scorpion *Pandinus cavimanus.* The red arrow indicates the pectines, visible in a palpating position.

Chapter 2 introduces scorpions as model systems for the study of sensory-motor systems and reviews current literature about the neurobiology of scorpion mechanoreception. Finally, this chapter describes previous studies that have led to this thesis.

Chapter 3 describes the methodology of the extracellular recordings and mechanical stimulation, together with a survey of other methods that were applied.

Chapter 4 presents the results of the anatomical, morphological and electrophysiological experiments.

Part II, Modeling cuticular mechanoreceptors

This part describes the construction of biomimetic, physical models of the previously investigated hair sensilla and examines their main characteristics:

Chapter 5 provides an introductory review of existing mathematical and technical models of cuticular mechanoreceptors of arthropods and describes the reasons for constructing physical models of these hairs.

Chapter 6 describes the methods applied for the technical modeling. The construction of artificial and hybrid sensors is explained and the application of fiber optics in the transducer is described.

Chapter 7 presents the main characteristics of the constructed sensors. In addition, suggestions for further processing of sensor outputs are provided.

Part III, Discussion

In this part (*chapter 8*), a discussion of the biological and modeling results is presented and the results are compared. The main achievements, limitations and implications of this work are discussed and an outlook for further studies is given.

Part I

Cuticular mechanoreceptors on the pectines of scorpions

Chapter 2

Introduction -
Neurobiology of scorpion mechanoreception
and role of the pectines

> In this chapter, scorpions as models for neurobiological research are introduced. An overview of the anatomy of the nervous system of scorpions is provided, the knowledge about their mechanical senses is shortly outlined and the pectines bearing the examined hair sensilla are described. Finally, the available knowledge about scorpions and their pectines is related to the objectives of this thesis.

Scorpions are intriguing animals for research. They appeared in the middle Silurian (425-450 million years ago), probably as aquatic, marine or amphibious species. The first terrestrial scorpions appeared in the early Carboniferous (325-350 million years ago) (Polis, 1990b). They almost certainly evolved from the Eurypterida. Since their first appearance as terrestrial animals, scorpions have populated all major land masses except Antarctica (Polis, 1990a) and occur in different, often extreme environments. Scorpions can be found in tropical forests, at high altitudes and deserts, but also in intertidal zones or as cave dwelling species (Polis, 1990a). Despite this diversity, which is reflected by the approximately 1500 existing species, scorpions posses a basic body plan that is extremely similar between different species. Furthermore, existing scorpions show external similarities to the fossil records of earliest scorpions (Polis, 1990b).

Among the reasons making scorpions fascinating objects for research are their complex behaviors. Two examples of such behaviors are the *promenade à deux*, a dance during the ritualized and intricate courtship (Polis and Sissom, 1990), or the ability of some species to catch flying insects in midair (McCormick and Polis, 1990). Latter demonstrates the efficiency of scorpions as predators on various arthropods and other small animals. Other examples of astonishing features are the extremely low metabolic rates of

some species (McCormick and Polis, 1990), their complex poisons containing neurotoxins (Simard and Watt, 1990), the ability of a couple of species to withstand supercooling with body temperatures down to -11.9 °C (*Paruroctonus utahensis*) or desert species shortly withstanding temperatures exceeding 50 °C (Hadley, 1990). Furthermore, scorpions possess highly sophisticated sensory systems (see section 2.2 for an overview of the mechanical senses). With regard to the ancestral body plan, which perhaps represents a good approximation to a common arthropod ancestor, and their relationship to other arthropods, they are interesting animals for comparative research (Root, 1990).

Within the Arthropoda, scorpions belong to the Arachnidae (subphylum Chelicerata). They exhibit an unmistakable appearance which distinguishes them from other Arachnids. Fig. 2.1 illustrates the general anatomy of scorpions with a schematic view of the scorpion *Pandinus cavimanus*, which was primarily used in this work. The body is divided into the prosoma and the ophistosoma (abdomen). The prosoma bears the median and lateral eyes. The ophistosoma is subdivided into the broader mesosoma (I-VII) and the narrow, tail-like metasoma (VIII-XII). Scorpions belong to the chelicerates, having three-segmented chelicerae modified for feeding. Among the most conspicuous structures of scorpions are the pedipalps, modified appendages for prey immobilization, defense and sensory experience (e.g. trichobothria). Each walking leg is divided into seven segments: coxa, trochanter, femur, patella, tibia, basitarsus and tarsus. Distal of the last metasomal segment is the anus, followed posterior by the telson with the sting. Other unique structures of scorpions are the pectines, ventrolateral appendages of the 2nd mesosomal segment that will be described in section 2.3.

2.1 The nervous system

The nervous system of scorpions probably has an ancestral structure, especially in comparison with other Arachnids or Arthropods. Nevertheless, with highly sophisticated sensory-motor systems, scorpions are capable to perform complex behaviors. Arachnids in general, and spiders in particular, show a highly centralized nervous system. In addition to a very large cephalothoracic nervous mass, scorpions possess a ventral nerve cord with segmental ganglia (Root, 1990). Despite some recent studies, which shed some light on the anatomy and physiology of the nervous system of scorpions, the knowledge is still sparse (Root, 1990), especially when compared to the knowledge about the nervous systems of insects (e.g. bees, locusts, moths, ...) or crustaceans (e.g. crayfish). Although, to some extend, several sensory and motor systems in the periphery are described rather well, this is not true for central nervous processing.

Fig. 2.2 shows the gross anatomy of the central nervous system (CNS) of scorpions (Babu, 1965), with a schematic view of the CNS of *P. cavimanus*, as it was observed
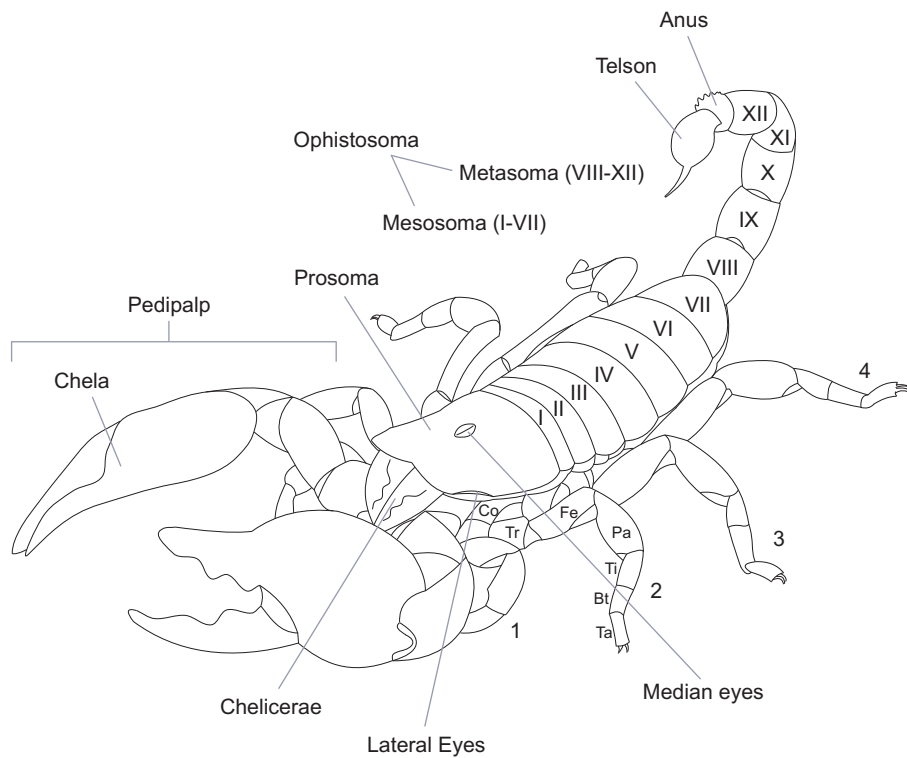
Fig. 2.1: Dorsolateral view of the scorpion *Pandinus cavimanus*. The prosoma is dorsally covered by the carapace, segments I-XII constitute the ophistosoma (abdomen) which can be subdivided into the mesosoma (I-VII) and the metasoma (VIII-XII). 1-4 illustrate the according pairs of walking legs. The segments of a leg are Co, coxa; Tr, trochanter; Fe, femur; Pa, patella; Ti, tibia; Bt, basitarsus and Ta, tarsus. The nomenclature follows Hjelle (1990).

during the experiments. In the prosoma, the cephalothoracic mass (CTM) is easily distinguished. It consists of two connected parts; the larger part is the ventral subesophageal ganglion whereas the smaller part is the dorsal supraesophageal ganglion with the esophagus located in between (not shown). Several major nerves originate from the CTM, the cheliceral nerves (Chn), pedipalpal nerves (Pdn), the four pairs of ambulatory nerves (Amn1-4), the pectinal nerves (Pctn) and the connectives (Cv). Also originating from the CTM are the abdominal nerves 3 and 4 (Abdn3-4) which innervate mesosomal segments III and IV. Caudal of the CTM, the ventral nerve cord with its seven abdominal ganglia is visible. Three abdominal ganglia are located in the mesosoma (Abdg 1-3) and four in the metasoma (Abdg 4-7). Nerves originating from the mesosomal ganglia innervate the remaining three mesosomal segments (V-VII) and nerves originating from the metasomal ganglia innervate the according segments in which they are located. The posterior metasomal ganglion (Abdg7) also innervates the metasomal segment XII, the

telson and the sting. Overall, the central nervous system of scorpions is less cephalized than the CNS of spiders but still shows the general tendency of arachnid centralization. For *P. cavimanus*, no distinctive differences from the general scheme presented in the mentioned literature are discernible.

A more detailed description of the CNS of *Heterometrus* was conducted by Babu (1965). This study also presents various older findings and provides a comparison of these. A review of the scorpion CNS can be found in Root (1990). A more recent study of Horn and Achaval (2002) deals with the CNS of *Bothriurus bonariensis*.

In this study, mechanoreceptors on the pectines were examined and therefore, details of the locations and processes of the pectinal nerves (Pctn), provided in the literature mentioned, will be described (following description is based on Babu, 1965; Root, 1990; Wolf, 2007). The pectinal nerves arise on either side of the connectives, slightly ventral to these. They are nearly as large as the connectives themselves. The pectinal nerves run parallel to the connectives until the bundle of nerves crosses a circumneural part of the endosternite, the diaphragm. Posterior to the diaphragm, the pectine nerves process straight through the muscles at the pectine bases and enter the pectines. The pectine nerves contain mainly sensory and some motor fibers and they are similar in diameter to the connectives.

In the subesophageal ganglion, two ventromedial neuropil areas have been described (on each side), with the larger area located posterior (Wolf, 2007). The same study also shows a glomerular and layered structure of the posterior neuropil and indicates that the motor neuron supply of the pectines is similar to that of other limbs. Both areas are thought to act as association centers (Babu, 1965). They obtain additional input from the ventral nerve cord and from the midventral tract. Via the pectinal tract and (further on) via the midventral tract they are connected to brain centers (Babu, 1965).
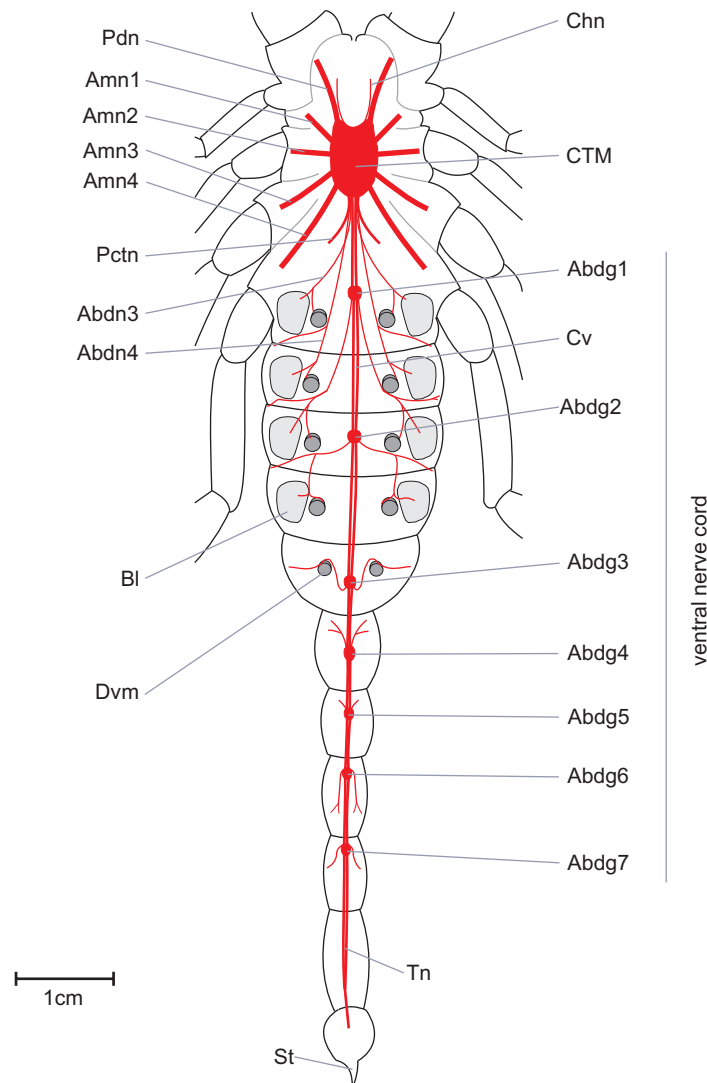
Fig. 2.2: Gross anatomy of the central nervous system of *P. cavimanus*. The illustration shows a dorsal view of the central nervous system of *P. cavimanus*. The dorsal cuticle, hepatopancreas, genital system and connective tissues are removed. The nervous system is identical to the data provided in literature. At the anterior end is the cephalothoracic mass (CTM), the most centralized nervous structure. From the CTM, several major nerves originate, the cheliceral nerves (Chn), the pedipalpal nerves (Pdn) and the nerves to the walking legs (ambulatory nerves, Amn1-4). Other large nerves are the pectine nerves (Pctn), the connectives (Cv) and the nerves innervating mesosomal segments III and IV, the abdominal nerves (Abdn3-4). Among other structures, these mesosomal nerves innervate the according pairs of booklungs (Bl) and dorsoventral muscles (Dvm). Posterior to the CTM, the ventral nerve cord with its seven abdominal ganglia (Abdg1-7) is visible. The first three abdominal ganglia are located in the mesosoma and the next four are located in the metasoma. Abdg7 innervates the last two metasomal segments, the telson (telsonic nerve, Tn) and the sting (St).

2.2 Mechanical senses

Scorpions primarily depend upon the input from their mechanical senses (Root, 1990). Ablation of specific mechanical senses leads to a reduction of their interaction with the environment. For example, if trichobothria are removed, the ability of scorpions to locate flying prey is diminished (Krapf, 1986). Another example shows that removal of long hair sensilla leads to a general floppiness of the whole body with absence of withdrawal responses (Babu et al., 1993). Typically, the mechanical senses can be distinguished in proprioceptors and exteroreceptors. The latter will be illustrated in the following.

Sensory hairs

The numerous hairs embedded in the cuticle are one of the prominent features of a scorpion. Some of these are probably chemoreceptors (short, curved hairs) but the majority is mechanoreceptive (Root, 1990). Several studies suggest a classification of the mechanoreceptive hairs into trichobothria, long, straight hairs and short, thick-walled bristles (e.g. Foelix and Schabronath, 1983a; Kasaiah et al., 1989):

- **Trichobothria** are slender hairs on the pedipalps of scorpions. They are easily distinguished from other cuticular sensilla as weak air currents lead to passive oscillations of the hairshafts. Their sockets display typical features (the bothrium) and single hairs always move along one axis. Although a sensory function was suspected very early, they were primarily used as a taxonomic character. The trichobothria are about 5-10 μm in diameter, 500-1500 μm long (Hoffmann, 1967; Messlinger, 1987) and probably innervated by several sensory neurons, with the number dependent on the species or family (e.g. Messlinger, 1987; Kasaiah et al., 1989). Physiological analysis has shown that trichobothria are primarily receptors of weak air currents (e.g. Hoffmann, 1967). These physiological findings were confirmed by behavioral studies suggesting that scorpions can orient by air currents using their trichobothria (Linsenmair, 1968) and that these hairs are probably required to detect flying prey (Krapf, 1986).

- **Long, straight hairs (LHS)** are numerous hairs which are ubiquitously distributed on the scorpion body, with highest densities found on the pedipalps and the first pair of walking legs. Anatomical and physiological knowledge is mostly based on a series of studies on the scorpion *Heterometrus fulvipes* (Babu and Sanjeeva Reddy, 1967; Babu et al., 1993; Babu and Jacobdoss, 1994; Kasaiah et al., 1989; Sanjeeva-Reddy, 1971; Sanjeeva-Reddy and Rao, 1970). These studies show that the LHS are 600-3800 μm long, with the longest found on the pedipalps. They have diameters of 50 μm at the base, tapering to ≤ 10 μm at the tip. Furthermore, the mentioned studies indicate a multiple innervation of the LHS. The anatomical

studies suggest that 7 sensory cells are associated with one LHS while electrophysiological studies revealed up to 4-5 units per LHS. A seven-fold innervation was also found in hairs on the tarsi and basitarsi of *A. australis*, *E. italicus* and *Buthus occitanus* (Foelix and Schabronath, 1983a). Interestingly, one study suggests that stimulation of a single LHS is able to elicit discharges of interneurons (Babu and Jacobdoss, 1994). Estimates on *P. cavimanus* suggest that about 3000-4000 LHS are distributed over the body (unpublished observations).

- **Short, thick-walled bristles** have been identified and distinguished on the walking legs. They are about 200-650 μm long (Kasaiah et al., 1989; Foelix and Schabronath, 1983a). The bristles are thought to be mechanoreceptors, but no further studies were conducted.

Slit sensilla

Slit sensilla are unique arachnid mechanoreceptors. They can occur as single slits or as groups (lyriform organs). Similar to spiders, a function as cuticular stress detectors is assumed. In comparison to spiders, scorpions possess more single slits than groups, but with typical patterns of arrangement (Barth and Wadepfuhl, 1975). Probably, the slit sensilla are multiple innervated (Foelix and Schabronath, 1983a). Other studies have shown that the basitarsal compound slit sensillum (BCSS) is involved in the detection of substrate vibrations (together with tarsal hairs) and that the input of these two types of receptors on the legs can also be used to determine the direction and distance to the source (Brownell and Farley, 1979a,b).

2.3 The scorpions pectines

The pectines are bilateral, ventrolateral appendages of the 2nd mesosomal segment, synapomorphic for scorpions and present in all extant and fossil species (Farley, 2001). They have a comb-like structure, consisting of 3 marginal lamellae and depending on the species a varying number of median lamellae, fulcra and teeth. In some species, either the fulcra or the median lamellae can be absent. Fig. 2.3 illustrates the general location and appearance of the pectines with an example of the pectines on the ventral side of the scorpion *P. cavimanus*.
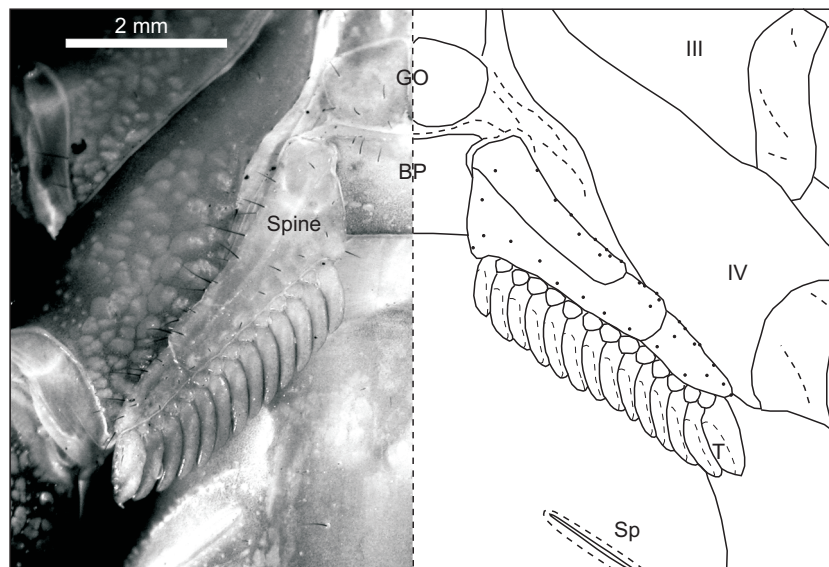
Fig. 2.3: Ventral view of a mesosomal section of *Pandinus cavimanus*. The pectines are located ventromedially on the body. Between the pectines, the basal plate (BP) is located directly posterior to the genital operculum (GO). The pectines consist of a spine (marginal, median lamellae and fulcra) and teeth (T). III-IV: according pair of walking legs, Sp: spiracle, opening to the book lungs

Three types of sensory hairs can be found on the pectines: chemosensory pegs grouped proximal on the ventral surface of each tooth; short, probably chemosensory hairs distributed all over the pectines and long hair sensilla (pectinal hair sensilla, PHS) distributed on the median lamellae (Fig. 2.4).

Cloudsley-Thompson (1955) provides an enjoyable review about earlier works on the pectines and the speculations about pectine function. These ranged from tactile, chemotactic or vibrational functions, an auxiliary role in respiration, interlocking of the lamel-
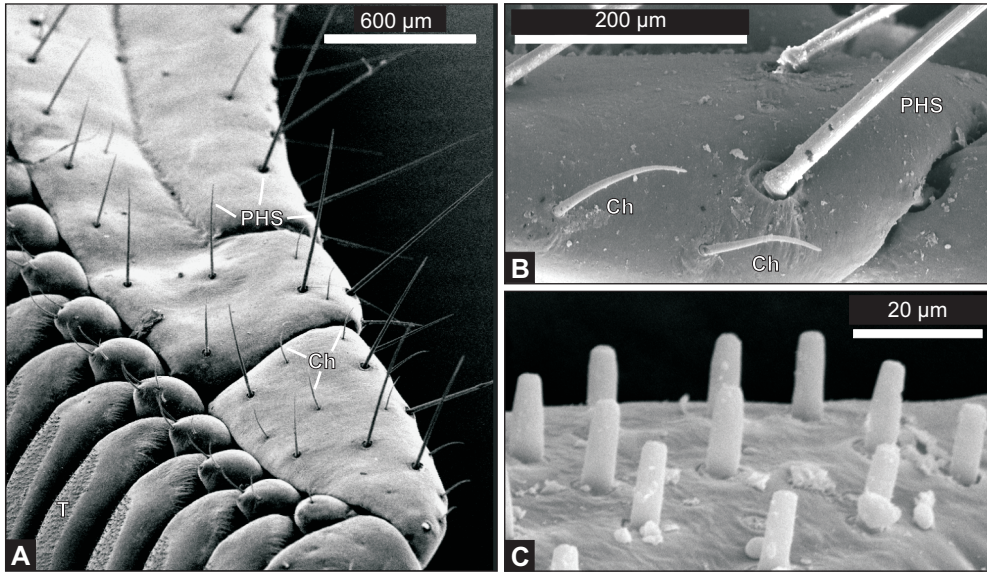
Fig. 2.4: Sensory equipment of the pectines. **A** shows a SEM image of a pectine. The long straight pectinal hair sensilla (PHS) and the short, curvy chemosensory hairs (Ch) on the spine (median and marginal lamellae), as well as the fields of chemosensory peg sensilla on the teeth (T) are visible. **B** shows a detailed SEM image of the PHS and the Ch. **C** displays a SEM image of the peg-sensilla (a small part of a field on a single tooth is visible).

lae during mating, equilibration and audition to a function as holders for the young during birth. Basically, this account shows that the function of the pectines was rather obscure, but that there was already evidence of a sensory function. Morphological studies on *Euscorpius italicus* suggested a mechanosensory function as the pectine nerves contained sensory fibers from cuticular sensilla, especially from the numerous peg sensilla on the teeth (Hoffmann, 1964). The same study also found that deflection of a single peg-sensillum led to twitches of single teeth or the whole pectine. Abushama (1964) conducted a variety of studies on *Leiurus quinquestriatus* and suggested that the pectines are sensitive to touch, temperature and odor. These suggestions were supported by the studies of Carthy (1966, 1968) on the same species, who also proposed that the pectines are used to choose a suitable location for the spermatophore during mating.

A detailed ultrastructural analysis of the pectines of *E. italicus* and *Androctonus australis* revealed structures of putatively chemosensory function in both, small hairs and peg-sensilla (Foelix and Schabronath, 1983b). This study further suggested, that the peg sensilla additionally possess one mechanoreceptive dendrite, and that chemoreceptive sensory cells make synaptic contacts with each other. Therefore, they concluded a dual function as chemo- and mechanoreceptors. These results were confirmed by studies of Brownell and Gaffin, who primarily studied the chemosensory function of the peg

sensilla and respectively the pectines of several species (Brownell, 1988, 1989; Gaffin and Brownell, 1992, 1997a,b, 2001; Gaffin, 2002). They also conclude, that the pectines are probably one of the most suitable arachnid preparations for the physiological study of chemoreception (Gaffin and Brownell, 1997b). Some of the most recent studies concerning the pectines have investigated pectine behavior in detail and provide first ethograms and motion-analysis (Gaffin and Walvoord, 2004; Mineo and Claro, 2006).

All these studies have established the view that the pectines are primarily chemosensory appendages – analogous to the insect antennae – with additional mechanosensory properties. Nevertheless, only the peg-sensilla have been analyzed in detail, while the responses of the other types of sensilla have not been physiologically analyzed in detail. The motor system of the pectines has only been examined in behavioral studies. So far, there is only sparse knowledge about muscles, proprioceptive feedback or central nervous processing.

A previous study by Schneider (2002) suggested – for the first time – a connection between contact of the pectines with an obstacle and reflexive body-height adjustments. Of the three types of sensilla that are located on the pectines, hair sensilla (PHS) which protrude in frontal and ventral directions seemed to be reasonable candidates for eliciting this reflex. Therefore, a subsequent work was conducted, showing that these sensilla indeed are mechanosensors, basically capable of detecting obstacles (Kladt, 2003). The work of Kowalski (2006) suggests, that stimulation of these sensilla alone is able to elicit reflexive retraction of the pectines.

The analysis of the long hair sensilla on the pectines provided in this work contributes to the knowledge of the pectines. This is of importance as the pectines represent a major chemosensory input source. A better understanding of these organs may eventually allow analysis of multimodal input, reflexive feedback loops and central nervous processing. Furthermore, only a few mechanosensory model sensilla have been described in arachnids, and especially in scorpions. This study provides a detailed description of the response characteristics of a basic 'touch' receptor that will help to establish an overall picture of scorpion mechanoreception.

Chapter 3

Methods

This chapter introduces the experimental animals, describes the methods of the morphological studies on the pectines and the cuticular hairs, the cobalt-stains that were applied to examine the innervation of the pectinal hair sensilla (PHS) and presents the methods of the electrophysiological experiments that analyzed the response characteristics of the PHS. The last section deals with the mechanical stimulation that was applied in the electrophysiological experiments.

3.1 Experimental animals

The primary species used in this study was the red-clawed scorpion *Pandinus cavimanus* Pocock, 1888 . In addition, some of the morphological experiments (neuroanatomy, pectine morphology) were conducted with the emperor scorpion *Pandinus imperator* C.L.Koch 1841. The large size of the specimen and their harmless sting make these species popular among hobbyists and therefore easy to obtain from specialized wholesalers (Tropenhaus Marxsen, Hamburg).

The genus Pandinus Thorell, 1876 currently includes 5 subgenera and 24 species (Fet et al., 2000). However, a comprehensive listing and classification does not exist (Fet et al., 2000). Despite the size of some species which attracts hobbyists as well a researchers, only little specialized literature can be found (Lourenco and Cloudsley-Thompson, 1996). *P. cavimanus* belongs to the subgenus Pandinoides Fet, 1997 and occurs in East Africa (northeast Congo, Kenya, Somalia, Tanzania) (Fet et al., 2000) where it can be found in tropical forests. *P. imperator* occurs in West Africa (Benin, Côte d'Ivoire, Ghana, Guinea, Liberia, Nigeria, Togo) with forest and savannah populations (Lourenco and Cloudsley-Thompson, 1996). It is important to note that *P. imperator* is

one of three CITES[1]-listed scorpion species (Meeting of the Nomenclature Committee, 2003, CITES appendix II, other species are *Pandinus dictator* and *Pandinus gambiensis*).

Individuals of *P. cavimanus* were kept isolated to prevent cannibalism while animals of *P. imperator* were kept in groups. The size of the terraria was 30 x 20 x 20 cm (L x W x H). The substrate consisted of a mixture of chopped bark and mold, always kept slightly moist. A substrate height of 4-5 cm allowed natural digging behavior. The temperature in a terrarium was kept between 20 °C and 35 °C, in reference to temperature distributions in natural hideouts of *P. imperator* (Mahsberg et al., 1999) – which seems reasonable as these two species live in similar habitats. The animals were kept in a 12:12 inverted day-night cycle, fed with crickets, mealworms and locusts every 1-2 weeks and water was supplied *ad libidum*. Adult animals of both sexes were used for the experiments. Animals were excluded if the pectines were obviously injured, the animals showed strong mite infestations, or imminent ecdysis was indicated by a turgid appearance of the mesosoma.

3.1.1 Animal dissection

Two of the applied recording methods (see section 3.3.2) and the nerve stains (see section 3.2.3) required dissection of the animals. The basic dissection procedures are illustrated in Fig. 3.1. The animals were cooled and dissected under crushed saline ice (buffering solution according to Bowerman, 1976)[2] to prevent clotting of the hemolymph. Following basic dissection procedure was applied:

1. The cooled animal was opened ventrally from mesosomal segment 2 to the prosomal somites VI-VIII, until the sternum or part of the sternum could be removed (Fig. 3.1B, cuts 1-4) (nomenclature according to Hjelle, 1990).

2. After removal of connective tissue and fat, the connectives (Cv), pectinal nerves (Pctn), ambulatory nerves (Amn2-4) and possibly the posterior part of the sub-esophageal ganglion (CTM) were visible (Fig. 3.1C). For the recording method using the whole animal preparation (see section 3.3.2D), the animal was further opened by removing parts of the fused coxae (2-4). This allowed easier access to the pectinal nerves during the experiments.

3. In the next step, the circumneural diaphragm (Di) was removed and the pectinal nerves were loosened from remaining tissues between the CTM and the base of the pectines (p) (Fig. 3.1C, cut 5). This was also the last step for the recording method using the whole animal preparation.

---

1   **C**onvention on **I**nternational **T**rade in **E**ndangered **S**pecies of wild fauna and flora.
2   20.47 g/l NaCl, 0.84 g/l KCl, 1.08 g/l $CaCl_2$, 0.16 g/l $MgCl_2$, buffered to pH 7.2 with TRIS.

4. Dissections that required the isolation of a pectine followed the pectinal nerve to the base of the pectines where further cuts around the pectine base isolated the pectine (Fig. 3.1C, cuts 6-7).
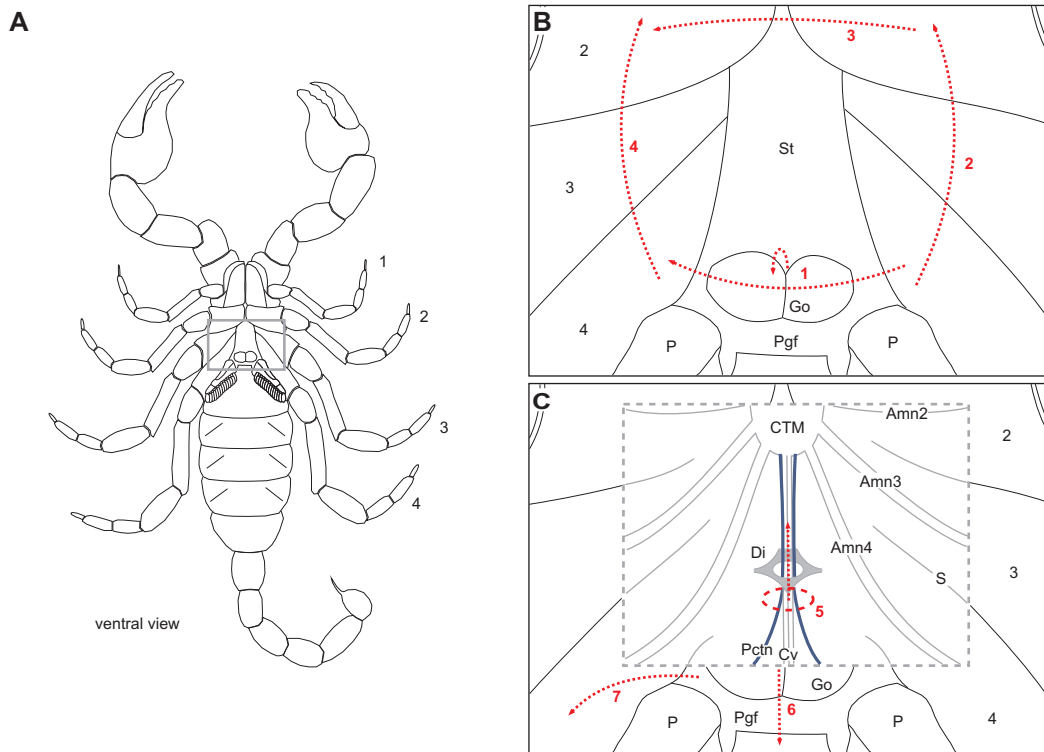
Fig. 3.1: Dissection procedure. Two of the applied recording methods and the nerve stains required dissection of the animals. **A** shows a ventral view of the whole animal and the area in which dissection was necessary. **B** illustrates the four cuts necessary to dissect the animal without damage to the pectine nerves *Pctn*. The first cut (1) had to be done carefully, the genital operculum *Go* was lifted and a flat cut through the postgenital fold (Pgf) opened the body. After this cut, the cuticle for the next cuts (2-4) could be lifted and by cutting through the coxae *2-4*, damage to the pectine nerves was prevented. Finally, the sternum *St* was removed. **C** shows the view once the cuticle was removed. Starting from the cephalothoracic mass *CTM*, the main leg nerves *Amn2-4* and the connectives *Cv* can be identified. Other landmarks are the remaining pieces of cuticle *S* between the fused coxae. The pectinal nerves are located on both sides of the connectives, slightly ventral to these. Their diameters, comparable to the connectives, allows distinguishing the pectine nerves from other smaller nerves. For a clear view, connective tissue and fat had to be removed from the nerves and the CTM. Following the connectives from the CTM, the circumneural diaphragm *Di*, a part of the endosternite, can be identified. The diaphragm was lifted by tissue which formerly connected it to the ventral cuticle and was flatly cut in anterior direction (cut 5). This was the most critical step of the dissection. Further cuts (6,7) around the pectine base *P* isolated the pectine.

3.2 Morphology and innervation

The outer morphology of the pectines as well as the innervation and morphology of the
PHS was examined in detail. These experiments were conducted with two different light
microscopes and a scanning electron microscope (SEM). The setup of the electrophysi-
ological experiments was equipped with a binocular dissection microscope (Wild Type
M8) which allowed a 125fold maximum magnification. This microscope was additionally
equipped with an adapter for a digital camera (Nikon CoolPix 4500) and an ocular mi-
crometer (max. accuracy $\pm$ 5 μm). In addition to the electrophysiological experiments,
the analysis of the outer morphology of the pectines were partly conducted using this
microscope.

For further examinations, another microscope (Leica, Leitz DM R) with a 100-700fold
magnification was used. This microscope was also equipped with an adapter for a digital
camera (Canon EOS 400 D).

The shutter and aperture of the digital cameras was manually controlled. The images
were processed with Photoshop Elements (Adobe Systems Inc., San Jose, U.S.). The
processing mostly consisted of brightness and contrast adjustments and sometimes an
unsharp mask filter was applied. Length measurements on the images were performed
with ImageJ (National Institutes of Health, U.S.) and calibrated with images of a mi-
crometer scale, taken with the same magnification and camera settings. Sketches of the
images were drawn with CorelDraw 12 (Corel Corporation, Ottawa, Canada).

3.2.1 Scanning electron microscopy (SEM)

For the SEM images, standard procedures were applied. At first, the specimen (mostly
whole pectines) were dried in a series of ethanol (50 %, 70 %, 80 %, 90 %, 98 %, 100 %,
100 %) and finally placed in acetone. A critical-point drying (Balzers CPD 030) removed
remaining water. The preparations were subsequently sputtered with a 60 nm gold-
coating (Baltec SCD 005, argon atmosphere). The scanning electron microscope (Vega
TS 5135MM, Tescan s.r.o.) was equipped with an electron backscatter detector and a
secondary electron detector. The images were processed with Photoshop Elements[3].

3.2.2 Direction of the PHS on the pectines

The direction in which the PHS protrude from the pectines was measured with a custom
made rotation platform (Fig. 3.2A). This platform allowed the measurement of the ro-
tations in spherical coordinates. The measurement was achieved with two orthogonally
positioned potentiometers (Spectrol 534 series potentiometers, 10 turns, 2KΩ $\pm$5 %, lin-

---

3   The preparation and the microscopy were conducted at the Berufskolleg Hilden, Mettmann, with the
     kind assistance of Dr. Hartmut Böhm.

earity ±0.25 %), where changes in resistance can be related to according rotation angles with great accuracy (Fig. 3.2A). Due to the arrangement of the potentiometers, firstly the azimuth (φ) and secondly the polar angle (θ) were rotated, i.e. each examined PHS was rotated until it was perpendicular to the optical axis of the dissection microscope (magnification 125fold). Thus, the rotation angles of the potentiometers represented the orientation of the PHS. Prior to the measurement of single PHS, the potentiometers were calibrated (Fig. 3.2B) and the animal axes were defined by appropriate rotations. The spherical coordinates were finally transformed into Cartesian coordinates as follows and plotted with Gnuplot (http://www.gnuplot.info/):

$$x = \cos\theta \cdot \cos\varphi \qquad (3.1)$$
$$y = \cos\theta \cdot \sin\varphi$$
$$z = \sin\theta$$
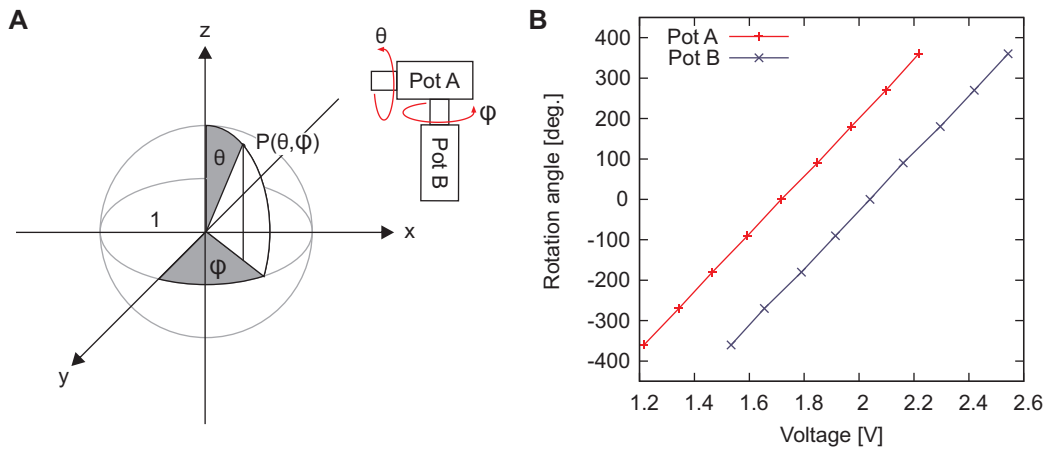
Fig. 3.2: Arrangement and calibration of the potentiometers. **A** The orthogonal arrangement of the two potentiometers (PotA, PotB) with the according rotation angles is shown. **B** Calibration curves of PotA and PotB. The voltage is plotted against the rotation angle. Both potentiometers show a high linearity.

3.2.3 Nerve-stainings

The innervation patterns of the PHS were studied with nerve fills of the pectine nerve in severed pectines. Staining with cobalt-chloride, nickel-chloride and cobalt-lysine was tested. As the stains with cobalt-chloride and nickel-chloride tended to be either over-stained or insufficiently stained and cobalt-lysine was most successful, only details for cobalt-lysine are described in the following. The labeling, development and silver-

intensification followed the procedures described in (Mesce et al., 1993), except that the timing was slightly modified and that electric pulses were applied during the labeling.

Labeling of the pectinal nerve

The respective animal was dissected as described in section 3.1.1. After freshly cutting the distal end of the pectine nerve, it was placed in distilled water for 10 minutes to open the axons and finally, 2-3 % cobalt-lysine solution was infused into the nerve by electric current pulses of 1 μA, delivered at a 1 Hz symmetric square wave pattern (Altman and Tyrer, 1980). The preparation was kept at 4 °C for 48-72 h. Prior to further analysis, the pectines were cut in 2-3 pieces of equal size to improve permeation of the solutions.

Tissue processing

After the infusion, the preparations were washed in buffering solution (see section 3.1.1) and the stain was developed with fresh ammonium-sulfide solution. The preparations were then either fixated with paraformaldehyde or glacial ethanol acid (10-15 minutes). Subsequently, the tissues were gradually dehydrated with a graded ethanol series (30 %, 50 %, 60 %, 70 %, 80 %, 90 %, 98 %, 100 %, 100 %, each 10 minutes). The preparations were placed in methylsalicylate for inspection under a microscope (300-700fold magnification).

Intensification

Some preparations were intensified with a silver intensification method (solutions are named according to Mesce et al., 1993)[4]. All following steps were performed on a nutator (BA-Wi-300, Bachofer) and controlled with a binocular microscope (10fold magnification). The rehydrated preparations (inverted ethanol dehydration series) were pretreated in 2 % sodium-tungstate, pH 10.5 in 1 % Triton X-100 solution for 20 minutes. For about 15 minutes, the pectines were placed in a mixture of solutions A and B before the intensification was started by placing the preparations in an 8:1:1 mixture of solutions A:B:C. The intensification was performed under visual control of the development for 10-20 minutes. Finally, the preparations were washed several times in distilled water and dehydrated for microscopy.

---

4   **Solution A:** 355 ml Distilled H_2O, 15 ml 1 % Triton X-100, 1.5 g Sodium acetate-3H_2O, 30 ml Glacial acetic acid, 0.5 g Silver nitrate.
  Solution B: 5 % Sodium tungstate, pH 10.5.
  Solution C: 0.25 % fresh Ascorbic acid.

3.3 Electrophysiology

3.3.1 Overview of the electrophysiological experiments

In the electrophysiological experiments, different extracellular recordings of the PHS were performed and single hairs were mechanically deflected with a custom-made mechanical stimulator. The experimental procedure was always similar. At first, an animal was prepared and the electrodes were positioned. Different hairs were tested on the quality of the recording and one hair was chosen for the experiment. The mechanical stimulator was positioned to the respective hair and the preferred direction of the hair was analyzed. Different series of mechanical stimuli were presented and the measured data was recorded. Finally, the hair deflection was calibrated and the experiment was stopped.

Depending on the quality of the recording, the signals were amplified 10^4-10^5fold, using custom made filter-amplifiers with low noise (5 μV peak-to-peak) and band pass filter set to the range of 0.3-2 kHz plus an additional 50 Hz filter. The amplified signals were digitized (20 kHz/channel) and saved on standard computers for further analysis using the 16bit analog-digital-converter (ADC) Power1401 and Spike2v5.13 (Cambridge Electronic Design, London). In addition, an audio-monitor was used during the experiments to control nervous activity and noise level.

The whole recording was supervised by a custom-written script (within the Spike2-software) which controlled the mechanical stimulator and the recording. This script generated three different windows. The first window (Fig. 3.3A) showed a slow, general view of the recordings with channels containing data from the recordings, feedback of the mechanical stimulator and channels for other internal parameters (e.g. TTL-marks for stimulus onset). The second window (Fig. 3.3B) only showed the recorded data, triggered to stimulus onset. The third window (Fig. 3.3C) was optional and only used if a preliminary online analysis of the data was performed during the experiments. The user could interact with the script via a toolbar and dialog boxes. In addition to standard functions, different types of mechanical stimuli could be chosen and their parameters set to required values (see section 3.4). After stopping the recording, the data and an according text file, which contained the stimulus settings, were automatically saved on hard disk.

Preliminary online analysis

Spike2 offers the possibility to analyze the data while sampling. This feature was built into the main controlling script and used during the electrophysiological experiments. For most stimulus types, the user could choose a preliminary online analysis (see Fig. 3.3) that was performed during the recording. For example, the number of spikes after each stimulus could be automatically counted and plotted against the varied stimulus

parameter. In the online analysis, action potentials (spikes) were detected if the data crossed a user-defined trigger level within the visible area of the triggered view B (the user had manual access to both axes). This was a fast and reliable method for instant control whether the chosen stimulus parameters matched the working range of a sensillum. Furthermore, it was used to quickly determine the preferred direction of a sensillum – which was always tested prior to the application of other types of stimuli.
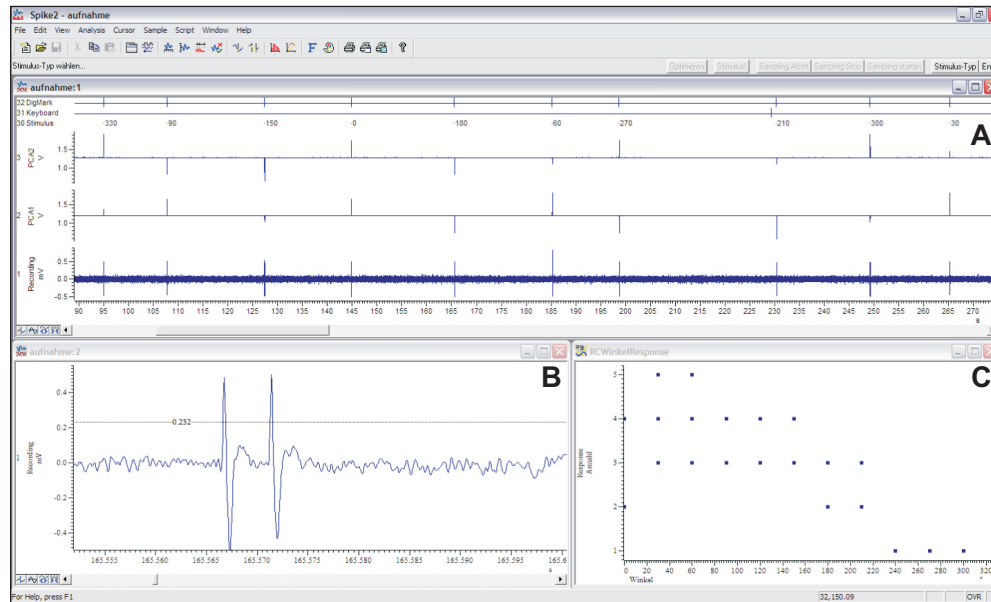

Fig. 3.3: Screenshot of the electrophysiological experiments. The script-controlled recording screen of the Spike2 software is illustrated. **A** Main recording window with channels for the electrophysiological data, the feedback of the stimulator, digital events (TTL-marks) such as stimulus onset/offset, and other parameters. **B** Triggered view. **C** Preliminary online analysis. In this case, stimulus direction is plotted against number of spikes. Above A, a toolbar is visible which is part of the script's user-interface.

3.3.2 Extracellular recording methods

Four different extracellular recording methods were tested and applied during the electrophysiological experiments (see Fig. 3.4). The initially applied method 1 recorded from the pectine base in restrained but otherwise intact animals (Fig. 3.4A). Method 2 extended the recording in intact animals by cooling the animal and recording directly from the socket of a hair (Fig. 3.4B). The other two methods required the dissection of the animal with method 3 recording from the main pectine nerve in isolated pectines (Fig. 3.4C) and method 4 using whole animal preparations to measure the activity of the main pectine nerve close to the cephalothoracic mass (Fig. 3.4D). In the following, all methods are described and subsequently compared.
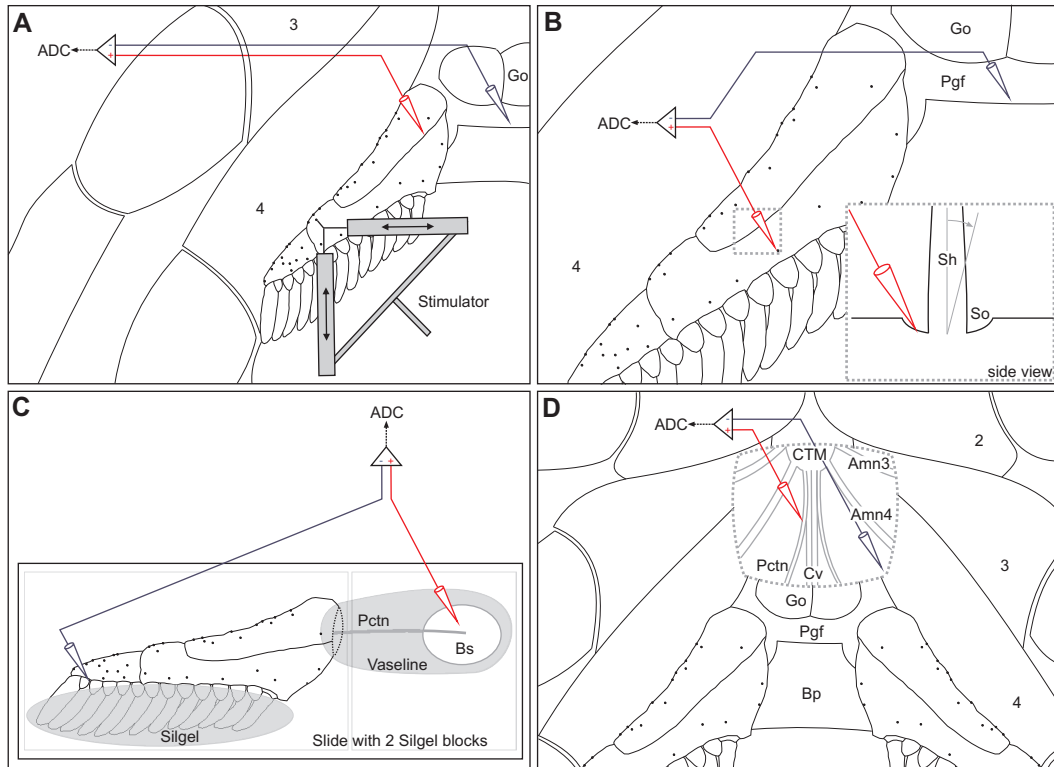
Fig. 3.4: Electrophysiological recording methods. **A**-**D** illustrate four different recording methods. The different types of electrodes are schematically represented by the cones. **A** Extracellular recording with tungsten electrodes in intact, restrained animal. **B** Extracellular recording from the hair socket with sharpened tungsten electrodes in intact, restrained and cooled animal (4-6 °C). **C** Extracellular recording from the severed pectinal nerve with silver-silverchloride electrodes. **D** Extracellular recording with hook electrodes from the pectinal nerve in whole animal preparations. *2-4* refer to the number of the pair of walking legs, *Go*: genital operculum, *Pgf*: postgenital fold, *ADC*: analog-digital-converter, *Sh*: hairshaft, *So*: hair socket, *Pctn*: pectine nerve, *Bs*: buffering solution, *CTM*: cephalothoracic mass, *Amn3/4*: according main leg nerve, *Cv*: connectives, *Bp*: basal plate. The stimulator is only shown in *A*, but it was applied in the same fashion in all experiments, regardless of the recording method.

Method 1: Recordings from the pectine base (Fig. 3.4A)

At first, animals were restrained with elastic bands on a custom-made preparation platform and the according pectine was further secured with double-sided adhesive tape on a small metal platform. For the recordings, tungsten electrodes (diameter 25/50 μm) were inserted into the base of the pectine, in particular in the interlamellar cuticle connecting two adjacent marginal lamellae. The indifferent electrode was sometimes inserted in the intersegmental membranes around the basal plate (e.g. the postgenital fold). Prior to an experiment, different sensory hairs were manually stimulated to test whether the recording was successful and which sensillum showed the best signal-to-noise ratio (SNR). The

preparation took 10-20 minutes but very often, the position of the electrodes had to be changed several times until a successful recording was achieved (e.g. changes of electrode distances). Sometimes, the experiments had to be interrupted as muscle activity (the animal squirming against the bonds) prevented the recording of sensory activity. The recordings lasted several hours up to one day.

Method 2: Recordings from the socket of a hair (Fig. 3.4B)

Movements of the animal that sometimes interrupted the recordings using method 1 were effectively prevented by cooling the animal on a cooling preparation platform to 6-8 °C in addition to the preparation of method 1. This allowed the insertion of sharpened tungsten electrodes (tip diameter 1-2 μm) into the socket of a sensory hair. In general, the SNR was better than in method 1 but again, several sensory hairs had to be tested to obtain a good recording. However, the insertion of the electrode had to be done carefully as it was easy to destroy the socket or the tip of the electrode. Furthermore, the angle of insertion had to be low to enable deflections of a sensory hair in each direction. Approximately 20-30 minutes were needed for the preparation and the recordings lasted 1-2 hours.

Method 3: Recordings from the pectine nerve in isolated pectines (Fig. 3.4C)

For the pectine preparation, the animals were dissected as described in section 3.1.1. The isolated pectine was placed in a petri-dish with buffering solution (solution according to section 3.1.1). Depending on the size of the animal, the dissected pectine nerve had a length of approx. 3-10 mm. Finally, the pectine was placed on a microscope slide and secured with Silgel (Elastosil RT 601, Wacker) in a way that sensilla protruding ventrally and frontally were free to move. The slide was covered with silgelblocks to enable insertion of the electrodes into the silgel (fastening the electrodes). Recordings were performed with stainless steel electrodes (approx. 50 μm) or with silver-silverchloride electrodes (approx. 50 μm), where the different electrode was positioned in a Vaseline-well surrounding the pectine nerve and the indifferent electrode was positioned in the tip of the pectine, in the soft cuticle between the lamellae and the teeth. Double recordings were performed by using two Vaseline-wells along the pectine nerve. This recording method was very successful. It showed excellent SNRs, allowed double recordings and lasted up to 4 h. About 30-50 minutes were needed for the preparation.

Method 4: Recordings from the pectine nerve in whole animal preparations (Fig. 3.4D)

For recordings in whole-animal preparations, animals were immobilized on custom-made preparation platforms with rubber-bands and two-component epoxy to prevent movements of the legs and the pedipalps. The pectine was further secured with double-sided adhesive tape on a small metal platform. The animal was then dissected as described in

section 3.1.1. Silver-silverchloride hook electrodes (diameters 50-100 μm) were attached to the nerve and insulated with Vaseline. Double recordings were performed by using two different hook electrodes on the same pectine nerve. Excellent SNRs and preparations lasting up to 4 hours were achieved with this method. Double recordings were possible which enabled distinction of afferent and efferent signals. Muscle activity sometimes masked the recordings and prevented further analysis, but it was weaker than in method 1 as the opening in the animal reduced the body pressure necessary for strong movements. Approximately 30-50 minutes were needed for the preparation.

3.3.3 Comparison of the recording methods

The recording methods differed in some crucial aspects. The recordings from the pectine base (method 1, Fig. 3.5A) allowed the registration of one type of action potential (AP) with a SNR of 3-11:1. Using this method, struggling animals often interrupted the experiments. Nevertheless, this method was quick, easy and the animals survived the procedure.

The recordings from the hair sockets in cooled animals (method 2, Fig. 3.5B) enabled the registration of two different AP-classes with a SNR of 4-17:1 for the larger class and 3-4:1 for the smaller one. The main advantage of this method were the diminished movements of the animals due to the cooling. The majority of animals survived the experimental procedure. Evident drawback of this method was the required insertion of an electrode into the hair socket. Sometimes, either the socket was damaged or the positioning of the electrode disabled large deflections of the hair shaft.

The recordings from isolated pectines (method 3, Fig. 3.5C) allowed the measurement of 2 and seldom 3 AP-classes with a SNR of 20-70:1 for the larger class and 3-5:1 for the smaller class. If three classes were measured, the smallest was always barely above the noise. The advantage of this method was the possibility to record from the isolated pectine nerve. Good recordings lasted for hours without changes in quality. Furthermore, double recordings were possible, no efferent signals were existent and the small size of the preparations allowed easy arrangement of the stimulator to several sensilla.

The recordings from the pectine nerve in whole animal preparations (method 4, Fig. 3.5D) allowed the registration of 2-3 different AP-classes. The largest class had a SNR of 20-80:1, the medium-sized class a SNR of 4-12:1 and the smallest class a SNR of 2-4:1. Therefore, the best registrations were achieved with this method. Double recordings were possible which enabled the measurement of afferent and efferent (motor) signals.

The main drawback was, that movements of internal muscles, in combination with body pressure, could lead to a loss of insulation on the hook electrodes and the nerve. Sometimes, the experiment had to be aborted, as it was not possible to achieve similar quality after re-insulating the nerve.
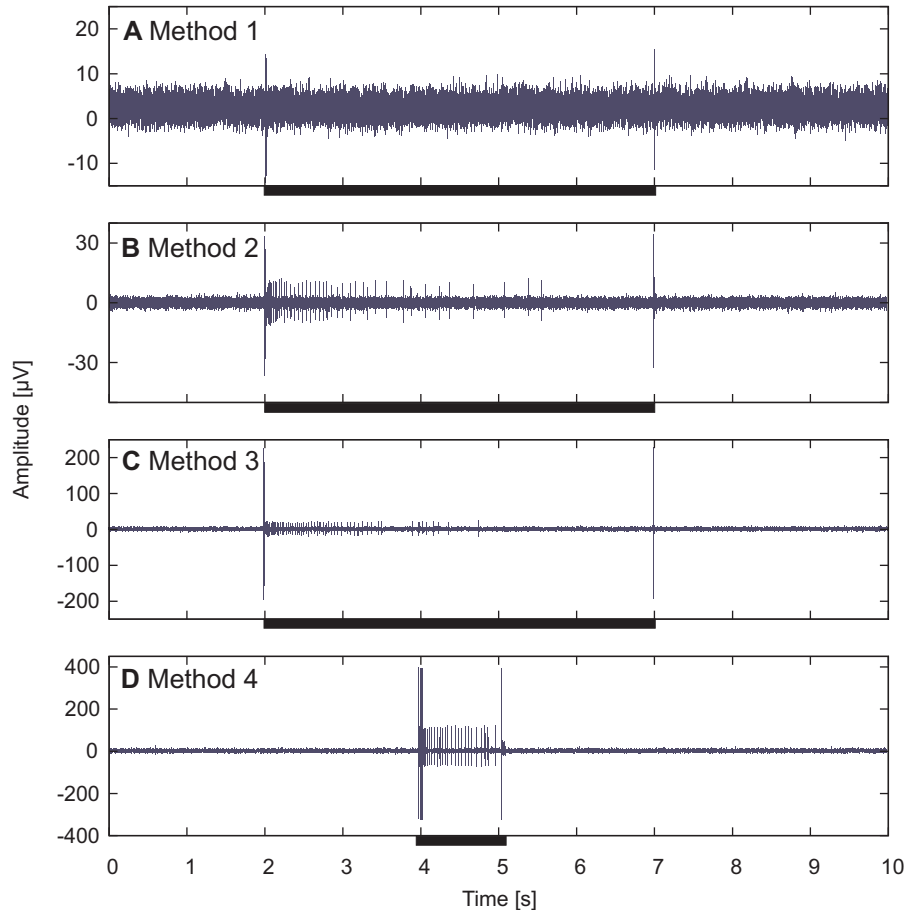

Fig. 3.5: Comparison of the electrophysiological recording methods. The different SNRs and number of recorded AP classes can be seen. **A** Method 1, recording from the pectine base. One AP-class with a SNR of 3-11:1 was measured. **B** Method 2, recording from the hair socket. Up to 2 AP-classes could be recorded with SNRs of 4-17:1 for the larger class and 3-4:1 for the smaller class. **C** Method 3, recording from isolated pectines. 2 and seldom 3 AP-classes could be distinguished. For the largest class, the SNR was 20-70:1, and for the intermediate class 3-5:1. The smallest class was barely above noise level. **D** Method 4, recording from the pectine nerve in whole animal preparations. Up to 3 AP-classes could be recorded. The largest class showed a SNR of 20-80:1, the medium-sized class a SNR of 4-12:1 and the smallest class a SNR of 2-4:1.

3.3.4 Analysis of the electrophysiological experiments

Electrophysiological data were analyzed with Spike2, Sigmaplot 9.0 (Systat Software, San Jose, U.S.) and Gnuplot 4.2 (http://www.gnuplot.info/). In addition to the al-

ready mentioned functions of Spike2 (save and display of data in connection with the Power1401, preliminary online analysis), it was used to discriminate different action potential (AP) classes and prepare the data for the export to other programs.

Spike identification

For the identification of different AP-classes in the electrophysiological data, the 'Spike shape' analysis of Spike2 was used. This classification is based on a shape identification algorithm which uses templates to distinguish different action potentials. A template is a series of data points where each point has a width, a minimum and a maximum value. Basically, the algorithm works as follows:

1. An action potential (spike) is detected, if a manually set trigger level is crossed.

2. Each detected AP is compared against each template to see if sufficient similarity exists.

3. If a spike is sufficiently similar to an existing template, it is added to it.

4. If the AP does not belong to a template, a new one is created.

This only describes the basic principles, the user had the possibility to adjust many parameters of this algorithm, e.g. how templates are created, what happens to a template if an AP is added, or the template width. For larger APs with low variability, the detection proved to be extremely stable and reliable, but for small APs with a SNR of 2:1 to 3:1 or even less, it was necessary to control and possibly modify the results of the detection. For further analysis, the first peak of each identified spike was used to create a digital event (TTL-mark) in another channel created offline (for each template a different channel was used).

Data export

Spike2 was used to record the data, detect and classify the action potentials within the recording. All following analysis were performed in Sigmaplot and Gnuplot. Custom written programs (scripts) allowed the export of the identified spikes. The exported data was saved in files with Tab-separated values. Following functions were available:

- *Spike count:* All spikes following a stimulus were counted. The exported file contained the stimulus value (e.g. direction), the number of spikes for each stimulus as well as their time in reference to the according stimulus onset.

- *Spike frequencies:* All spikes following a stimulus were counted. The exported file contained the stimulus value, the number of spikes for each stimulus, the mean time (in reference to the according stimulus onset) and the frequencies between pairs of successive spikes.

- *Spike phase:* For frequent, sinusoidal stimuli, this script allowed the export of the phase of each spike in reference to the sine wave (zero-crossing). The exported file contained the stimulus frequency, the number of spikes per cycle and the phase of each spike.

- *Conduction velocity:* This script allowed the comparison of two recording channels and the determination of the conduction velocity between the two recorded traces. Identified spikes of each channel were compared in their time and the conduction velocity was calculated with the user set value of the electrode distance. Prerequisite of this script was an exact identification of spikes. Furthermore, both channels had to contain the same types of spike classes. The exported file contained the conduction velocities of the pairs of related spikes.

- *Binned spike frequencies:* The same calculations as in the spike-frequency export script were performed, but instead of exporting the frequency of each pair of successive spikes, the frequencies of all spikes (per stimulus) were binned with a user set binsize and averaged for export. Instead of the time and frequency for pairs of spikes, the exported file contained the mean time of each bin (in reference to stimulus onset) and the mean frequency within the bin.

Mean response vector

The mean response vector allows the analysis of circular data. For electrophysiological data, each action potential can be regarded as a unit vector R_i expressed by its Cartesian components with the direction of the stimulus angle/phase α_i. The length R ($0 \leq R \leq 1$) of the mean response vector for N action potentials can be defined as the sum of these N unit vectors, indicating the strength or directedness of a response (Batschelet, 1981):

$$R = \frac{\sqrt{\left(\sum_{i=1}^{N} \cos \alpha_i\right)^2 + \left(\sum_{i=1}^{N} \sin \alpha_i\right)^2}}{N} \tag{3.2}$$

with the direction P given by:

$$P = \arctan \frac{\sum_{i=1}^{N} \sin \alpha_i}{\sum_{i=1}^{N} \cos \alpha_i} \tag{3.3}$$

The mean response vector was used for the analysis of directional characteristics and for the frequency response curves where the length R of the mean vector was plotted as intensity and the direction P of the mean vector as phase against stimulus frequency (Horsman et al., 1983).

Curve fitting

In some cases, functions were fitted to the data for further analysis. For these (non-linear) least-square fits, the Marquardt-Levenberg algorithm, included in Gnuplot and Sigmaplot, was used.

Calculation of conduction velocities

Conduction velocities were calculated using double recordings (recording methods 3 and 4). The maxima (peaks) of individual action potentials of each recording were identified and the time between two corresponding action potentials was taken. The distance was the visually measured minimum distance between the two Vaseline wells (method 3) or the distance between the two recording electrodes (method 4).

3.4 Mechanical stimulation

The analysis of mechanosensory properties requires devices for appropriate mechanical stimulation. In this context, a variety of methods for mechanical stimulation are established. Oscillating flow fields (Barth et al., 1993), electrostatic attraction (Birukow, 1958) or modified loudspeakers (Caldwell and Hatcher, 1972; Thurm, 1963; Hoffmann, 1967) are some examples.

In this study, the mechanical stimulator consisted of a combination of two piezoelectric actuators (PCAs) (P-871.127, PI Ceramic GmbH, Lederhose, Germany) which could be driven by a controller (E-651, PI Ceramic GmbH) in open-loop or closed-loop operation (Fig. 3.6). The combination of two PCAs allowed arbitrary movements of the stimulator tip within a plane. This arrangement enabled the delivery of different stimulus directions without rearranging the position of the stimulator in reference to the sensory hair.

Several properties of the piezoelectric actuators were crucial for the choice: deflection amplitudes of ± 250 μm with a precision of 0.1 μm or better, a force up to 1 N and a reduced operating voltage of 60 V. Furthermore, small dimensions and low weight made it possible to attach the whole stimulator to a micromanipulator. The PCAs were purchased calibrated, equipped with fullbridge strain gage sensors and a controller which allowed very accurate closed loop operation (see Fig. 3.7A).

Each actuator was installed into an aluminum frame, which also connected both PCAs. A needle was glued to each PCA with two-component epoxy and held in place by a glass capillary with constricted ends. This setting restricted the movements of each needle to one axis. Finally, both actuators were arranged orthogonally in a way that the needles could be glued together. For the attachment to single sensilla, a thin tungsten-hook (diameter approx. 50 μm), was glued to the tip of the actuator-setting (Fig. 3.6).

3.4.1 Stimulator characteristics

The calibration provided by PI showed great linearity of the deflection to the input voltage, with a nonlinear deviation below 0.2 %. The feedback of the strain gages was adjusted to match the input voltage. A control of these values confirmed the calibration (Fig. 3.7A). Nevertheless, the mechanical arrangement inevitably led to a loss of precision, caused by the gluing of needles to the PCAs and by the mechanical attachment of the two stimulators. Therefore, the accuracy was controlled with an optical calibration using 125fold magnification (accuracy approx. $\pm$ 5 μm). This indicated: (1) the actual deflection of the tip was lower than the amount of bending, caused by the position of the needles on the PCAs (not on uppermost position where maximum deflection is achieved) and (2) the changes in amplitude/direction showed linearity at least above visual accuracy.
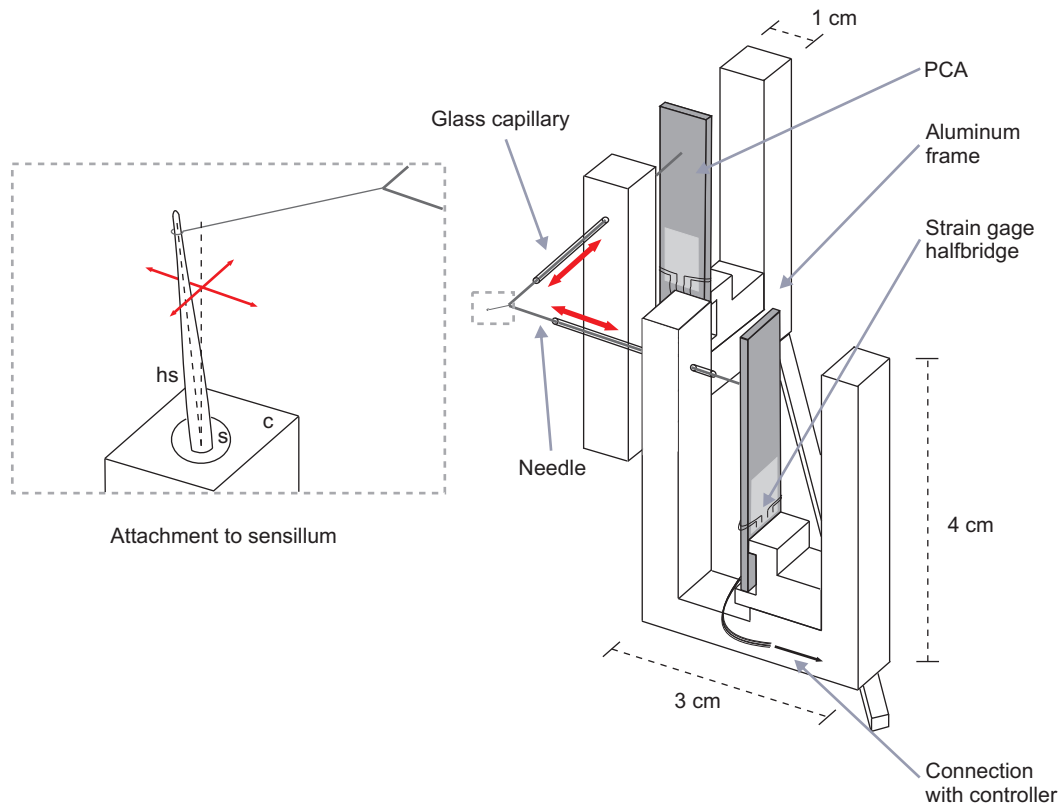
Fig. 3.6: The mechanical stimulator. The stimulator consisted of two PCAs which were arranged and connected by an aluminum frame. Needles were glued to the PCAs and positioned by glass capillaries which restricted movements of each actuator to one axis. A strain gage full-bridge on each actuator (halfbridge on each side) gave feedback to the closed-loop controller. The inset shows the attachment of the stimulator tip to a sensory hair. The orthogonal arrangement of both PCAs allowed arbitrary deflections of a sensory hair within a plane. *c*: cuticle, *hs*: hair shaft, *s*: hair socket

The stimulator response to frequent sinusoidal stimuli was tested (Fig. 3.7B). This showed that in closed-loop operation, the amplitude of the oscillations started to decrease from an amplitude of approx. 20 Hz (the controller was optimized for precision). In open-loop condition, the stimulator never reached the desired amplitude but instead remained rather constant in its level up to frequencies of 100 Hz. This was of importance, as for experiments with frequent, sinusoidal stimuli, the amplitudes had to be corrected accordingly (see section 3.4.2).

The only exception of this total accuracy occurred at large deflection amplitudes (above 150 μm). At these amplitudes, it was observed, that especially different deflection directions led to different amplitudes with a deviation of approx. 10-20 μm. This was
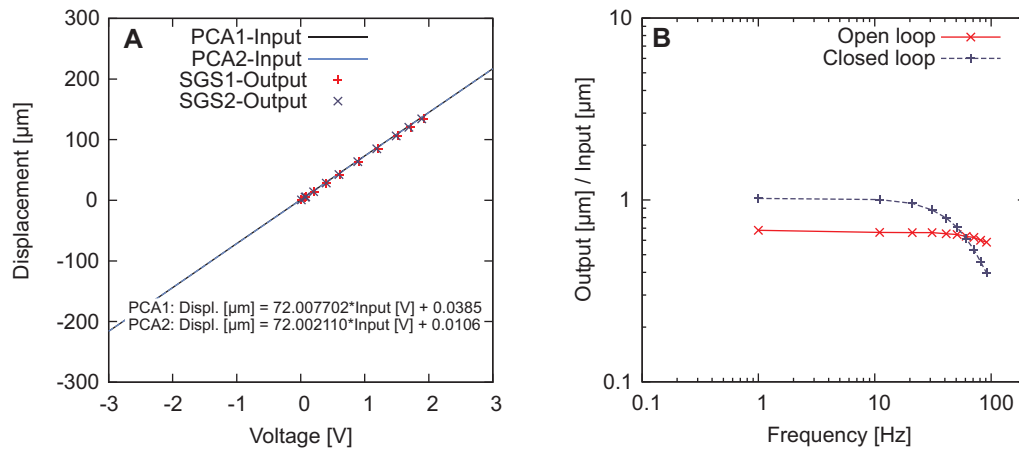
Fig. 3.7: Calibration of the mechanical stimulator. **A** Control measurements (0° direction) with the strain gage feedback confirm the linearity of the provided calibration curves. The calibration curves were used in the computer-controlled generation of stimuli. PCA-input corresponds to the intended amplitude and SGS-output to the measured strain gage feedbacks. **B** The response to frequent stimuli (0° direction, 100 μm amplitude) was tested by analyzing the feedback. The observed differences between closed- and open-loop operation had to be considered in the experiments.

probably caused by bending forces decreasing the amplitudes especially in 0° and 180° directions. If these large deflections were used in other stimulus directions, the optically measured values were linear within the optical precision.

The closed-loop operation did also lead to a delayed response to fast step function stimuli (Fig. 3.8A). Inaccuracy caused by the mechanical arrangement could also be seen in the strain gage responses of other stimulus types, e.g. the maximum deflections of slow ramp-stimuli showed small distortions (Fig. 3.8B).

3.4.2 Stimulus generation

The PCAs were driven by a two-channel controller which allowed either closed- or open-loop operation. To prevent hysteresis (in open loop mode, hysteresis could make up 10% of the stimulus amplitude, especially when the stimulus direction was changed), the controller was mostly used in closed-loop mode. The Spike2 script, which handled the sampling, additionally controlled the generation and control of the mechanical stimuli by using the two analog outputs (0-5 V) of the Power1401 (DACs). These were connected to the controller, which had an input range of 0-5 V/PCA (minimum - maximum deflection).

The stimulator consisted of two orthogonally arranged PCAs, where each PCA repre-
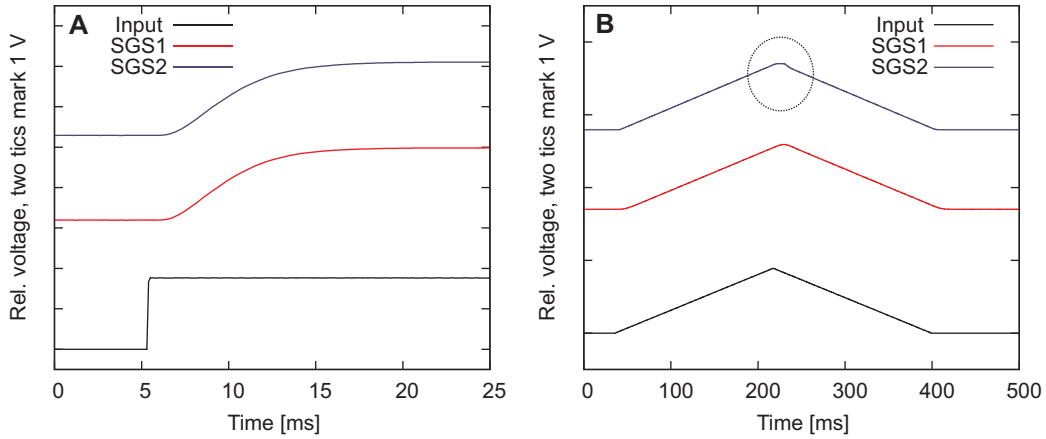
Fig. 3.8: Attenuation and accuracy of the mechanical stimulator. **A** Attenuation together with a small delay caused by the closed-loop operation can be observed in the responses to step-stimuli. **B** Inaccuracy caused by the mechanical arrangement can be seen in the feedback. In this case, the deflection by slow ramp-stimuli showed these effects at the tip of the maximum deflection (indicated by the black, dotted circle).

sented one axis of movement. To achieve a stimulus in an arbitrary direction α with an amplitude A, the single PCA components were calculated, including the provided calibration of each PCA. The necessary input voltage $A_{PCA}(V)$ can then be calculated as follows, with b, m representing the values of the linear calibration curves ($f(x) = m \cdot x + b$, see Fig. 3.7A):

$$A_{PCA1} = \underbrace{\frac{A - b_1}{m_1}}_{cal.A_{PCA1}} \cos\alpha \ ; \ A_{PCA2} = \underbrace{\frac{A - b_2}{m_2}}_{cal.A_{PCA2}} \sin\alpha \qquad (3.4)$$

Details of the script for the mechanical stimulation

The control of mechanical stimuli with a Spike2-script enabled pseudo-randomized generation of all kinds of stimulus patterns. The user could choose different stimulus types and had accurate control over the parameters of the stimuli. After the user had set the type of mechanical stimulus and the according parameters, the script performed necessary calculations and created a set of instructions which could be loaded afterwards to drive the DAC outputs, a sequencer code (machine-code like sequence of instructions). The script then initialized the sampling configuration and allowed the user to start the recording. Once the sampling was started, the script used an 'idle' function which only got called whenever processing time was available (sampling had priority). During sampling, this function controlled the start and the timing of stimuli by calling the sequencer code which was then stepped through, allowed the user to stop or abort the sampling

and controlled – if set by the user – the preliminary online analysis.

Although this procedure did not allow the change of stimulus parameters once the sampling had started, it was necessary to ensure that the output sequencer and the sampling itself had enough working memory for optimal performance. Previous tests had shown that especially the required trigonometric calculations took processing time and that interactive, immediate changes in stimulus parameters (press a button and a stimulus is delivered by adjusting variables) were inadequate. The applied procedure had several advantages: easy user interaction (especially during an experiment where a lot of other parameters had to be controlled), the desire to keep the size of the data files small (still up to 200 MB) and most importantly, a simple method to create series of stimuli with one or several parameters automatically randomized.

Once the sequencer started the output, it was as precise as the sequencer speed allowed. Therefore, the maximum possible sequencer speed with a clock frequency of 10 μs was used which resulted in a resolution of 1 μs. Each output instruction required $<1\mu$s, with cosine output having a penalty of additional 0.55 μs and ramps 0.5 μs. The clock speed was shared between the output sequencer and the data sampling. During an output tick, no sampling or analysis was possible and vice versa. The sampling always had priority over output. Therefore, it could happen that the output was delayed until processing time was available. Overall, this did not have much effect on the stimuli and sampling as the applied sampling frequencies were below the limits of the Power1401 and therefore, the available clock speed was sufficient to serve all instructions.

Available stimulus types

As already mentioned, the script allowed the generation of different types of stimuli which could be delivered in series with randomly varied parameters. All available stimuli could be delivered in any direction and with randomized intervals between single stimuli of a series, set by user chosen values for minimum and maximum intervals. Following stimuli were available (see Fig. 3.9):

- **Step-stimuli (Fig. 3.9A).** These stimuli could be delivered with automatic variations in amplitude and duration by setting the according minimum and maximum values and an interval-value for the amplitude. For the preliminary online analysis, the user could choose that either the number of spikes or the spike interval of the first two spikes was plotted against the stimulus amplitude.

- **Ramp-and-hold stimuli (Fig. 3.9B).** In addition to the options available for the step-stimuli, the user could set on- and off- ramps by adjusting the ramp velocity. The ramp velocity could vary and was set with minimum, maximum and interval values. The optional online analysis was identical to the analysis of the step-stimuli.

- **Ramp stimuli (Fig. 3.9C).** This type of stimulus had an on- and off- ramp without a hold duration in between. The user could set and vary the velocity, duration or amplitude of the ramps with both ramps being identical. For the optional online analysis, the number of spikes or the spike interval could be plotted against the varied value.

- **Stair-stimuli (Fig. 3.9D).** This stimulus was delivered for the determination of discrimination thresholds at different deflected positions of a PHS. It consisted of a user-defined number of steps with according step size and step duration. No online analysis was available.

- **Stair stimuli with sine-modulation (Fig. 3.9E).** This stimulus type was based on the stair-stimulus. In addition to a step size, a sine wave with a change in amplitude was applied to each step by setting the values for sine frequency and number of amplitude-intervals per step. No online analysis was available.

- **Frequent sinusoidal stimuli (Fig. 3.9F).** A user could choose this type of stimulus with a variation in frequency (minimum, maximum and interval values) at a given amplitude and duration of the stimulus. As the Bode plot of the stimulator revealed that the amplitude of the delivered stimulus was strongly dependent on the stimulus frequency (from 20 Hz upwards), this had to be corrected. Therefore, it was implemented that the amplitude of each frequency was increased until the amplitude of a previously released 1 Hz stimulus was reached (by analyzing the strain-gage feedback). This feature proved to be rather instable and therefore either open-loop stimuli were delivered or different amplitudes were applied and afterwards determined which amplitudes actually fit together. Furthermore, an offset of the sine could be defined to allow experiments with a predeflected position of a PHS. No online analysis was available.

Prior to every experiment, the preferred direction of the chosen sensillum was determined. This was done with another series of stimuli, where the deflection direction was automatically varied. These directional characteristics series were available with ramp-stimuli and single sinusoid stimuli.
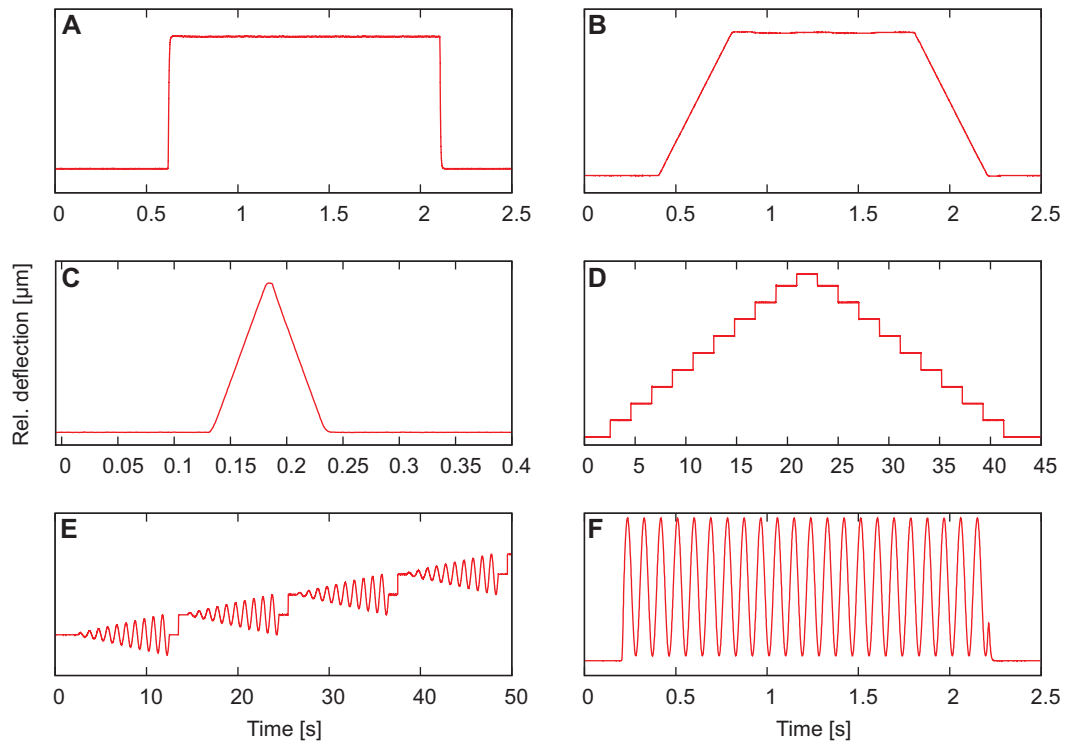
Fig. 3.9: Available mechanical stimuli. Different series of mechanical stimuli could be set by the user. **A** Step-stimuli with variations in amplitude. **B** Ramp-and-hold stimuli with variations in amplitude and ramp-speed. **C** Ramp-stimuli with variations in ramp-speed, duration or amplitude. **D** Stair-stimuli with a user-defined number of steps and step height. **E** Stair-stimuli with a superimposed sine wave modulation on each step. Only a part of the stimulus is shown, the whole stimulus stepped up and down as in *D*. **F** Frequent sinusoid stimuli with variations in frequency. Additionally, an offset for the sine wave could be set. The presented data represents strain-gage feedback of real stimuli.

3.4.3 Calculation of angular deflection

The stimulator allowed linear translation of the tip (μm). Because a sensillum rotates around its pivot point in its socket, the deflection was measured as angular deflection (°). Therefore, the length of a hair l and the deflection of the hairtip x was measured for each experiment. This enabled the calculation of the angular displacement α:

$$\alpha = \tan^{-1}\left(\frac{x}{l}\right) \tag{3.5}$$

Carefully, the stimulator tip had to be positioned orthogonal to a sensillum and not directly at the hairtip but somewhat lower. This approach ensured that the rotation of the hair did not disconnect the stimulator (with rotation, the distance of the hairtip to the cuticular surface decreases). The deflection of the hairtip was measured in different directions (0°, 90°, 180°, 270°, preferred direction) and with different stimulus amplitudes. This was necessary to calculate the angular deflection, but also to control the linearity of the stimuli and orthogonal positioning of the stimulator.

In this study, rather large angular deflections were applied (up to 30°). Therefore, the relation between stimulator deflection and angular deflection of a sensillum was analyzed. Fig. 3.10 illustrates that a linear relation can be assumed.
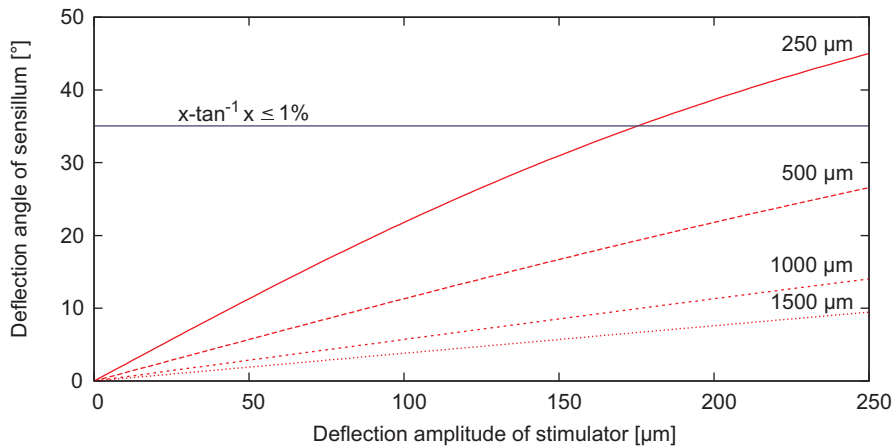

Fig. 3.10: Calculation of deflection angles. Equation 3.5 is plotted for different hairlengths. It can be observed, that in the range of applied stimulus amplitudes the deflection angle of a sensillum shows a linear relation to the stimulator deflection. The blue line indicates that below a deflection angle of 35°, the deviation between a linear function and the arctan function is less than 1%. The according equation was numerically solved using Matlab (The MathWorks, Inc., Natick, U.S.).

Chapter 4

Results

This chapter describes the main results of the neurobiological experiments. It begins with a brief examination of scorpion and pectine morphology and describes the morphology and innervation of the pectinal hair sensilla. The main part presents an electrophysiological analysis of the hair sensilla. Finally, a possible role of the PHS for reflex behaviors is examined.

P. cavimanus, the main species used in this thesis was only sparsely studied so far. Therefore, several biometric characters were measured to obtain information about the morphological parameters of the animals. This characterization included the weight, the total length of the main body (prosoma & mesosoma), the length of the 5th metasomal segment (segment XII) and the number of pectinal teeth. The data was collected directly after acquisition of a scorpion and in some cases controlled several times later on. This control was done to confirm that the animal care conditions were satisfactory, but no long term measurements were performed.

The first examination analyzed the relation between the main morphological parameters of an animal. As the weight was assumed to be proportional to the volume of an animal, the cube root of the weight was assumed to be proportional to the length of the animal (Brown, 1997). Therefore, the cube root of the weight was plotted against the parameters body length and length of the 5th metasomal segment (Fig. 4.1). The results indicate, that these parameters are weakly correlated to each other. Although the sexes were known, possible differences between these were not examined and the linear regressions were performed on the whole data set containing all animals. The main reason for ignoring possible sexual differences was that the animals were purchased. For the acquisition, both sexes were asked for and as larger males are easier to distinguish from females, a bias of the data could not be excluded.
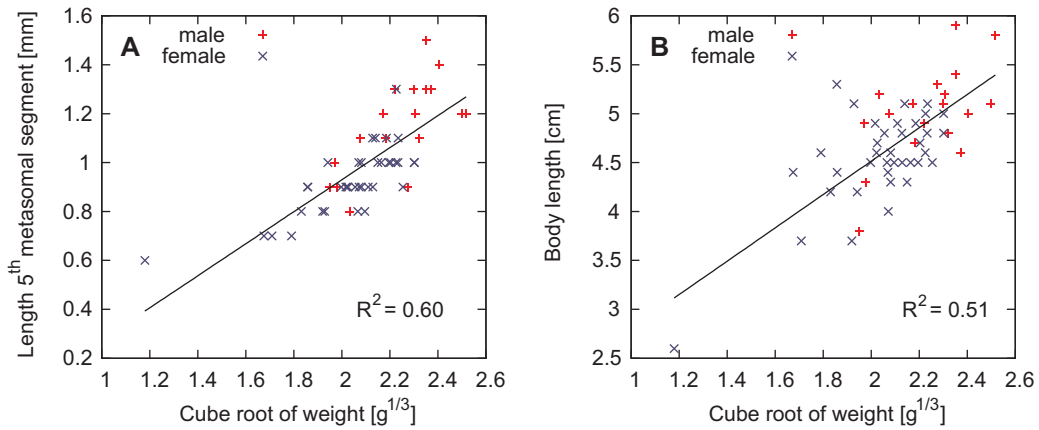
Fig. 4.1: Correlation between morphological characters of *P. cavimanus*. **A** illustrates the weak positive linear correlation between the cube root of the weight and the length of the 5th metasomal segment (segment XII). **B** shows the weak positive linear correlation between the cube root of the weight and the body length which was defined as the sum of lengths of the prosoma and the mesosoma. Although the sexes can be discriminated, sexual differences were not analyzed.

4.1 Outer morphology of the pectines

The outer morphology of the pectines of *P. cavimanus* and their equipment with cuticular sensors was analyzed in detail. As mentioned in chapter 2, the pectines are bilateral appendages of the 2nd mesosomal segment with a distinct shape (lamellae and teeth). An overview of the ventral and dorsal surface of the pectines as well as a cross section is illustrated in Fig. 4.2.

On the ventral side, three marginal lamellae and a varying number of teeth could be identified (Fig. 4.2A). This is in accordance with the general scheme provided in literature. In males, between 12 and 16 teeth and in females, between 11 and 16 teeth per pectine were found. Between the teeth and the lamellae, fulcra were visible. The teeth counts further indicated that there was always one tooth more than fulcra. Interlamellar membranes (interlamellar cuticle) could be identified in between the different lamellae and fulcra.

The outer morphology of the dorsal side differed from the ventral side of the pectines (Fig. 4.2B). In addition to the marginal lamellae, three median lamellae were found on the dorsal side and instead of the fulcra, the bases of the pectinal teeth were visible. These bases were embedded in a strap of interlamellar membrane which facilitated movements of the teeth. The interlamellar membranes were generally more pronounced on the dorsal side than on the ventral side.

In pectine preparations, several pectine base muscles were found which were located between the pectine base and the endosternite, probably responsible for rotations of the

whole pectines. Cross sections through a pectine revealed a flattened structure with a width:height ratio of approx. 6-8:1 (Fig. 4.2C).

Three different types of cuticular sensilla are located on the pectines (see Fig. 2.4 and chapter 2): chemosensory pegs in fields on the distal side of each tooth as well as short, probably chemosensory hairs and long mechanoreceptive hair sensilla (PHS) on the lamellae. In addition to these already known locations of the different sensilla on the pectines, some additional details were found.

On the pectines of *P. cavimanus*, the short, whitish (probably chemosensory) sensilla were not only located on the lamellae but were also found on the fulcra and often on the most distal tooth. The PHS, which were analyzed in this study, were mainly found on the ventral side and the frontal edge of the lamellae, with a few PHS located on the lamellae of the dorsal side (Fig. 4.2).
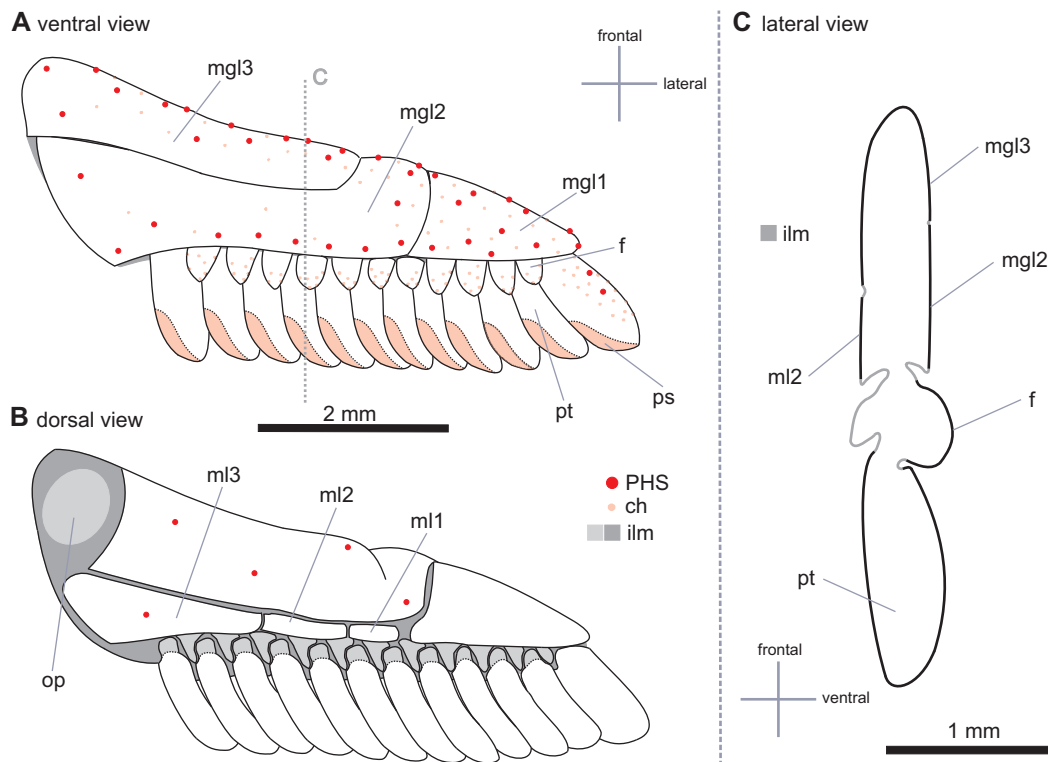

Fig. 4.2: Outer morphology of the pectines. **A** Ventral view of a pectine. **B** Dorsal view of a pectine. **C** Lateral cross section of a pectine. *mgl1-3*: marginal lamellae, *ml1-3*: median lamellae, *f*: fulcra, *ps*: fields of peg sensilla, *pt*: pectinal tooth, *PHS*: pectinal hair sensilla, *ch*: chemosensory hairs, *ilm*: interlamellar membrane, *op*: connection of the pectine to the body.

In some scorpion families, the pectines show a strong sexual dimorphism (see section 4.1.2). This dimorphism is mostly characterized by the number of teeth and the number of peg sensilla per tooth. However, no distinct sexual dimorphism was found in *P. cavimanus*. A comparison of teeth numbers on the pectines suggested that males tend to have more teeth than females (Fig. 4.3), with 27.89 ± 1.73 teeth per animal in males and 25.82 ± 1.85 teeth per animal in females. As the number of teeth did not correlate with animal size (see Fig. 4.4), it was inferred that males tend to possess one more tooth per pectine than females. Interestingly, the number of teeth often varied between the two pectines of one animal. In about 39% of the animals, a difference of one tooth and in 6% of the animals, even a difference of two teeth was observed. No preference for either side or a sex was found in these variations.
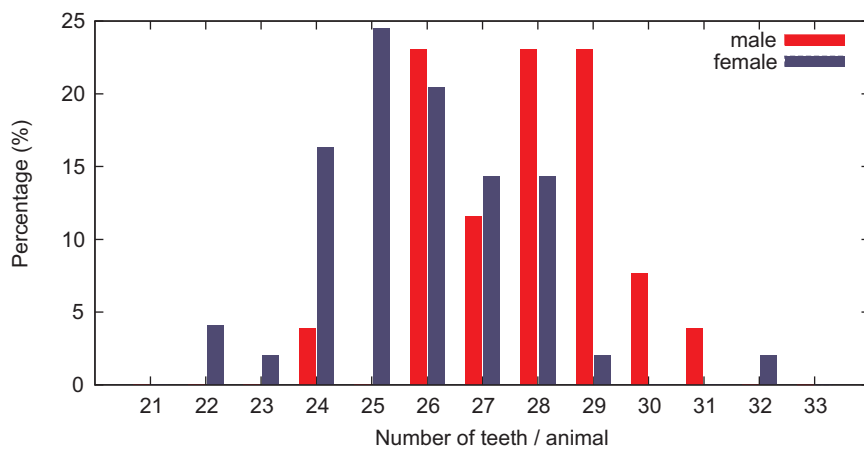

Fig. 4.3: Number of pectinal teeth. The distribution of the relative numbers of peg sensilla per animal is shown for both sexes. The mean values for males (N=26) and females (N=49) are: 27.89 ± 1.73 and 25.82 ± 1.85.

No linear correlation was found between the number of pectinal teeth and other morphological parameters such as the cube root of the weight or the length of the 5th metasomal segment (Fig. 4.4). Therefore, the number of teeth seems to be a fixed value for an animal. Furthermore, the results indicate that the number of teeth does not correlate with pectine length (R^2=0.04, N=18 pectines).

4.1.1 The pectines and their equipment with pectinal hair sensilla

Approximately 30-50 PHS were found on the pectinal lamellae (Fig. 4.5). Of these, most protruded from the ventro-frontal surface of the marginal lamellae and a few protruded from the dorsal surface of the lamellae. No pronounced sexual dimorphism was found in the number of PHS (Fig. 4.5).
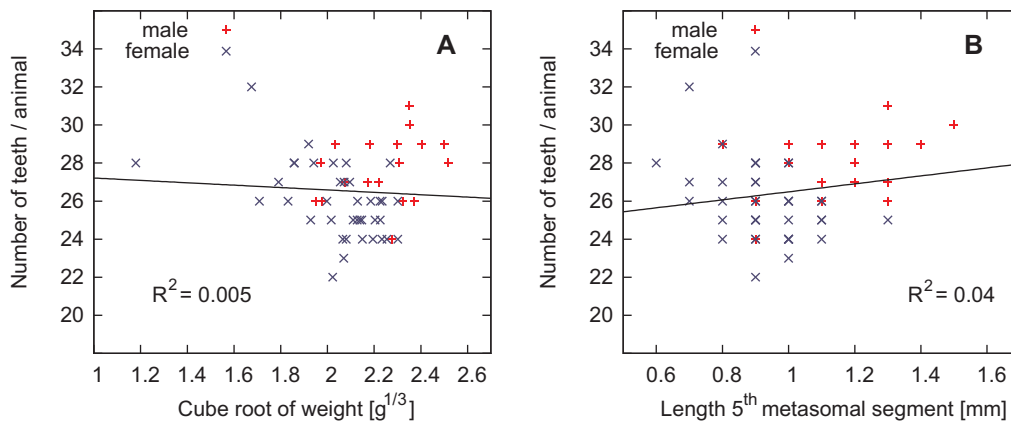
Fig. 4.4: Correlation between number of teeth and other morphological parameters of *P. cav-imanus*. Both plots indicate that the number of pectinal teeth does not correlate with the investigated morphological parameters. **A** Correlation between number of pectinal teeth and the cube root of the weight. **B** Correlation between the number of pectinal teeth and the length of the 5th metasomal segment.
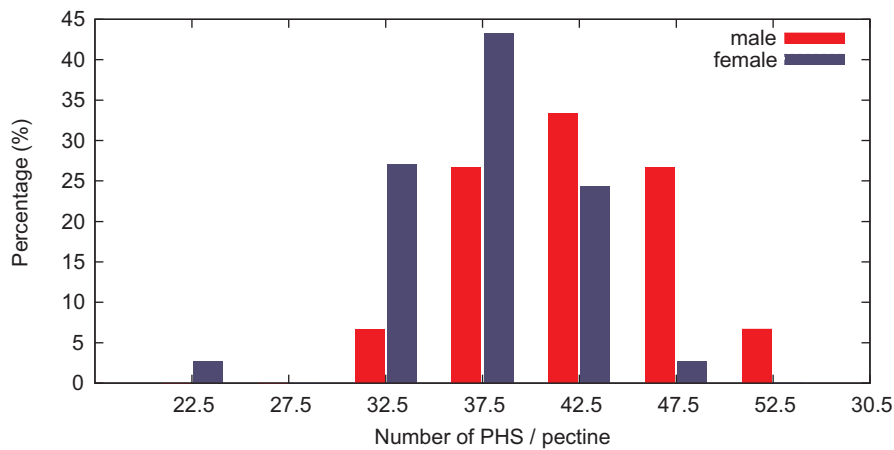

Fig. 4.5: Number of PHS on a pectine. The histogram shows the distribution of the numbers of PHS per pectine. The data was binned with a bin size of 5 PHS, the values on the abscissa represent the bin centers. The data comprises a total of N=15 males and N=37 females.

Reflexive movements of the pectines and the body require adequate sensory structures. In addition to appropriate sensitivities, this also includes suitable locations of the sensors. Because a role of the PHS as obstacle-detectors was suggested, the directions of their hairshafts were analyzed (the direction in which they protrude, for method see chapter 3.2.2). The results indicate that the PHS mainly cover a latero-ventro-frontal area (Fig. 4.6). However, these data were collected in reference to pectines in their resting position.

In this position, they are held close to the body at angles of 45±5 degrees in relation to the fronto-caudal axis. During palpation, the pectines rotate downwards from the pectine base and also perform small rotations along their longitudinal axis. Thus, a palpating pectine probably covers the complete ventro-frontal area with its PHS.
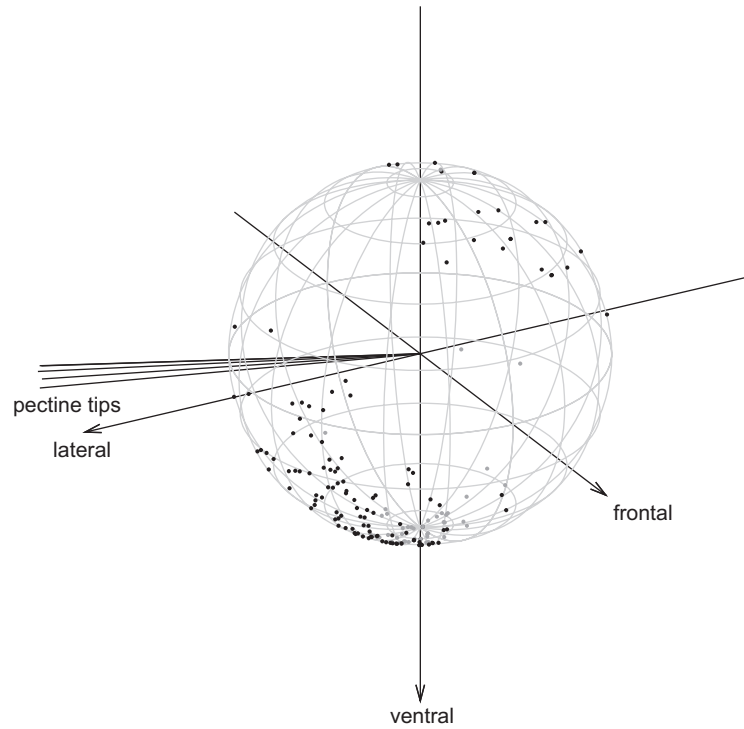

Fig. 4.6: Direction of the PHS on the pectines. This 3D graph illustrates the direction in which the PHS protrude from the pectines. Especially the latero-ventro-frontal area is covered. The pectines are represented by the origin of the sphere and the directions of the PHS by the dots. The frontal, ventral and lateral axes represent the main animal axes. The pectine tip axes indicate the direction in which the pectine tips show in resting position. Data points hidden by the perspective view are marked in gray. The data represents measurements of 4 pectines and a total of 174 PHS with the axes in relation to the resting position of the pectines.

4.1.2 Comparison with other species

A comparison of the number of teeth on the pectines of *P. cavimanus* with the numbers on the pectines of other species revealed that the Scorpionida in general do not exhibit a strong sexual dimorphism. In comparison, some species of the Vaejovidae and the Buthidae show strong sexual differences of more than 8 teeth per animal (table 4.1). However, the examined literature indicates that males always possess the same number or more teeth than females.

Family	Species	# teeth / pecten	
		♂	♀
Bothriuridae	*Brachistosternus intermedium*[◇]	25-26	20-21
	Brachistosternus montanus[◇]	26-30	23-25
	Brachistosternus quiscapata[◇]	29-32	24-26
	Brachistosternus titicaca[◇]	24-27	20-21
Buthidae	*Androctonus australis*[#]	34.2±1.48	26.3±1.25
	Buthus occitanus tuneatus[#]	32.3±1.77	27.6±1.08
	Centruroides exilicauda[*]	25	22
	Parabuthus pallidus[*]	36	31
Chactidae	*Superstitionia donensis*[*]	6	6
Diplocentridae	*Didymocentrus comondae*[*]	8.5	7.5
Euscorpiidae	*Euscorpius italicus*[†]	8	8
Scorpionidae	*Pandinus cavimanus*	13.94±0.96	12.91±1.01
	Pandinus gregoryi[*]	18	17
	Pandinus imperator[#]	14-17	14-16
Vaejovidae	*Anuroctonuis phaiodactylus*[*]	8.5	7.5
	Nullibrotheus allenii [*]	12	8.5
	Paruroctonus bantai[•]	20-28	16-20
	Paruroctonus mesaensis[*]	37.5	24
	Paruroctonus shulovi[•]	18-22	11-17
	Paruroctonus simulatus[•]	18-24	12-17
	Uroctonus mordax[*]	13.5	10
	Vaejovis bilineatus[‡]	15-19	14-16
	Vaejovis confusus[*]	17	13.5
	Vaejovis spinigerus[*]	23	18.5

Tab. 4.1: Number of pectinal teeth in different species. A comparison of the number of teeth between different taxa and within a species between the sexes is shown. This table is a summary of data presented in [*](Gaffin and Brownell, 2001, table 7.1, p.191), [#](Mahsberg et al., 1999), [†](Foelix and Schabronath, 1983b), [‡](Yahia and Sissom, 1996), [◇](Ochoa and Acosta, 2002), and [•](Haradon, 1985). The data of *P. cavimanus* is based on 26 males and 49 females. The collected data only contains publications where variation data was presented, plain holotype/allotype descriptions were excluded.

A qualitative comparison of different species, with regard to their equipment with long hair sensilla and the overall complexity of the lamellar structure, indicated that the pectines of *P. cavimanus* are average in their size, number of teeth and number of long hair sensilla[1]. This comparison included scorpions of six families and 21 different species. As this comparison is only qualitative, no further details about the investigated species are presented. Overall, the examinations confirmed the data presented in table 4.1. Furthermore, *P. cavimanus* and *P. imperator* were among the species with the largest body size.

---

1 With the kind support of Dr. Bernhard Huber, the collection of scorpions of the Alexander Koenig Zoological Research Museum was accessible for this comparison.

4.2 Morphology and innervation of the pectinal hair sensilla

4.2.1 Basic morphological parameters

An examination of PHS morphology showed that they are straight, almost cylindrical structures with a length of 300-1400 μm (N=418 PHS). In Fig. 4.7, data of chemosensory hairs (Ch) and of metasomal long hair sensilla (mLHS) are presented and compared to the lengths of the PHS. According to their length distribution, the PHS could be distinguished from the curvy, chemosensory hairs (Ch) which are also present on the pectine surface. The mLHS were included for comparison, as they are a group of sensilla that were studied previously (e.g. Babu and Jacobdoss, 1994). The mLHS are much longer than the PHS, with lengths up to 3500 μm (Fig. 4.7).
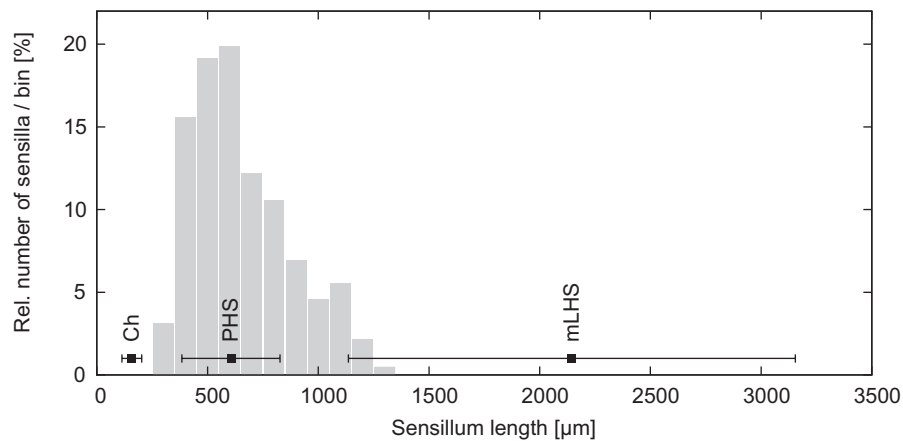

Fig. 4.7: Length-distribution of the PHS. Data of the PHS (N=418) are shown in comparison to the lengths of the chemosensory hair sensilla (Ch, N=56) on the pectines and metasomal long hairsensilla (mLHS, N=156). The different types can be distinguished by their lengths, especially the pectinal chemosensory hairs and the PHS. In addition to the mean±standard deviation (SD) which is presented for all types of sensilla, the histogram illustrates the length-distribution of the PHS.

Individual PHS were approximately 30 μm in diameter at the base and tapered to about 10 μm at the tip. Their lumen ranged from 5 μm at the base to 2 μm at the tip. In comparison, the trichobothria (Tr) on the pedipalps were thinner throughout, with the strongest difference in diameter in the base region. Here, the PHS showed a thickened structure, while the trichobothria were even slightly thinner at their base than in the more distal hair region (Fig. 4.8).
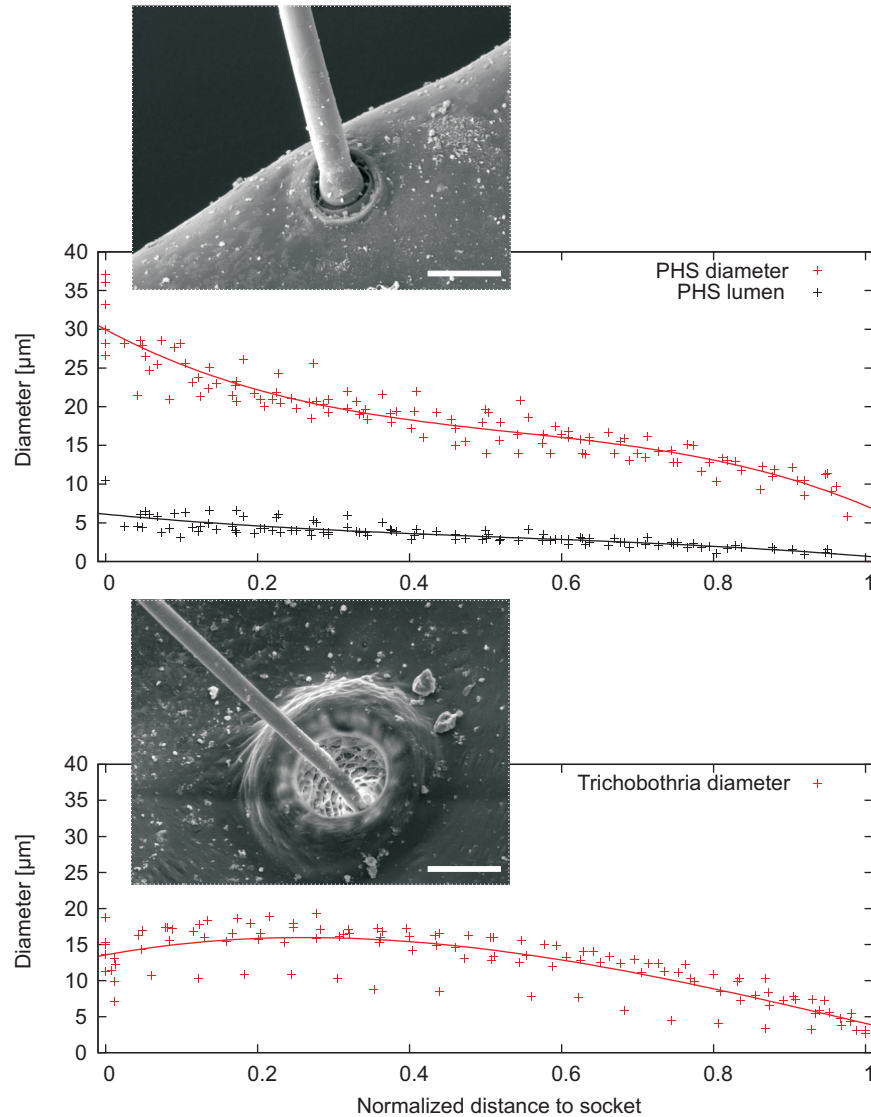
Fig. 4.8: Diameters of the PHS. The outer and inner diameters of the PHS (N=6) are illustrated in comparison to the outer diameter of pedipalpal trichobothria (Tr, N=5). Overall, the Tr are thinner than the PHS, with the strongest differences occurring at the base. The lengths of the individual sensilla were normalized. The SEM images illustrate the different diameters of the two types of hairs and the different shapes of their sockets. The white bars indicate 50 μm.

4.2.2 Morphology of the socket

The examinations indicate that the sockets of the PHS are low rimmed and allow wide range of displacements of the hair shafts (Fig. 4.8). According to the shape of the sockets, the PHS could be divided into two groups: (1) a group with round, flat sockets which did not show a morphological directedness and (2) a group that possessed sockets

with a higher rim at one side, indicating a morphological directedness. The second group is illustrated in Fig. 4.9A. Overall, the sensilla protrude from their sockets at angles of 90-75 degrees, relative to the surface of the pectine cuticle.

During the electrophysiological experiments, it was observed that a hair could be displaced in each direction up to an angle of 20°-30° without bending of the hairshaft. Preliminary measurements indicate that the sockets enable even larger displacements up to 40° without bending (Fig. 4.9B). The experiments were carried out using the dissection microscope with a 125fold magnification. Individual hairs were visible from the top and pulled in four different directions (0°, 90°, 180°, 270°) with a thin glass hook. Furthermore, the hairs were cut short to about 100-200 μm to maintain visibility of the socket and the hairshaft as well. Overall, this method was complicated and only rough data for a few hairs exist, therefore more exact measurements will have to be carried out in the future (see discussion, chapter 8.2.1).
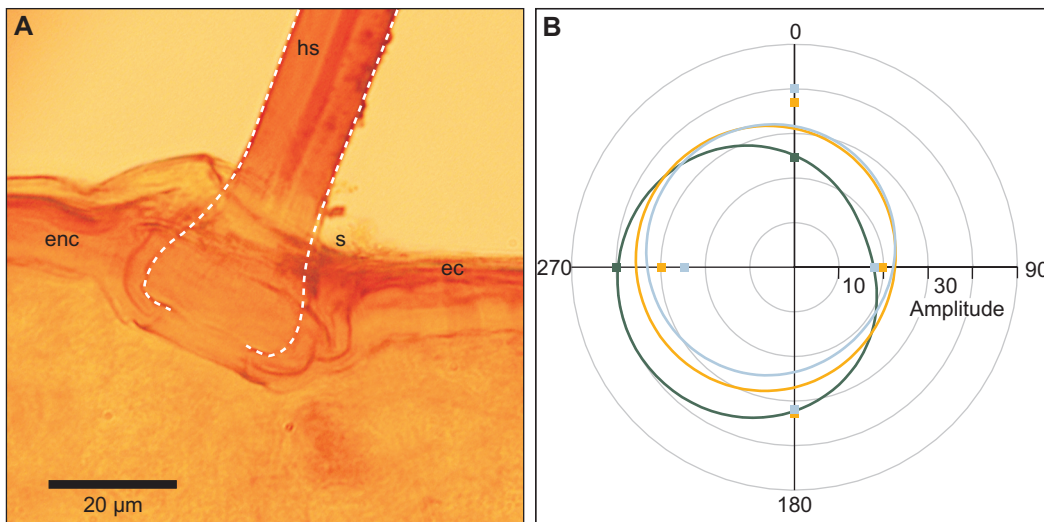

Fig. 4.9: Hair sockets and maximum deflections of the PHS. **A** Detailed view of a hairsocket as seen in a methylsalicylate embedded pectine. *hs*: hair shaft, *s*: socket, *enc*: endocuticle, *ec*: epi- and exocuticle. This particular hair belongs to the group of PHS that show distinct directional predisposition in their sockets. **B** Three examples of measured maximal deflections in 0°, 90°, 180° and 270° deflection direction. The deflection amplitude (°) is plotted as polar distance. The PHS sockets allow a wide range of deflections until the hair shafts touch the sockets and start bending by further deflection. The polar angle is in no relation to the animal (N=3 hairs).

4.2.3 Innervation

With the applied staining-protocol (see chapter 3.2.3), successful labeling of sensory cells in more than 19 pectines was achieved. The samples shown in Fig. 4.10 indicate that each sensillum is associated with a cluster of bipolar cells, approx. 70-100 μm below the hair socket. The cells' axons fasciculate to form a small nerve some 50 μm proximal to the soma cluster. Similarly, the dendrites fasciculate to make contact with the hair base at a common attachment site, excentric to the hair's central line. The stains never marked all the hairs within a given pectine. However, in at least 10 preparations, groups of cell bodies were labeled below several PHS. Taking into account only intense stains, the number of cell bodies within the cluster of a single hair sensillum was determined as follows: 23 clusters consisted of 5 cell bodies, 10 clusters exhibited 4 somata and 3 clusters consisted of 6 cells.
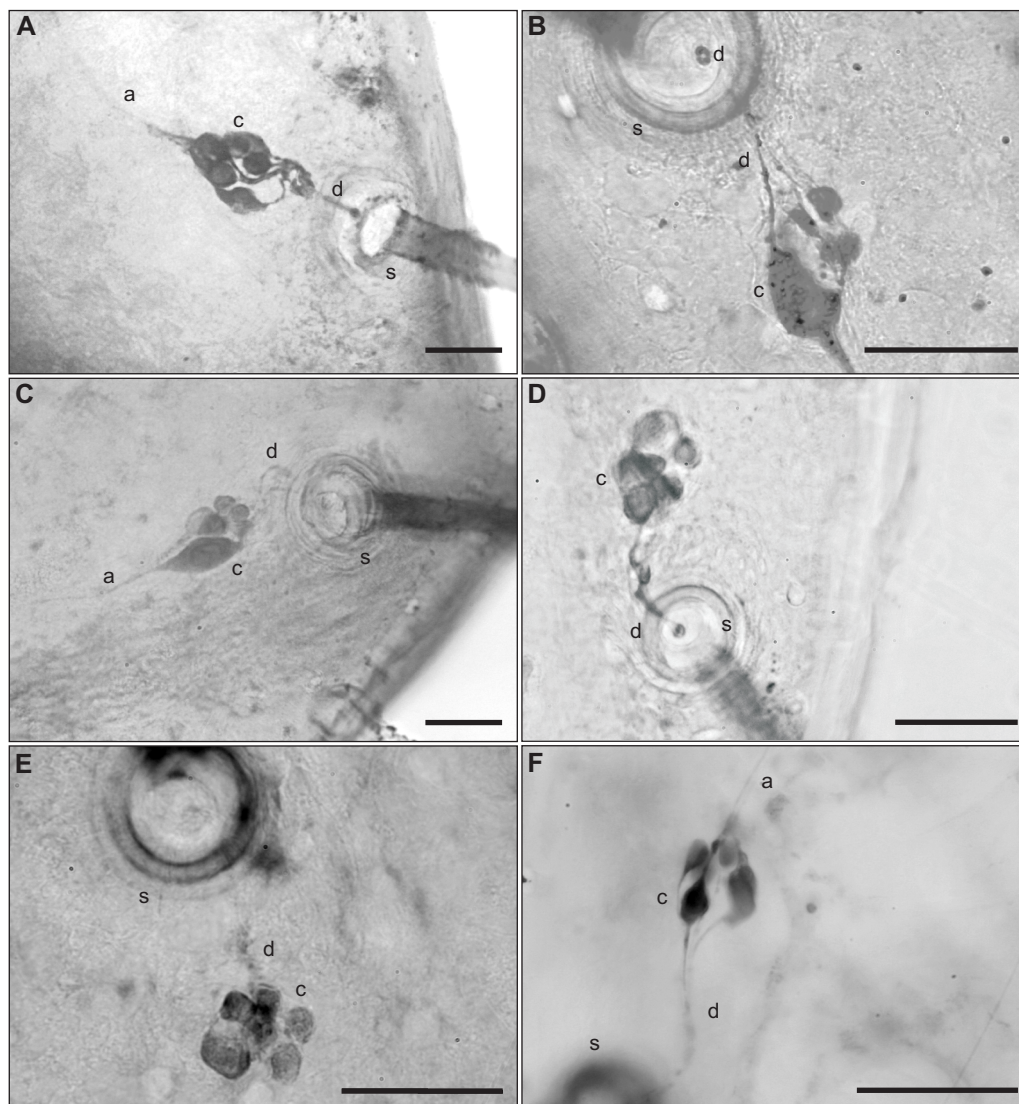
Fig. 4.10: Innervation pattern of the PHS. **A**-**F** show six different examples of stainings with cobalt-lysine. Structures of the sensory cells are labeled with the initial letters: *a*xons, *c*ell bodies, *d*endrites and the hair *s*ockets can be distinguished. The clusters of 4-6 sensory cells are approx. 70-100 μm below the socket. Scale bars 50 μm.

4.3 Electrophysiological response properties of the pectinal hair sensilla

The electrophysiological experiments consisted of several experimental series which investigated different aspects of the response characteristics. For each analysis, appropriate types of mechanical stimuli were presented during the recordings. These examinations included experiments concerned with directional characteristics, the response to variations in velocity and frequency as well as amplitude and time response characteristics. Furthermore, the timing between sensory and motor activity with regard to the role of the PHS in reflex behaviors was investigated.

The electrophysiological results are based on measurements with all applied recording methods (see chapter 3.3.2). The data of the smaller AP-class are mostly based on measurements using isolated pectines and whole animal preparations (methods 3 and 4, see chapter 3.3.2). The results are supported by approximately the same number of experiments (PHS) where the recording either had to be interrupted after a short time or the measured signal-to-noise ratio was insufficient for detailed examination.

In the majority of recordings (N>50), only one large AP-class (L-unit) was present. In 17 further preparations an additional medium-sized class (M-unit) was evident, and in 10 experiments a third, small class (S-unit) could be distinguished (Fig. 4.11). Average recordings exhibited amplitudes of 100-200 μV for the L-unit, 20-50 μV for the M-unit and 10-20 μV for the S-unit (chapter 3.3.3). An average experiment lasted for about 2-4 hours, but some experiments lasted more than 10 hours. During an experiment, series of stimuli were presented with stimulus intervals of 20-60 seconds. Between two successive series, no stimuli were presented for 1-10 minutes to prevent adaptation of the hairs.

Each experiment consisted of several preliminary tests which included (1) the choice of a sensillum for recording and (2) determination of the preferred direction of the respective sensillum. Usually, responses of up to 20 different PHS were visible in the recordings when stimulating one sensillum after the other. In most cases, these PHS could be distinguished by the maximum amplitudes of their recorded responses. Because of the directional characteristics of the hairs, it was important to deflect each sensillum in several directions to determine the quality of its recording. As all hairs showed similar response properties with respect to static, dynamic, and spatial characteristics, the full set of stimulus presentations was only performed with the sensillum that displayed the best signal-to-noise ratio. Of particular importance was the fact that several, large and small AP-classes exhibited good signals. Furthermore, the sensillum had to protrude at an angle from the cuticular surface that allowed positioning of the stimulator. Each experiment was initiated by determination of the preferred direction of the chosen hair using the according stimulus program (chapter 3.4.2). Except for the examination of
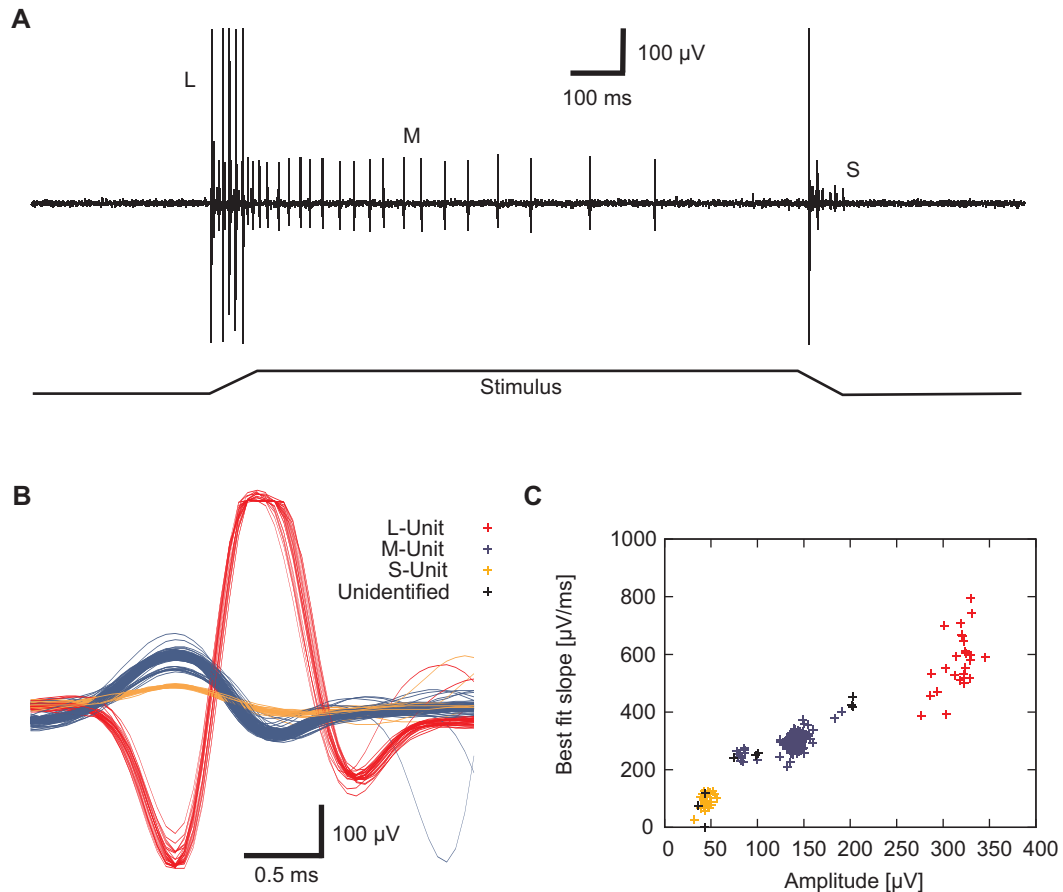
Fig. 4.11: Identification of AP-classes. **A** The response to a ramp-and-hold stimulus (approx. 20° and 200 °/s ramp speed) identifies 3 different spike classes (units) according to size as well as response characteristics. While the largest (L-) and the smallest (S-) units only respond to the dynamic (ramp) component of a stimulus, the medium-sized (M-) unit also responds to maintained deflection of the sensory hair. The discharge frequency of the M-unit decreases continuously over time. None of the units shows spontaneous activity. **B** Identification of different AP-classes according to size and shape. **C** Plotting several characteristics of the AP-classes against each other facilitates discrimination and allows control of the identification.

directional characteristics, all measurements were performed in the preferred direction of the respective sensillum.

Fig. 4.11A illustrates a recording where three different AP classes could be distinguished. All recordings had in common, that spontaneous activity was never observed in any of the spike classes, or by inference, sensory cell units. Depending on the type of recording method, up to three different units were repeatedly identified when stimulating an individual hair. This identification was based upon the size and shape of the impulses and different response dynamics of the units. For further analysis, the spike shape was examined as described in chapter 3.3.4. This enabled a fast classification and

identification of the different action potentials (Fig. 4.11B). However, two cases had to be considered when applying the semi-automatic classification. Firstly, motor activity had to be excluded from the traces as this confused the automatic classification. Secondly, the classification was not very robust for small AP units, in particular when these were sometimes masked by larger units. On that account, the results of the spike shape analysis were confirmed by plotting different parameters of the identified spikes against each other, for example the best-fit (rising) slope was plotted against the peak-to-peak amplitude (Fig. 4.11C). This enabled fast detection of possible errors (wrongly identified or unidentified spikes) and following manual revision of the identification.

Another criterion that may be used to distinguish different sensory cells is their conduction velocity. Double recordings were used to determine the conduction velocities of the different units (see chapter 3.3.4). In all examined samples, the L-unit had the highest conduction velocity, while the S-unit was the slowest (Fig. 4.12A). The conduction velocities ranged from 0.7 to 1.8 m/s for the L-unit, from 0.4 to 0.8 m/s for the M-unit and from 0.3 to 0.5 m/s for the S-unit, as determined at room temperature (Fig. 4.12B).
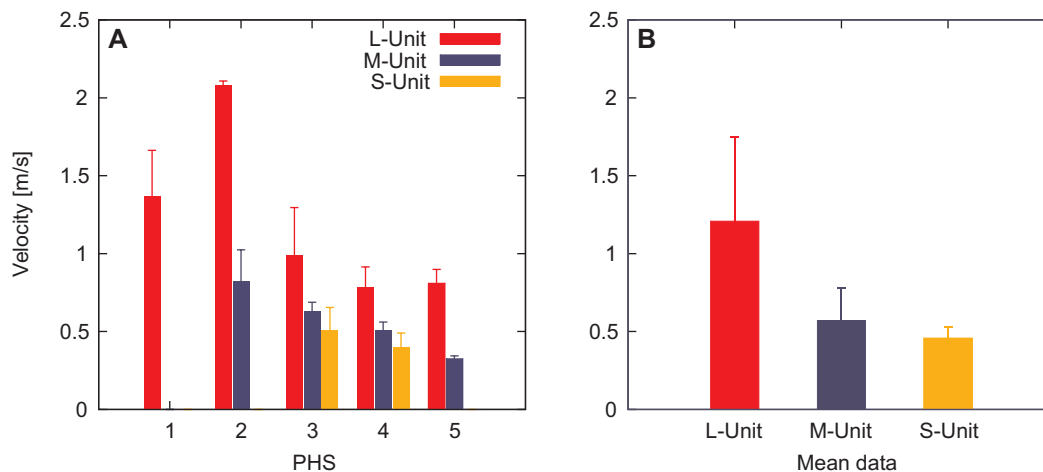

Fig. 4.12: Conduction velocities of different PHS units. **A** Measurements of five PHS are shown. The L-unit always showed the highest conduction velocity and the S-unit always the slowest conduction velocity. **B** Mean values of the different units. The L-unit ranged from 0.7 to 1.8 m/s, the M-unit from 0.4 to 0-8 m/s and the S-unit 0.3 to 0-5 m/s. The velocities were determined at room temperature (L-Unit: N=5, M-Unit: N=4, S-Unit: N=2 PHS).

4.3.1 Amplitude and time response characteristics

The L-, M-, and S-units showed different dependencies on the stimulus amplitudes (deflection amplitude, DA) and different response dynamics to sustained deflections (Fig.

4.11). Step stimuli with varying amplitudes and durations were presented to examine their responses (L-unit: N=15, M-unit: N=10, S-unit: N=2 PHS). These experiments showed that the L- and S-units responded to the dynamic part of a step stimulus (phasic behavior), while the M-unit also responded to sustained deflections (phasic-tonic behavior). A typical response to deflections of different amplitudes is illustrated in Fig. 4.13. Even at large stimulus amplitudes above 10°, the response of the L-unit terminated
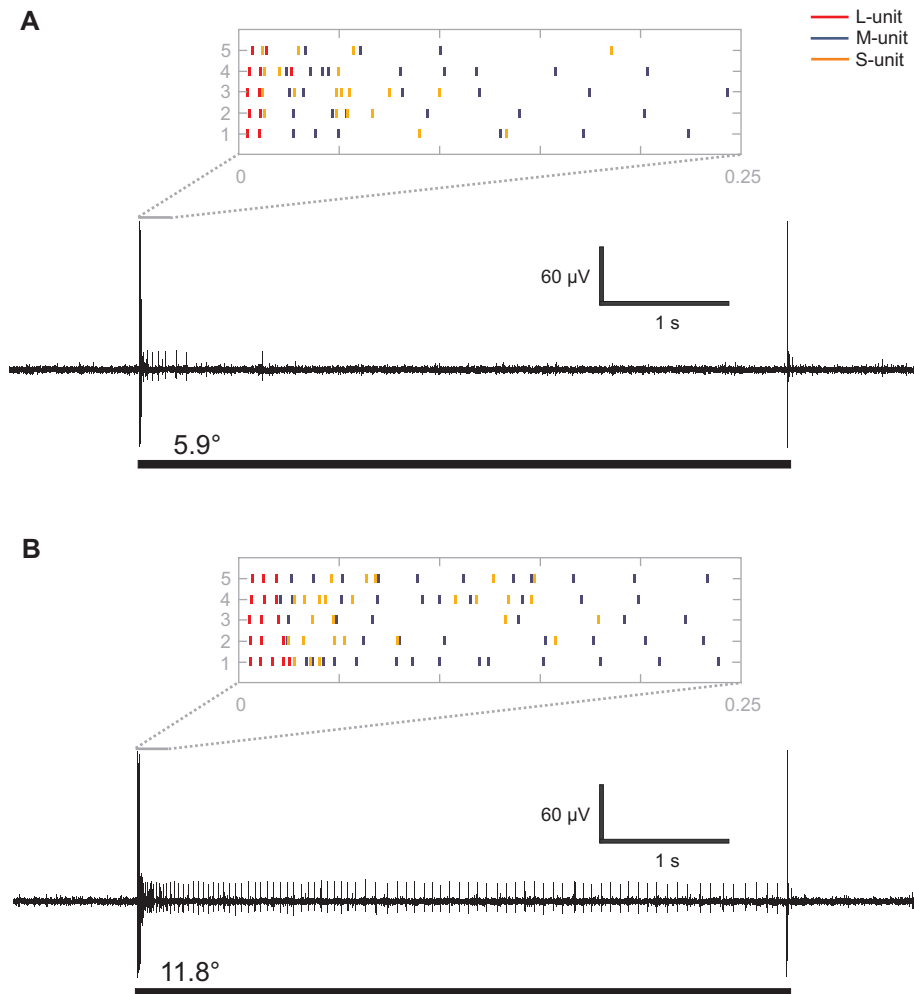

Fig. 4.13: Temporal characteristics of the PHS. The original traces and raster plots of five stimuli per deflection amplitude illustrate the responses of the L-, M-, and S-units of one PHS. Step stimuli with a 5 s duration were presented at deflection amplitudes of 5.9° (**A**) and 11.8° (**B**). While the L- and S-units showed phasic behavior, the M-unit showed a phasic-tonic response, with the response persisting throughout the duration of the stimulus at higher deflection amplitudes. The raster plots illustrate the first 250 ms after stimulus onset to display the phasic responses of the L- and S-units (L-unit: N=15, M-unit: N=10, S-unit: N=2 animals).

within the first 50 ms after stimulus onset and the response of the S-unit ceases within the first 250 ms. The stimulus offset led to similar, but overall weaker responses of these two units. In contrast, the M-unit responded to large deflections with activity that sometimes sustained a whole stimulus duration of 5 seconds. A comparison of the two stimulus amplitudes also shows that all units displayed a positive dependency of the response to the deflection amplitude (Fig. 4.13).

While the L- and the S-units responded to the dynamic part of a stimulus, the M-unit also responded to maintained deflection of a sensory hair. For an exemplary hair, this is illustrated in Fig. 4.14. The plotted example represents single stimulus presentations of three deflection amplitudes. The responses showed a high initial discharge frequency of up to 200 Hz which decreased over time. The M-unit showed a positive dependency on stimulus amplitude, higher amplitudes led to stronger and longer-lasting responses. This example is based on single stimulus presentations, values of mean frequencies will be presented in Fig. 4.17.
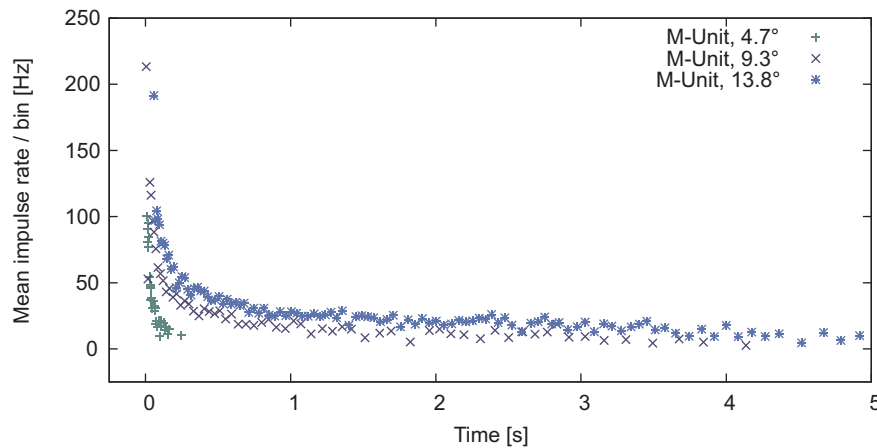
Fig. 4.14: Temporal response characteristics of the M-unit. The response of a M-unit recording of one PHS is shown, to step deflections of 5 s duration with different deflection angles. The data represents one stimulus presentation per amplitude. After an initial response with discharge rates of about 100-200 Hz, spike frequency decreases fast.

Fig. 4.15 illustrates the amplitude response of the L- and M-units of a representative PHS. The L-unit only responded with a few spikes to stimulus onset and offset. Beyond deflection amplitudes of about 10°, the spike discharge saturated at a level of about 4-8 impulses. Overall, the response to stimulus onset was more pronounced, with maximum discharges around 5 impulses, while release from a deflection elicited weaker discharges of up to 1-2 spikes. The S-unit activity was similar but somewhat prolonged for the ON-response (Fig. 4.15). However, due to their similar response properties, activity of the S-unit was always masked by discharges of the L-unit (Fig. 4.15B). Nevertheless, the

S-unit also seems to respond to the dynamic part of a stimulus, similar to the L-unit, but with a slower decline of activity.
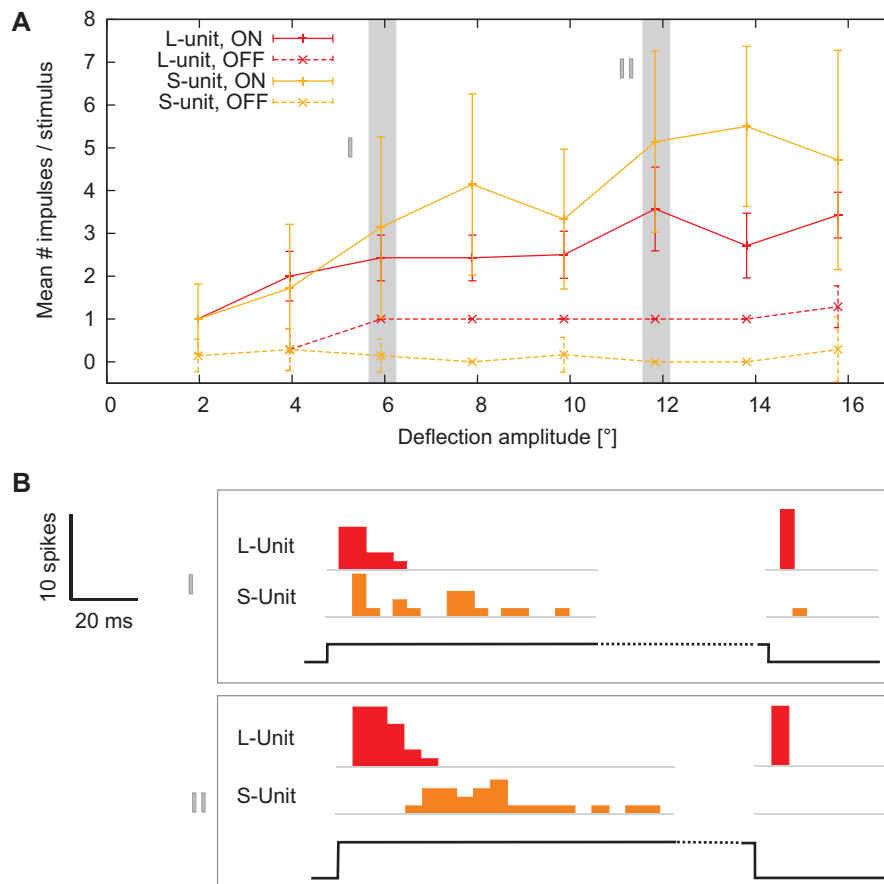

Fig. 4.15: Temporal characteristics of the L- and S-units. The responses of the L- and S-units of one PHS to step deflections of 5 s duration and different amplitudes is shown. **A** The spike discharge is plotted versus deflection amplitude (7 repeats / DA). **B** Spike histograms of L- and S-unit discharges are displayed for two stimulus amplitudes of *A*, *I* and *II*. The bottom trace represents the stimulus (5 ms bins; 7 repeats / DA). The L-unit typically responds to the dynamic portion of the stimulus with up to 4-8 impulses. The response to the deflection is more pronounced than the response to the release. The S-unit exhibits a phasic response, although with a somewhat slower decline. Due to their small size in the recordings, activity of the S-unit was often masked by L-unit activity.

For further analysis of the amplitude characteristics, three different parameters were examined – mean number of spikes per stimulus, mean frequency and maximum frequency (Fig. 4.16). An analysis of the responses of one exemplary PHS indicates a positive dependency of these parameters on stimulus amplitude. The L-unit increased the number of spikes to less than 10 responses, its mean impulse rate increased from 100-150 Hz to 150-200 Hz. The maximum impulse rate was slightly higher than the mean

impulse rate. However, the deviations between single stimuli with the same amplitude were high in comparison to the changes by variation of the amplitudes (Fig. 4.16). The M-unit response indicated a different behavior. The response increased up to a number of 100 impulses per stimulus for a step stimulus of 5 s duration. The saturation at higher amplitudes was also caused by the M-unit responding throughout the whole stimulus. The mean impulse rate, representing the M-unit impulses between 1 and 2 seconds after stimulus onset, increased slightly from about 5 Hz to 20 Hz. The maximum impulse rate was not evaluated as M-unit activity of the first 50 ms was masked by activity of the L-unit, especially at higher amplitudes (Fig. 4.16).
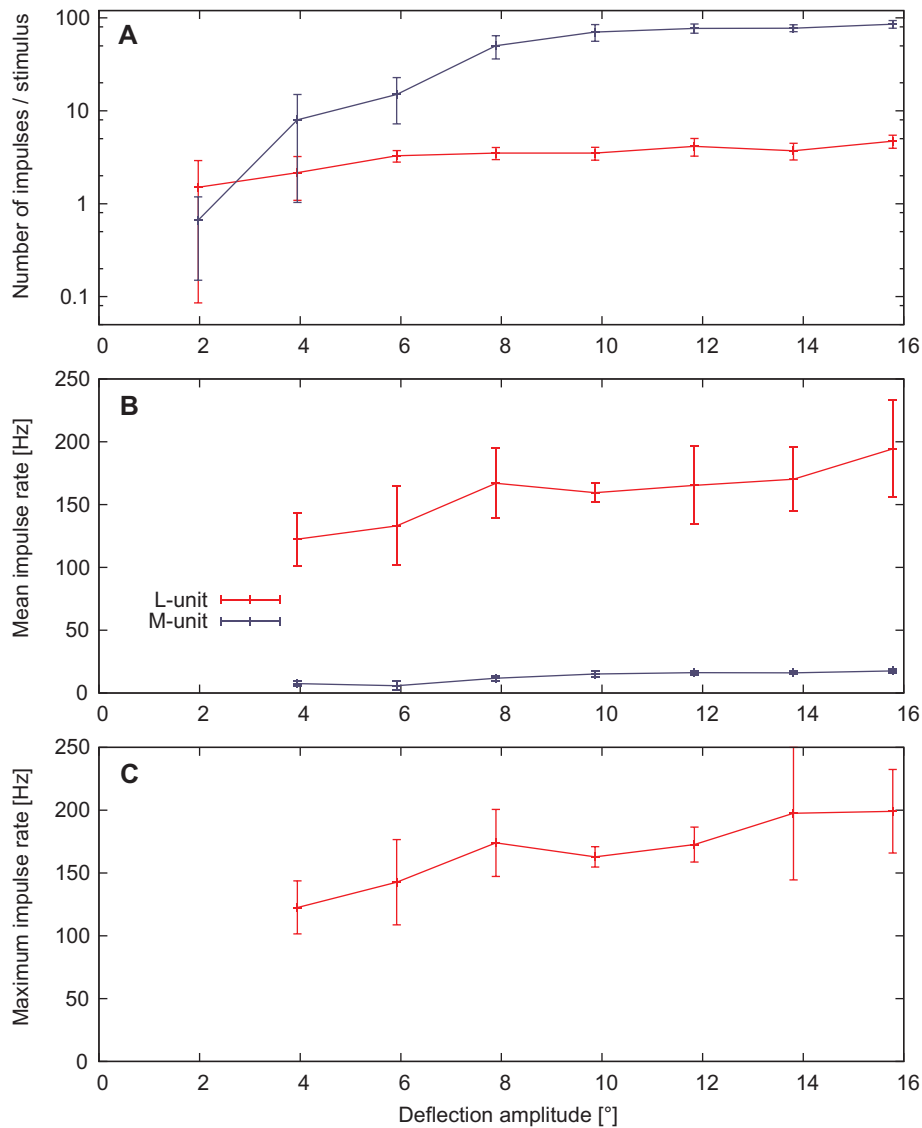
Fig. 4.16: Amplitude response characteristics. One example of a PHS (L- and M-units) to changes in deflection amplitudes is shown. Three parameters were plotted against the deflection amplitude to characterize the responses. **A** Number of impulses per stimulus. The y-axis is plotted on logscale as the M- and L-units show more than a 10fold difference in their total impulse numbers. **B** Mean impulse rate per sample. For the L-unit, the mean impulse rate was measured from total activity per sample. For the M-unit, only responses between 1 and 2 seconds after stimulus onset were used to calculate a mean rate. **C** The maximum impulse rate was averaged over the samples and plotted. As the first APs of the M-unit are hidden by activity of the L-unit, especially at higher amplitudes, only the data of the L-unit is shown (N=5-10 samples / stimulus amplitude).

Comparison of different PHS

In general, the response characteristics of the L- and M-units of most PHS were similar. The experiments suggest that the amplitude threshold of all units is approximately 1°. Stair stimuli and stair stimuli with sine-modulation (see chapter 3.4.2) confirmed that both units (L, M) not only respond to deflections from an undeflected position but also respond to changes in deflection from deflected positions. As already seen in the OFF-responses of the L-unit, they are also capable to detect decreases of deflection. The discrimination threshold from different pre-deflected positions was not examined in detail.

A comparison of the M-unit responses shows that the initial discharge frequency was around 150 Hz and decreased over time to below 10 Hz (Fig. 4.17). This decrease was linear in a double-logarithmic plot, indicating that the phasic response component follows a power function (general form $f(x) = ax^k$). Higher stimulus amplitudes led
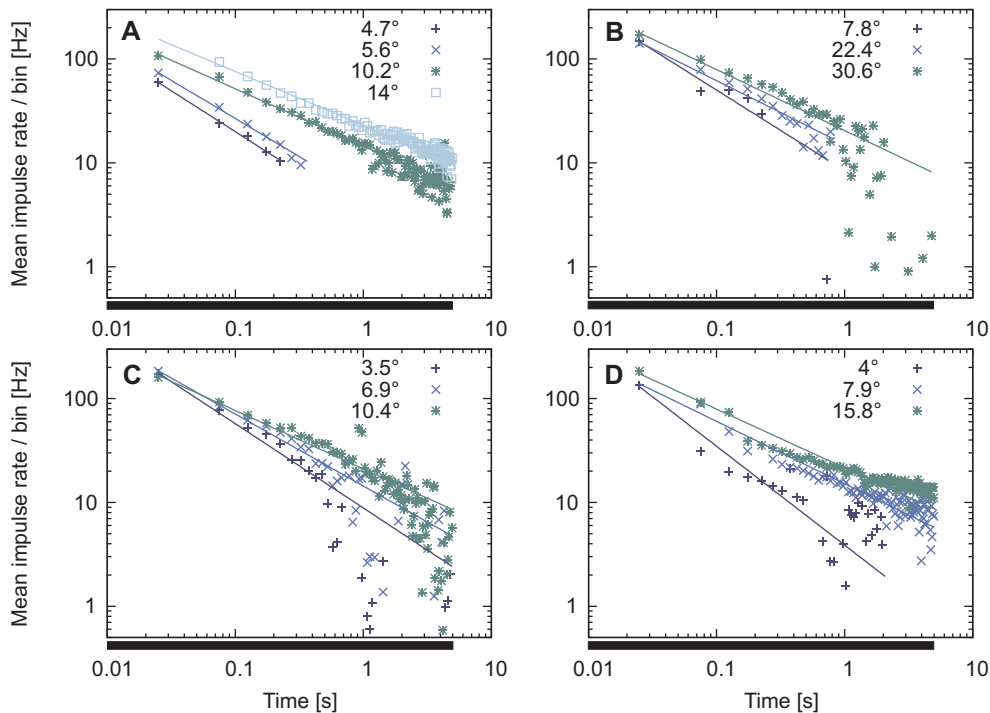

Fig. 4.17: Comparison of M-unit responses. **A-D** Four examples of M-unit recordings are shown. They illustrate the responses to step deflections of 5 s duration with different deflection angles (samples per stimulus: **A**: 7, **B**: 5, **C**: 10, **D**: 5-10). The mean impulse rates were calculated in 50 ms bins. All examples show an initial response with discharge rates of around 150 Hz and a following decrease in spike frequency according to a power function (note logarithmic scales on axes). However, initial discharge frequencies at the highest deflection angles are only rough values since spikes of the M-unit were often masked by activity of the L-unit. The black bars indicate the duration of the step stimuli.

to stronger and longer-lasting responses of the M-unit. Depending on the deflection amplitude, mean frequencies of 10-20 Hz were still observed 4-5 s after stimulus onset (Fig. 4.17).

The number of impulses per stimulus was chosen as a measure to compare different L-unit responses (Fig. 4.18). Common to all experiments was the fast decline of the responses within the first 50 ms after stimulus onset. The comparison shows that at a deflection amplitude of about 6-10°, the L-unit responses saturated at a level depending on the individual PHS, ranging from an average of 2-3 spikes per stimulus to 6-8 spikes per stimulus. However, these differences also occurred if the amplitude measurements were conducted at the beginning of an experiment. Therefore, adaptation caused by the continued presentation of stimuli during the experiments can probably be excluded.
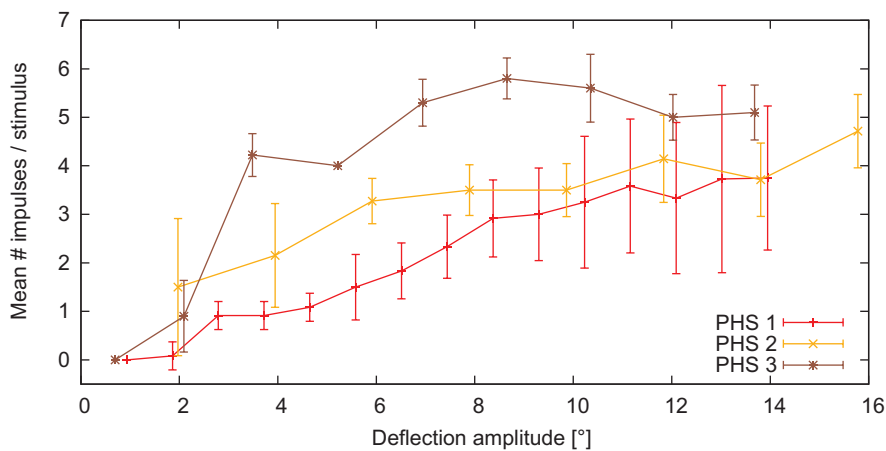

Fig. 4.18: Comparison of L-unit responses. For three different PHS, the mean number of impulses per stimulus is plotted against the deflection amplitude. The responses start to saturate with 2-8 impulses per stimulus at an amplitude of 6-10°.

The latency of the L-unit saturated beyond deflection amplitudes of 8-14 degrees, with latencies reaching a minimum of 2.5-7.5 ms including the conduction time (Fig. 4.19). Latencies of 1-2 ms or even less can be estimated if average conduction velocities and distances between recording sites and sensilla are assumed.
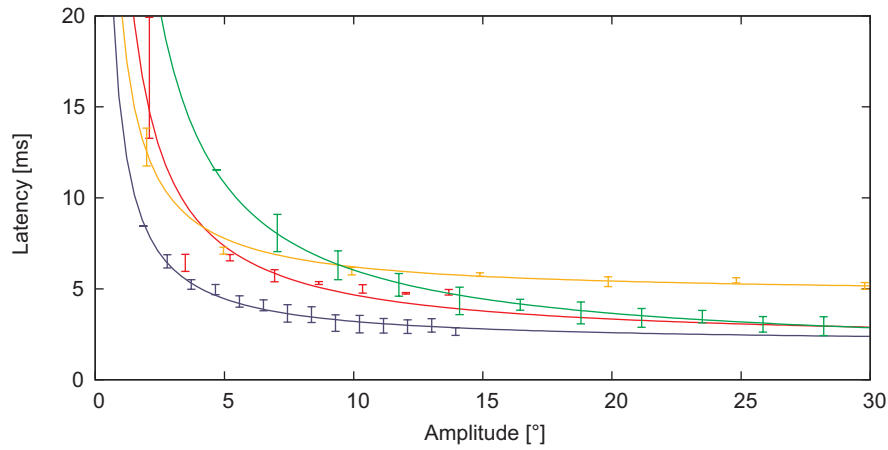

Fig. 4.19: Relative latencies of the L-units. The response time (latency) of 4 PHS is plotted against the deflection amplitude. The latencies start to saturate at amplitudes between 8° and 12°. The absolute delay was estimated to be 1-2 ms or even less, as the latencies were measured without further examination of conduction velocities or distances between recording sites and the sensilla.

M-unit variability and number of AP classes

In comparison of all experiments, the M-unit showed most variability in its responses with regard to the time characteristics. Although the previously described behaviors applied for most experiments, some experiments showed that the M-unit responses to large stimulus amplitudes ceased after 1-2 second following stimulus onset. It is not clear, whether this was caused by different adaptational states of the respective M-units or whether several units with extremely similar amplitudes possessed similar behaviors.

Fig. 4.20 illustrates the single experiment where more than three distinct units could be measured. Especially the medium sized units (2) and (3) could both be M-unit like types while the largest and the smallest showed typical L- and S-unit responses. However, this experiment has to be regarded with care; e.g. the assumed L-unit amplitude was not as pronounced as in usual experiments. Nevertheless, this example is an indication that there are possibly more than three different, electrophysiologically active units.
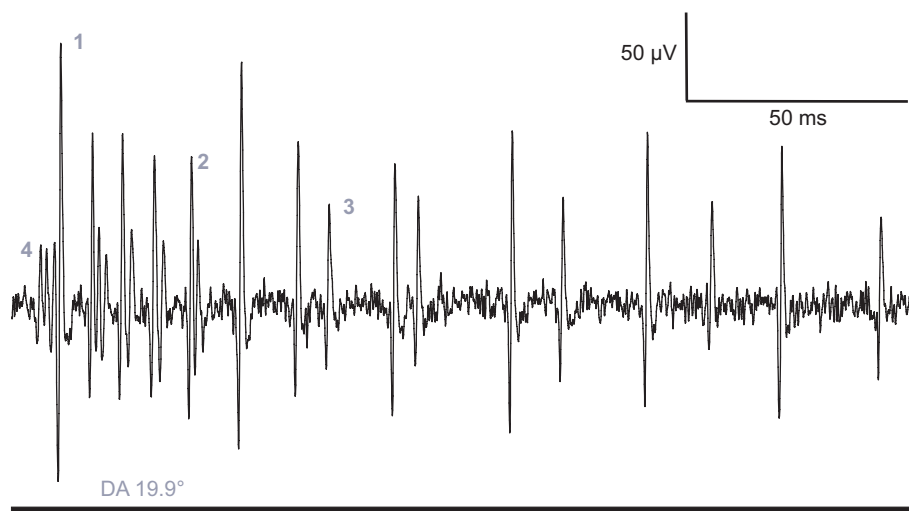

Fig. 4.20: Example of a single measurement with more than three units. This example illustrates the single experiment where more than three different units could be recorded at stimulation of a single PHS. About the first 250 ms of a step stimulus with 19.9° DA are illustrated. Unit (1) is assumed to be a L-unit, unit (4) is probably a S-unit and units (2) and (3) showed M-unit like behavior. However, this represents a single experiment, conducted using recording method 3, the pectine preparation.

4.3.2 Velocity response characteristics

Ramp and ramp-and-hold stimuli with varying durations, amplitudes and ramp-speeds were applied to investigate whether the responses of the L- and M-units showed different dependencies on stimulus velocity (L-unit: N=8 animals, M-unit: N=5 PHS). According to the analysis of the amplitude characteristics, the parameters mean number of impulses

per stimulus as well as mean and maximum impulse rates were plotted against stimulus velocity. Fig. 4.21 illustrates the dependency of these parameters on the stimulus amplitude for a representative PHS.
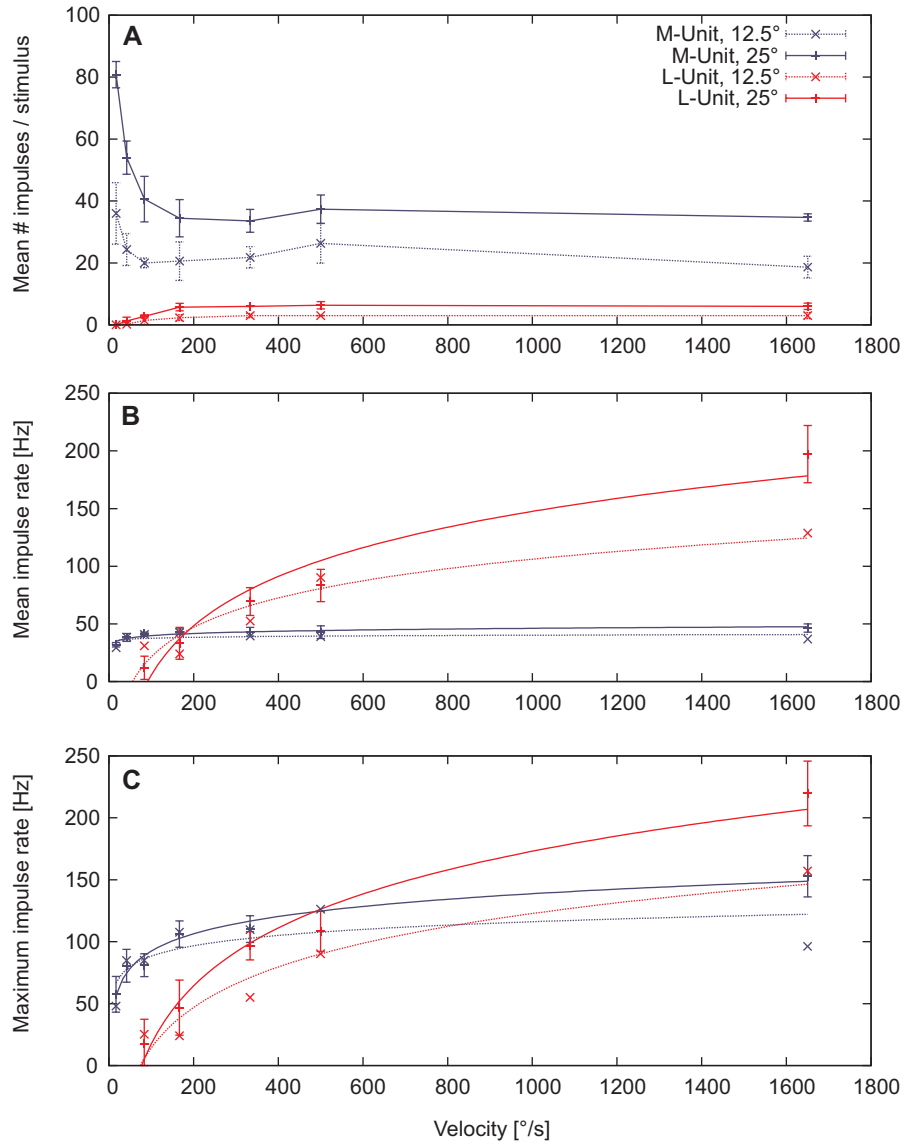

Fig. 4.21: Velocity response curve of a single PHS. L- and M-units show different responses with regard to the angular velocity of a ramp (and-hold) stimulus. Different thresholds and working ranges of the L- and M-units are discernible. Different parameters are plotted against the angular velocity for two different deflection amplitudes. **A** Mean number of impulses per stimulus (±SD). **B** Mean impulse rate (±SD). **C** Maximum impulse rates (±SD), the maximum of each sample was used to calculate a mean value. For better visibility, only the standard deviations of the 25° deflection amplitude are shown. Each stimulus was delivered 3-7 times (N ≈ 5 samples per stimulus).

Especially the mean and maximum frequencies seem to be a good measure of the relation between the responses and the stimulus velocity. The velocity threshold for the M-unit was between 2 and 5 °/s while the L-unit started responding beyond velocities of 50-100 °/s. The working range, defined as the range of angular velocities which is coded by changes in impulse frequencies, covered velocities of 2 to 500 °/s for the M-unit and 50 to 2500 °/s for the L-unit. Saturation occurred at velocities above these working ranges, at maximum impulse rates of 150-200 Hz for the M-unit and 200-250 Hz for the L-unit (Fig. 4.22). However, these values also depended upon the stimulus amplitudes.
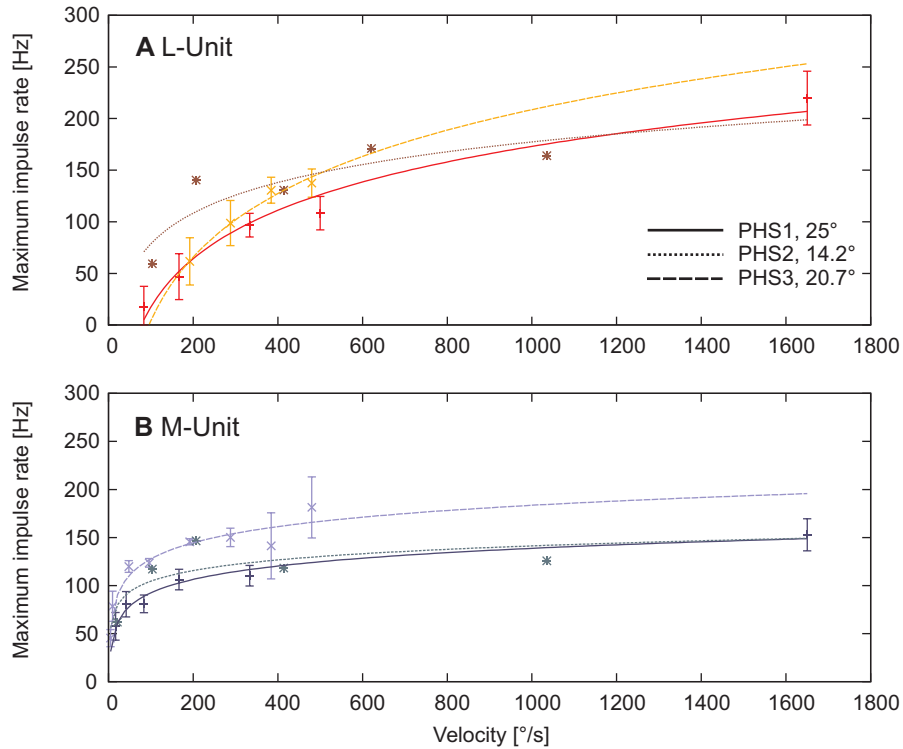

Fig. 4.22: Comparison of velocity response characteristics. Most examined PHS showed similar response characteristics in reference to the angular deflection velocity. Three representative examples (PHS1-3) are compared with regard to the responses of their L- and M-units by plotting the maximum impulse rate against the angular velocity. **A** Comparison of L-units. **B** Comparison of M-Units (samples per stimulus: PHS1, N=5; PHS2, N=10; PHS3, N=10).

4.3.3 Frequency response characteristics

Working ranges corresponding to those noted for ramp stimuli were observed with the application of sinusoidal stimuli (see chapter 3.4.2). The different characteristics of the L- and M-units are illustrated in a frequency response diagram (Fig. 4.23), plotting response amplitude (number and density of spikes per stimulus cycle converted into a mean

response vector, see chapter 3) and response phase against stimulus frequency. Corresponding to its phasic-tonic response to ramp and step stimuli, the M-unit answered sinusoidal stimuli down to very low frequencies indeed, with a frequency threshold certainly below 0.1 Hz. The response of the M-unit declined sharply between 10 and 50 Hz, with best responses below 10 Hz. Above 10 Hz, this unit responded with just one spike per stimulus cycle and exhibited a pronounced phase delay. The L-unit, by contrast, did not respond to stimuli below 1 Hz, with the threshold in the range between 1 and 5 Hz, but covered frequencies of 100 Hz and above. At frequencies above 20 Hz, only 1-2 impulses were produced per stimulus cycle.

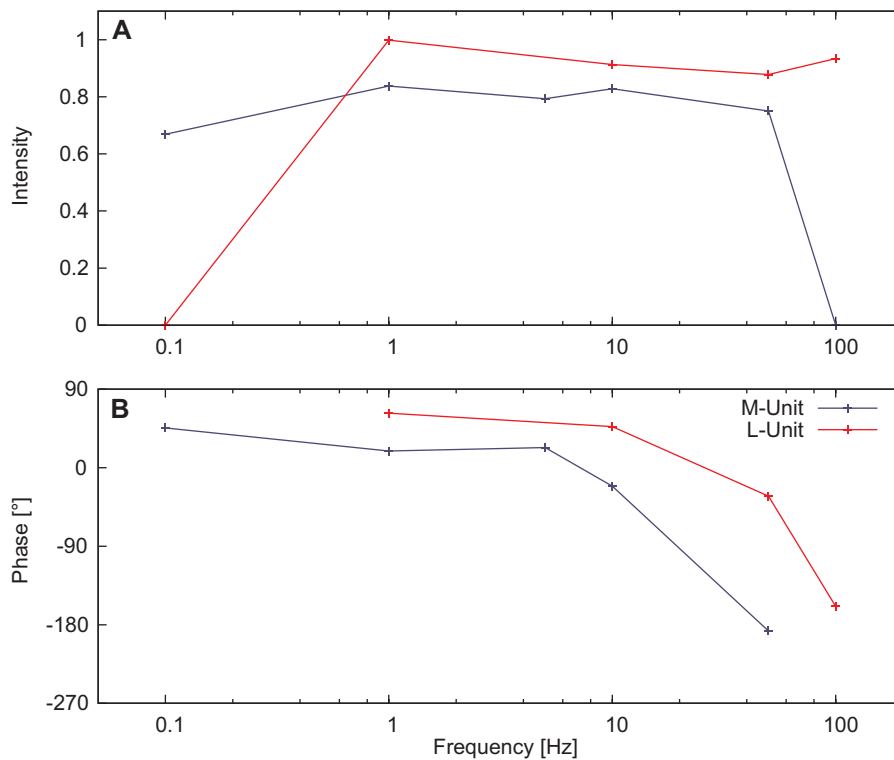**Fig. 4.23:** Frequency response characteristics. **A** plots the intensity (length of the mean response vector, see chapter 3.3.4) and **B** plots the relative phase in reference to the deflection maximum (phase 0°) against stimulus frequency. The deflection amplitude of the example was 11°, each data point represents the mean value of 4 stimulus presentations at 0.1 Hz and up to 150 at higher frequencies (N=4 PHS).

Fig. 4.24 illustrates the scattering of the impulses for three different frequencies. At low frequencies (1 Hz), the M-unit responded with several impulses per cycle while the L-unit responded only with a few. However, the M-unit responses decreased with increasing frequency showing only a few, scattered responses at higher frequencies (50 Hz), while the L-unit still responded rather continuously with at least one spike per second.
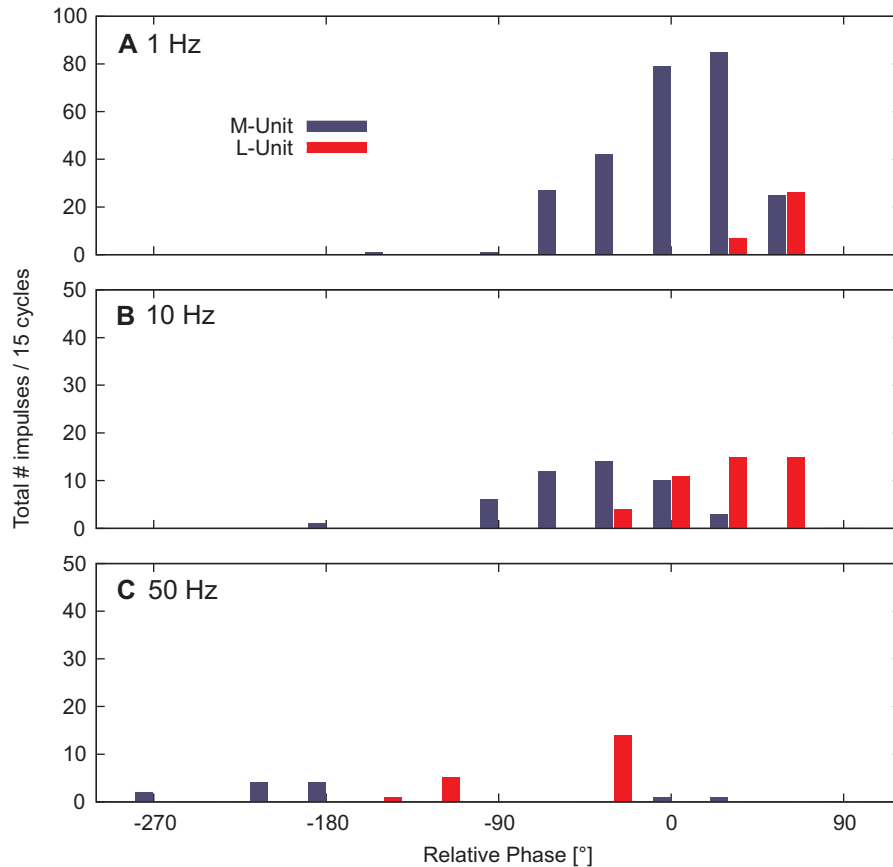

Fig. 4.24: Frequency response histogram. The response of the L- and M-units to sinusoidal stimuli are presented. Stimulus frequencies of 1 Hz, 10 Hz, 50 Hz are compared. The diagram shows the total number of impulses of 15 stimulus cycles, plotted against mean phase. The relative phase is plotted in reference to the deflection maximum (this plot shows the same PHS as Fig. 4.23) (N=4 animals).

4.3.4 Directional characteristics

Directional selectivity is an important characteristic of cuticular sensilla such as the PHS. For a variety of sensilla, directional selectivity has been shown (e.g. filiform hairs of cockroaches or spider trichobothria). Ramp and ramp-and-hold stimuli were applied to test the directional characteristics in the responses of the different units of a single

PHS. The results indicate that a least the L- and M-units of the PHS show broad directional tuning (Fig. 4.25). This broad directional sensitivity is reflected by small mean response vector lengths, ranging from 0.2 to 0.6. Nevertheless, the maximum response in the preferred direction was clearly larger than in the opposite direction. The directional tuning of the two units in a given sensillum was found to be similar (Fig. 4.25A-C), and the directional tuning was not dependent on stimulus amplitude as the overall response equally increased to deflections in each direction (Fig. 4.25D).
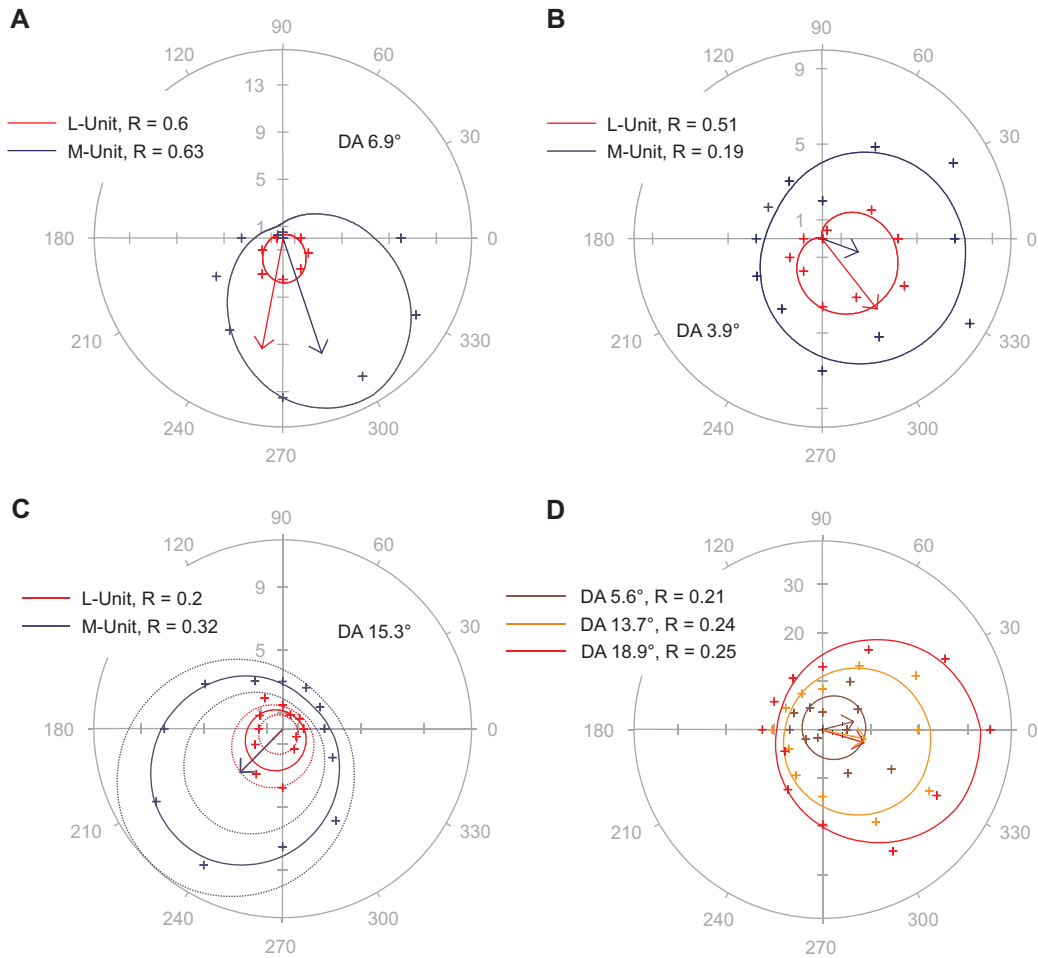

Fig. 4.25: Directional response characteristics of the L- and M-units. **A-D** show polar plots of individual sensillum responses. The mean number of impulses per stimulus is plotted as the polar distance. The polar angle on the horizontal plane is defined as the angle to the frontal ridge (0°) of the pectine. The data points represent mean numbers of impulses per stimulus and per direction, the solid lines show the cardioids calculated from these data. Dotted lines in *C* indicate standard deviations. **A-C** show three typical samples of directional responses. **D** illustrates L-unit responses for three different deflection amplitudes, recorded in one sensillum. The arrows indicate the mean response vectors that were calculated from the directional responses (number of experiments L-Unit: N>50 animals, M-Unit: N=15 animals).

From other sensilla, microphones or antennae, different characteristic curves are common to describe the directional tuning (e.g. omnidirectional, figure eight or cardioids). For a more detailed analysis of the relationship between stimulus direction (Θ) and response as well as comparison with other types of sensilla, the L-unit data from 40 experiments were compared. Their responses were normalized for each sample to a range between 0 and 1, their individual preferred direction was set to zero and finally, all data were plotted into one diagram (Fig. 4.26). A cardioid function of the form

$$R(\Theta) = \frac{1 + \cos(\Theta)^z}{2^z} \tag{4.1}$$

was fitted to the data, with z representing the broadness of the directional tuning. The best fit was achieved with z = 1.69 (R^2 = 0.46). Therefore, the directional tuning of the L-unit is slightly narrower than a standard unidirectional cosine (z=1) (Fig. 4.26). Overall, the results suggest a directional sensitivity of the PHS.

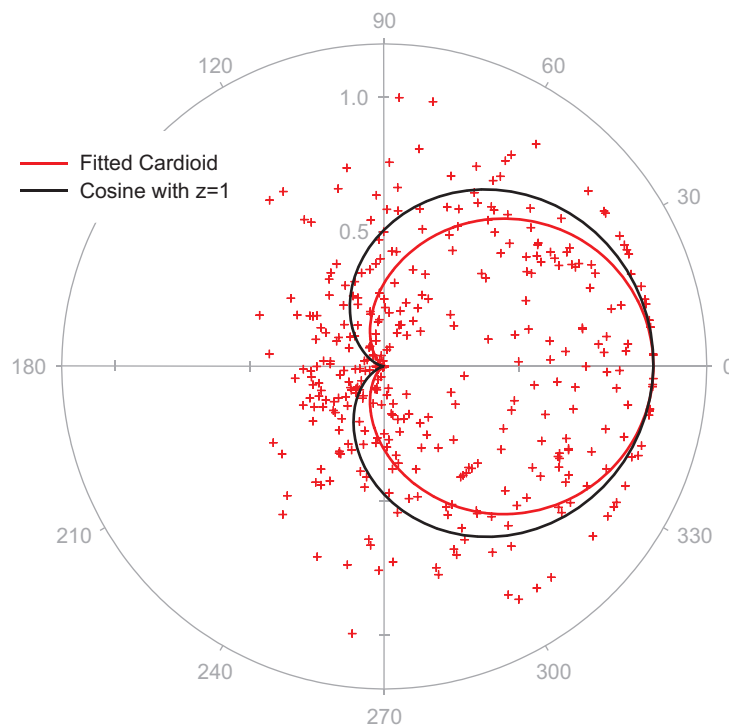**Fig. 4.26:** Cardioid fit of the directional response characteristics. The plot shows the pooled response of 40 different L-unit samples. The stimulus direction is normalized to the preferred direction (0°) and the response is normalized to values between 0 and 1 (angular axis). The red curve represents the fitted cardioid ($R(\Theta) = \frac{1+cos(\Theta)^z}{2^z}$) with z=1.69, the black curve shows a cosine with z=1 for comparison.

4.3.5 Possible role of the pectinal hair sensilla for reflex behaviors

While stimulating a single PHS in restrained but otherwise intact animals, it was often observed that part of the pectine or the whole pectine twitched; sometimes the animal started fighting against the immobilizing bonds. These behavioral responses were characterized and confirmed by several observations.

1. Double recordings from the main pectine nerve revealed that with a delay of 5-15 ms, sensory impulses were followed by motorneuron impulses coming from the cephalothoracic mass. The conduction velocities of the motorneurons were approximately 0.5-0.7 m/s and always lower than the conduction velocity of the L-unit (0.7-1.8 m/s) (Fig. 4.27A,B).

2. Recordings from the bases of the pectines in restrained animals showed that stimulation of a single PHS and resulting generation of sensory impulses (observed in the L-unit) elicited reflexive muscle potentials. The delay between sensory and motor activity was approximately 50 ms (Fig. 4.27C). This is explainable by the conduction velocities and the relatively long distance (up to 3 cm) between the hairs and the cephalothoracic mass.

Although these are only preliminary data, they suggest a role of the PHS for reflexive pectine movements and perhaps for lifting the whole body.
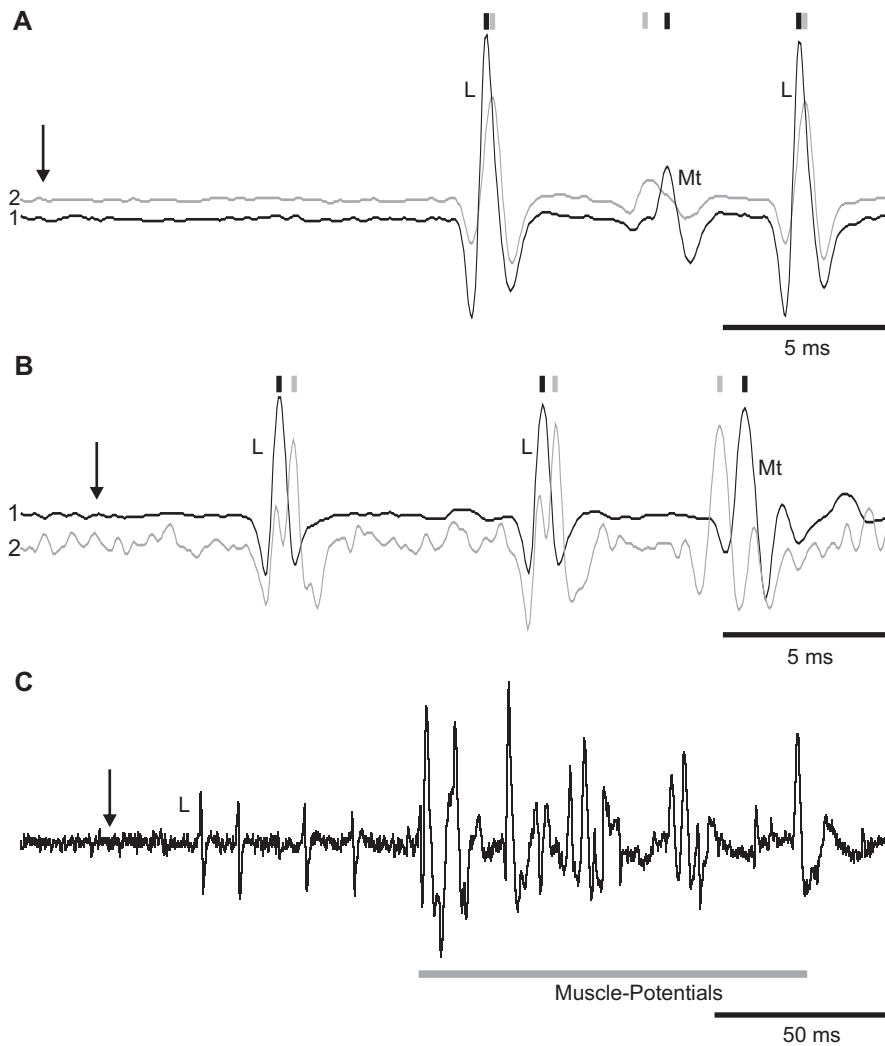
Fig. 4.27: Timing of sensory and motor activity. Three examples are presented for the timing between sensory activity, due to the stimulation of single PHS, and reflex motor activity. **A**, **B** show double recordings from the main pectine-nerve (see chapter 3, method 4). From the direction of the impulses, L-unit responses (L) and motor neuron spikes (Mt) can be distinguished. Although the exact timing depends on the distance of the recording site to sensillum and cephalothoracic mass, the first sensory spike is measured 5-15 ms after stimulus onset and motor activity follows 5-15 ms after the first sensory spike. **C** shows a recording from the pectine base (measuring activity in the pectine nerve as well as muscle-activity, method 1) in a restrained, but otherwise intact animal. 20 ms after stimulating a single PHS, the first sensory impulse is measured which is followed after approx. 50 ms by motor-activity.

Part II

Modeling cuticular mechanoreceptors

Chapter 5

Introduction - Arthropod mechanoreceptors as models in biology and engineering

This chapter provides an introduction into mathematical and physical modeling with an emphasis on models of cuticular mechanoreceptors of arthropods. After introducing modeling as a tool for biological research, the main reasons for the construction of a biomimetic mechanosensor are described. A general model of arthropod mechanoreceptive hairs is presented, physical modeling of cuticular hairs is outlined and transducer designs for tactile sensors are examined with an emphasis on fiber optic methods. Finally, examples of already existing biomimetic models are described.

In many scientific contexts, models are one of the principle tools. This general use as a major instrument has led to a complex terminology, where different types of models are classified in various ways (e.g. idealized models, scale models, phenomenological models, ...). The importance of models has also led to increasing attention in philosophy about the general nature of models and modeling (e.g. How does a model relate to reality?) or how new insights can be gained by the use of models (Frigg and Hartmann, 2006). An interesting survey of the scientific basis of models and modeling with regard to biorobots as models of biological behavior is presented by Webb (2001).

In this thesis, models are considered as tools to test hypotheses about mechanisms underlying biological processes. They are used to generate predictions about biological systems that can ideally be tested by comparison with measurements on real organisms. Two basic types of models are distinguished:

- **Mathematical models:** The use of equations that abstract basic principles of the target system. This can involve analytical examination and/or approximation

with numerical methods. The Hodgkin and Huxley (1952) model of the ionic mechanisms of action potential initiation and propagation in the squid giant axon is a typical example of a widely recognized mathematical model. If the models become more complex, they often require numerical methods and the use of computers. Then, the terms **computer model** and **computer simulation** are used.

- **Physical models:** Physical models, also referred to as **technical models**, involve a 'real-world' implementation. Like mathematical models, they require simplifications and abstraction. Equivalent circuits of nervous membranes are typical examples of physical modeling in a biological context. The most ambitious types of physical models in biological research can probably be found in biorobotics that aim to represent animal behavior.

There are probably two main reasons why physical modeling is sometimes preferred over mathematical modeling and computer simulation. The first reason is that animals represent **embodied systems**[1], i.e. they are part of, and intricately coupled to the environment. The second reason is that the physical nature of the environment surrounding an animal can be very complex and difficult to simulate. Therefore, simulations have the risk to neglect important parameters by simplification. Physical models as implementations in the real world try to solve this problem by eliminating the environmental simulation.

These two reasons illustrate why physical models – and especially biorobotics – are increasingly applied in neuroethology. However, there are also drawbacks to the application of physical models. They also require simplifications and abstraction, therefore they are also susceptible to misinterpretations. Furthermore, they can be expensive, require long development cycles and may fail for pure technological reasons and not for erroneous assumptions about the biological system that is modeled (Chiel and Beer, 1997).

Building technical devices that are physical models of biological systems is not only of interest to biology but also to engineering that can benefit from various, often ingenious solutions found in nature (Barth, 2003). Depending on the point of view, this area of research is often termed **Technical Biology**, **Bionics** or **Biomimetics** (Barth, 2003). This can lead to the quite confusing situation that a physical model is termed **biomimetic** or **bio-inspired**, but is of no use for the generation of new hypotheses about the biological system it was built to mimic (Chang, 2001, in the context of biorobotics). Therefore, the **biological relevance** has to be specified.

---

1 Embodiment is a concept applied in robotics and artificial intelligence, claiming that an autonomous agent (robot, neural network) has to be intimately coupled to the environment and that it also has to be part of the environment to achieve levels of complexity which can be compared to biological systems.

Webb (2001) suggests a framework for such a characterization of models, consisting of 7 dimensions:

1. **Accuracy:** To what extent do mechanisms of the model reflect mechanisms of the biological target?

2. **Biological relevance:** Is the model able to generate new hypotheses or does it predict behavior of the biological system?

3. **Generality:** How many biological systems does the model represent?

4. **Abstraction:** How many details of the biological target are included in the model?

5. **Medium:** What materials were used to implement the model?

6. **Level:** What level of the biological system is modeled? (e.g. chemical processes, neural networks, ecological processes, ...)

7. **Behavioral match:** How well does behavior of the model correspond to behavior of the biological system?

There are reasons to believe, that biorobotics has the potential to become a powerful tool for the analysis of animal behavior and the underlying processes (see Webb, 2001). However, although engineering has benefited from biological inspiration, only a few examples exist where the opposite is the case (Niebur et al., 2001). The reasons are manifold, e.g. biorobotics is a relatively new field, the development of models is often more expensive and tedious than the implementation of computer simulations, they lack standard materials and every model has to be developed from scratch (Niebur et al., 2001). Furthermore, roboticists sometimes too easily conclude a biological relevance from the performance of their robots (Chang, 2001; Delcomyn, 2001; Selverston, 2001).

The lack of standardized tools and modules (Niebur et al., 2001) as well as components that do not possess the properties of biological counterparts (e.g. sensor or muscle properties) are probably two of the main hindrances for the recognition of biorobotics as an important tool.

This study attempts to cross the bridge between biology and engineering by constructing a biomimetic tactile sensor that mimics the response characteristics of the previously examined mechanoreceptive hairs of scorpions. One objective of the design is that the functional mechanics of the biological sensillum are closely copied. The artificial sensillum has to be deflected in a way similar to the biological counterpart. Instead of a mechano-neural transduction, the rotation of the hairshaft is transduced with a technical method. Important guidelines for the design of the biomimetic tactile sensors are appropriate scaling, an analog transduction process and possible use of biological components.

5.1 Basic models of arthropod sensory hairs

Modeling can be conducted on different levels of analysis. With regard to arthropod sensory hairs, it is possible to model transduction processes on the molecular level up to behavioral-ecological processes. A plethora of studies on cuticular hair sensilla of arthropods exists. These studies include many aspects, ranging from the molecular level, ultrastructural analysis, electrophysiological response characteristics or behavioral functions to evolutionary considerations. In the context of this thesis, only studies concerned with modeling structural aspects of arthropod mechanoreceptors are presented (as these are of relevance for the attempt to construct a biomimetic sensor).

In cuticular mechanoreceptive hairs, two basic types of sensors can be distinguished (see Fig. 5.1): **medium flow sensors** (e.g. trichobothria, filiform hairs) and **touch sensors** (various bristles). While considerable amount of research was performed about the physical parameters that influence medium flow sensitive hairs, only a few studies have considered the physical parameters of touch sensitive hairs (Dechant et al., 2001).

One of the most simple models that can describe cuticular hairs is a lever. The outer lever arm represents the hairshaft that rotates around a pivot point located in the socket. Rotation of the inner lever arm, which is a hundredfold shorter than the outer lever arm, elicits nervous activity. A better simple model to describe cuticular hairs is the damped harmonic oscillator (*restoring force+damping force=hair-mass* x *acceleration*).

Fig. 5.1 illustrates a more elaborated model of sensory hairs (based on a damped harmonic oscillator) that includes several mechanical parameters of the hairshafts and the sockets (Barth and Dechant, 2003). Here, the hairs with length L and diameter $d(L)$ are suspended in a socket represented by its damping constant R and its spring stiffness S. The socket resists deflections of the hairshaft and restores the hair to its initial position after a deflection.

In Fig. 5.1A, a medium flow sensitive hair (e.g. trichobothrium) is shown. The hair is deflected by drag forces along the whole hairshaft. For example, these drag forces are caused by air currents. These hairs work in the boundary layer of the cuticular surface. Therefore, the optimal stimulus frequencies depend on the hairlenghts, with shorter hairs having higher optimal frequencies (Barth, 2000). In response to air currents, the hairshafts become deflected like rigid rods, with restoring constants of the sockets in the range of 10^{-12}-10^{-14} Nm/° (Barth, 2000). Therefore, the mass of the hairshaft and its torsional inertia are the main parameters that influence their mechanical behavior (Barth and Dechant, 2003).

Touch sensitive hairs are illustrated in Fig. 5.1B. The force acting on the hairshaft not only leads to deflections of the hair, but also to considerable bending of the shaft (Dechant et al., 2001). This is caused by higher elastic restoring constants of the sockets than in medium flow hairs, with values in the order of 10^{-8}-10^{-9}Nm/° (Albert et al., 2001;
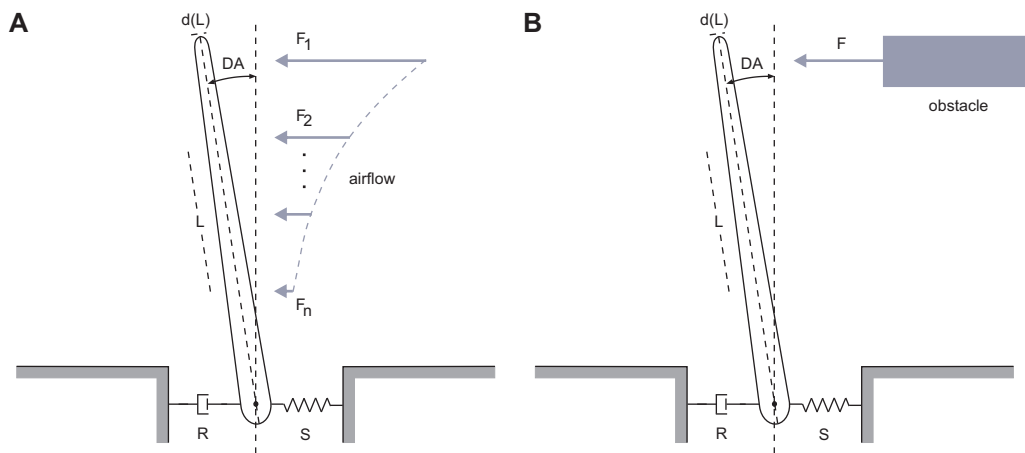
Fig. 5.1: Schematic models of arthropod mechanoreceptive hairs. **A** Medium flow sensitive hair. The hair is deflected by drag forces (F_1,...,F_n) along its hairshaft. **B** Tactile hair. An obstacle that is moved against the hair produces a force F that leads to hair deflection. Deflection amplitudes DA, hairlength L, hair diameter as a function of length $d(L)$, damping constant R, restoring constant S (modified figure, based on Barth and Dechant, 2003).

Barth et al., 2004). Furthermore, the external forces that deflect the hair are generally larger. Major biomechanical parameters that influence the behavior of a tactile hair are Young's modulus and the second moment of area along the hairshaft (Dechant et al., 2001; Barth and Dechant, 2003).

Mathematical models of touch-sensitive hairs become complicated, as non-linearities (e.g. the shapes and mass-distributions of hairshafts) and large deformations of hairshafts and sockets have to be considered. Therefore, these models can not be solved analytically and require the use of numerical methods. The most advanced model of arthropod tactile hairs is probably described by Dechant et al. (2001). This model applies a finite element method to discretize the problem and enables calculation of hairshaft bending with regard to shape and material properties of the hairshaft and the socket.

In addition to the basic models that describe cuticular hairs, different behavioral functions have to be considered. For tactile hairs, two extremes can be described, with real hair functions probably somewhere in between:

1. **Obstacle detection**: The hair is deflected by a large force (surface, large object). The only information of interest is the time of contact (and the position of the hair).

2. **Texture discrimination**: In contrast to obstacle detection, more information is obtained from contact with another object. This can include roughness, hardness, size or texture. The information can be obtained by a single, prolonged contact (e.g. sweep over surface) or by repeated contacts.

5.2 Physical modeling of arthropod mechanoreceptors

In its abstract form, a sensor is the input transducer of some kind of information, providing the information to a processing system. The processing system subsequently activates appropriate output transducers (Fig. 5.2).
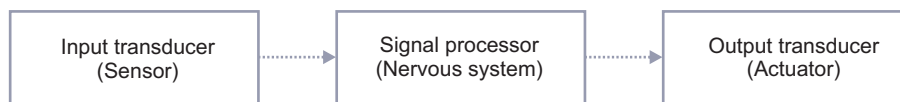

Fig. 5.2: Information processing scheme.

According to Russell (1990), the input to a physical transducer can be divided into six main categories (domains): radiant, mechanical, thermal, electrical, magnetic and chemical. Depending on the domain, different physical effects can be utilized for the transduction. However, the electrical domain can be manipulated best and therefore only examples of physical effects with electrical output are given in table 5.1.

According to table 5.1, arthropod mechanoreceptors measure signals of the mechanical domain. Although this seems to be a trivial statement, it is important for the definition of tactile sensors as different definitions are commonly used in engineering. With regard to arthropod mechanoreceptors, following definition is used:

A device or system that can measure a given property of an object or contact event through physical contact between the sensor and the object (Lee and Nicholls, 1999).

For example, this definition excludes optical distance sensors and includes not only the measurement of force and position, but also shape, texture, temperature or hardness of an object.

Domain	Measurand	Examples
Chemical	Concentration Crystal structure Aggregation Condition	Direct measurements of electric properties
Magnetic	Field intensity	Hall-sensors
Thermal	Temperature	Thermocouples
Mechanical	Force Velocity Size Place	Piezoelectric-sensors, strain gages, variety of capacitative and inductive sensors
Radiant	Intensity Frequency Polarization Phase	Photodiodes, position sensitive diodes, CCD-Sensors[*], interferometers, velocimeters

Tab. 5.1: Possible physical effects for the transduction into electrical signals. [*]Charge coupled devices, commonly used in digital photography (adapted from Middelhoek and Hoogerwerf, 1986, 1988).

So far, two main requirements for mechanical sensors have been described: (1) The sensor has to measure mechanical signals by contact and (2) The output should be electrical. However, auxiliary energy sources can be used for the mechano-electrical transduction, as illustrated in Fig. 5.3. In this work, optical methods, in particular fiber optics, were chosen to measure the deflection of the hairshaft (see section 5.2.1 and chapter 6). Therefore, the next section describes possible sensor designs using fiber optics.
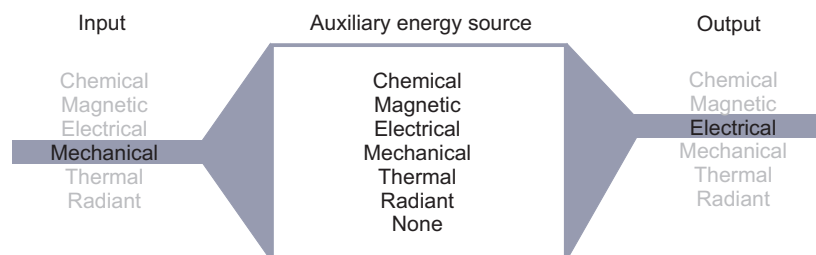

Fig. 5.3: Energy transformations within a transducer (adapted from Russell, 1990).

5.2.1 Fiber optic sensors

In this thesis, fiber optic technology was applied to mimic the transduction process of mechanosensory hairs. In the following sections, three main advantages are examined which have led to the application of fiber optics as transducer elements in the physical model sensors.

A general scheme of fiber optic sensors is illustrated in Fig. 5.4. Basically, they are optical sensors which allow spatial separation of the optical transducer unit (e.g. consisting of an optical fiber) and the optoelectronic unit (e.g. consisting of a light source, an optical detector and processing electronics). The spatial separation is achieved by using optical fibers as the optical communication channel.
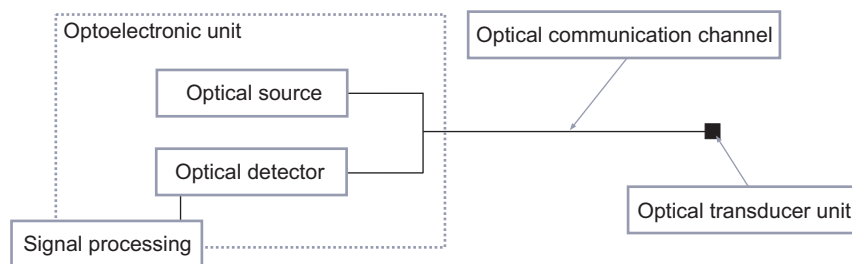

Fig. 5.4: Schematic diagram of a fiber optic sensor. (adapted from López-Higuera, 2002)

The previously presented diagram already illustrated the first important advantage of fiber optics that has led to the application in this context – the spatial distance between the optoelectronical unit and the optical transducer unit. This enables the use of the optical transducer even in very small sensors (López-Higuera, 2002).

The second major advantage is that different measurement methods exist which can achieve greatest known sensitivities (using interferometric techniques, López-Higuera, 2002). Table 5.2 summarizes possible utilizations of fiber optic sensors. Either intrinsic parameters of the fiber or extrinsic parameters such as the intensity of reflected light can be measured. In addition, different characteristics of light can be measured. For example, a simple method could measure modulations of the intensity of light. More complex methods could measure changes in phase or apply interferometric techniques.

The common availability of lasers, optical components and optoelectronics is the third major advantage. Nowadays, these devices can be purchased 'ready-to-use' and equipped with connectors that enable fast connection of single components (without requiring tedious positioning of fibers). However, comparatively high costs, especially for integrated optical and optoelectronical devices, are the main disadvantage of fiber optics.

Nature of transduction	**Intrinsic:** e.g. curvature of the fiber changes intrinsic characteristics of transmission or reflection **Extrinsic:** external device modulates light, e.g. changes in reflection of a mirror or intensity varied by blockage of transmission
Measurement principles	**Intensity measurements:** easiest method, only a few components are needed **Phase measurements or interferometry:** requires coherent light source, single-mode fibers and polarization control; greatest sensitivity, high costs and complexity

Tab. 5.2: Transduction methods of (fiber) optic sensors (based on López-Higuera, 2002).

5.2.2 Examples of technical models of biomimetic mechanosensors

A variety of tactile sensor models exist which basically apply all kinds of methods presented in table 5.1. The following list provides a broad classification of biological systems that are frequently referred to in the context of biomimetic tactile sensors (excluding proprioception). Furthermore, only mechanosensors in terms of the definition used in this study are included.

1. **Human sense of touch:** A lot of research is concerned with transferring the capabilities of skin and embedded cutaneous receptors into a technical counterpart, especially for application in robotic manipulation (Tegin and Wikander, 2005; Lee and Nicholls, 1999). Most of these sensors are either constructed from industrially available force and torque sensors (Tegin and Wikander, 2005; Russell, 1990) or mimic tissue electromechanics (De Rossi et al., 1988; Wettels et al., 2007).

2. **Whiskers and antennae:** The terms whiskers and antennae seem to be synonymously used in engineering. They are generally applied as proximity sensors to detect objects (Lee and Nicholls, 1999). This detection can include active articulation of the whiskers (Russell, 1990). Some examples of whisker designs can be found in Russell (1990), Wijaya and Russell (2002) or Kim and Möller (2005). Basically, the deflection of a whisker is measured with piezoelectric elements, strain gages or by contact of the whisker with a surrounding structure (closing an electric circuit).

3. **Cuticular hairs:** Only a few studies are available where arthropod mechanosensors are mimicked. For example, Chapman (2001) described analog and digital sensors that resemble filiform hairs (medium flow sensors). Other groups have

developed micromachined cantilevers that resemble filiform hairs (van Baar et al., 2003) or artificial hair cells (Chen et al., 2003a,b).

Overall, this list only provides a short survey of the available literature. Due to their possible simple designs, whiskers/antennae are commonly applied in (arthropod) biorobotics while cuticular hairs have only been used in a couple of preliminary studies.

Chapter 6

Methods

This chapter describes the methods that were applied for the construction of biomimetic tactile sensors. At first, the overall design of the sensor is illustrated. Details of the applied mechano-electrical transducers are subsequently presented and preliminary tests of the applied concepts and designs are described. Finally, the methods for the analysis of the constructed sensors are illustrated.

This thesis attempted to design technical sensilla that mimic structural and functional properties of arthropod mechanoreceptive hairs, in particular the previously examined PHS. Therefore, following main conditions had to be fulfilled:

1. Each sensor should contain a hairshaft and a socket, embedded in a surface. The sensors should allow deflections of the hairshafts up to 20-30 degrees without damaging the shafts or the sockets.

2. Similar scaling should be achieved, with hairshaft lengths < 1-2 mm and socket diameters of 50-100 μm.

3. The mechano-electrical transducers should measure deflections of the hairshafts within the socket.

4. The response characteristics of the sensors should equal the response characteristics of the PHS.

These requirements led to the conclusion that a modular design of the sensors was preferable, where the transducer (a), surrounding structure (b), socket with an elastic membrane (c) and hairshaft (d) could be addressed separately (Fig. 6.1). The issues concerned with the mechanical design of the sensor (b-d) were examined in close relation.
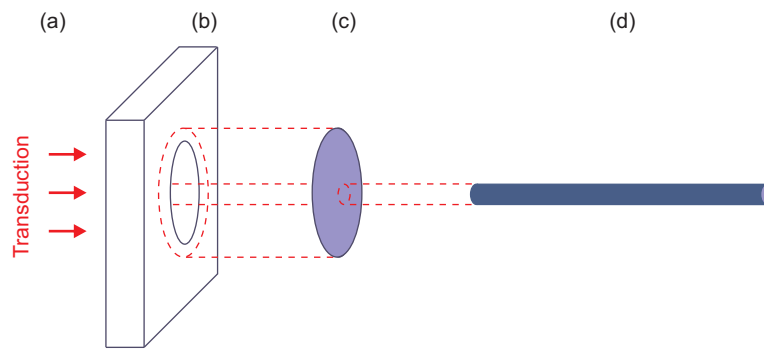
Fig. 6.1: Modular design of the biomimetic tactile sensilla. The construction of the sensors was divided into 4 distinct problems: **(a)** Design of a suitable mechano-electrical transducer, **(b)** surrounding structure that provides a mounting frame for the sensor, **(c)** A socket (50-100 μm diameter) with an elastic membrane that permits deflection of the hairshaft, **(d)** a hairshaft with a length < 1-2 mm.

6.1 Design of mechanical parts of the biomimetic sensors

Surrounding supportive structures (Fig. 6.1b)

The surrounding structure was intended to provide overall stability to the sensor. Furthermore, it should provide the anchor of the sensor, i.e. a hole where the socket (and the hairshaft) could be embedded. Therefore, the material had to be rigid and contain a hole. Several requirements had to be met: The hole for the socket had to be round (isotropy), with a diameter of less than 100 μm and the material had to be thin (thickness < 200 μm), to obtain suitable thickness-diameter relations.

Different materials for the surrounding structure were tested, including several plastic and metal foils with required thickness. At first, it was tested whether it was possible to create holes with required dimensions in the various materials. Although most materials allowed the creation of holes, e.g. by drilling or piercing, several properties made the created sockets insufficient for the use in sensors. For example, the holes had jagged shapes or the surrounding material was deformed and showed cracks. As copper etching is a widely applied technique, e.g. for etching circuit paths on electric boards, different etching techniques were tested to create holes in copper sheets. Etchings were performed either with iron(III)chloride or with sodiumpersulfate. Unfortunately, these techniques did not lead to repeatable and satisfactory results.

Finally, commercial pinholes, which are typically used in electron microscopy, were employed. These pinholes can be purchased in different specifications that seemed suitable for this work. The pinholes were provided as circular discs with a diameter of 3.05

mm and a thickness of 10-50 μm. They could consists of copper or nickel, optionally plated with platinum or gold. Hole diameters of 70 μm, 100 μm and 150 μm were available. For the sensors, copper plates with 3.05 mm diameters, 50 μm thickness and hole diameters of 70 μm were chosen (G2675C, Plano GmbH, 35578 Wetzlar, Germany). The copper pinholes showed constant, high quality and were used in all experiments.

Sockets with elastic membranes (Fig. 6.1c)
While the surrounding structure provided the shape of the socket, the socket itself had to be constructed from an elastic material that allowed deflection of the hairshaft. The socket also had to be rigid enough to support the hairshafts. Different materials were tested and finally, a two-component silicone rubber was chosen (Elastosil RT 601, Wacker Chemie AG, Germany). This rubber was flexible enough to allow deflections of the hairshafts but it was also rigid enough to support the shafts. Furthermore, the application of a two-component mixture that had to be cured enabled the insertion of the hairshaft into the socket in uncured state. This resulted in firm embeddings of the hairshafts during curing of the rubber and also firmly embedded the sockets into the surrounding material. Curing was either performed at room temperature for 24h or by heating the air around the sensor with a soldering rod (tip heat 400°C) for around 5 minutes.

Hairshafts (Fig. 6.1d)
The hairshafts had to be thin enough to be placed into the sockets and they had to possess lengths up to 1-2 mm. Different types of glass-fibers, glass-capillaries and carbon-fibers were tested. Basically all tested fibers could be purchased or constructed with required dimensions. Finally, either glass fibers with diameters of 10-50 μm or carbon fibers with diameters of ≤ 10 μm were applied (with varying lengths). Hybrid sensors were constructed where the hairshafts consisted of carefully torn out pectinal hair sensilla (PHS).

Construction procedure
For the construction, a pinhole and a hairshaft were positioned with micromanipulators using a binocular microscope with 125fold magnification. Prior to final positioning, a small drop of uncured silicone rubber was put into the hole of the pinhole with the help of another glass fiber. Final positioning was subsequently performed and the rubber was cured.

6.2 Design of the mechano-(opto)-electrical transducer

The transducer had to measure deflections of the hairshafts in close proximity of the sockets. For this purpose, optical techniques were employed – in particular fiber optics[1]. Background and reasoning for the application of fiber optics is provided in chapter 5. Different kinds of optical methods are available (e.g. intensity or phase measurements and interferometric techniques). In this study, measurements of intensity modulation were chosen for the transducer as they are easy and only require a few components (in comparison to the other methods). A variety of architectures are possible for intensity modulation measurements (García and Cuenca, 2002). Two different mechanisms were applied (Fig. 6.2). The first method (Fig. 6.2A) modulated light intensity by changes in reflection while the second method (Fig. 6.2B) modulated the transmission of light. Most results presented in this study are based on experiments employing the first method.

In both methods, light was generated by a red-light laserdiode and coupled to an emitting glass fiber. The intensity of the modulated light was measured with a photodetector that was connected to the setup via a receiving fiber. The use of optical fibers enabled the sensor to be small, with the laser and the photodetector positioned in some distance to the sensor.

Method A: Reflective configuration (Fig. 6.2A)
At first, the light emitted by the laser was sent into a 50/50-coupler. Therefore, only 50% of the emitted light reached the point of measurement in the sensor. The amount of light that was reflected back into the sensing fiber was dependent on the angle of the sensing fiber to a reflecting surface. After entering the sensing fiber, the reflected light again passed the 50/50-couper before reaching the photodetector.

Method B: Transmissive configuration (Fig. 6.2B)
This method followed an even simpler approach where the emitting fiber was connected to the laser and a second, receiving fiber was connected to the detector. Optical coupling of the two fibers was achieved by opposite positioning. The intensity was modulated by moving an object in between these two fibers.

In the following, the optical components of the transducer are described.

6.2.1 Fiber-coupled laser source

The light source was a fiber-coupled laserdiode (S1FC635, Thorlabs GmbH, Wetzlar, Germany) that emitted red light with a wavelength of 635 nm (Fig. 6.3). The laser consisted of a Fabry-Pérot laserdiode with a maximum output power of 2.66 mW. The accuracy of the output was ±0.01 mW with a stability of 0.1 dB / 24h (Data sheet,

---

1   The choice and design of the applied techniques was supported by Prof. Meschede and Dr. Alt.

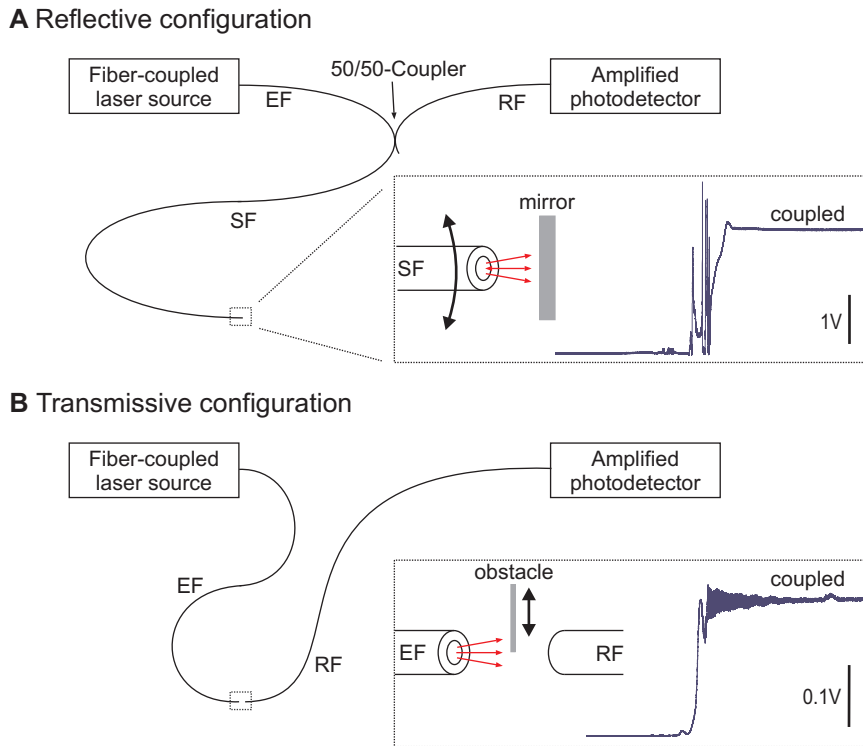**A** Reflective configuration

B Transmissive configuration

Fig. 6.2: Configuration of the mechano-opto-electrical transducers. **A** Reflective configuration. Light emitted by the laser was transmitted via a 50/50 coupler to the sensing fiber *SF*. A reflective surface (mirror) reflected light back into the fiber, with the amount of reflected light entering the fiber depending on the angle of the SF to the surface. The reflected light again passed the 50/50-coupler before it was transmitted to an amplified photodetector. **B** Transmissive configuration. An emitting fiber *EF* was coupled to the laser and positioned opposite of a receiving fiber *RF* that was connected to the detector. An obstacle that was moved in between these fibers changed the amount of transmitted light. In both configurations, manual coupling efficiency was sufficient for the experiments.

Thorlabs GmbH). The laser was internally coupled to a single mode fiber. Laser output was coupled to single mode fibers with a FC-connector. In the experiments, the laser was adjusted to an output power of 2.5 mW.

6.2.2 Amplified photodetector

A silicon photodetector with selectable amplification (0-70 dB) was applied (PDA36A, Thorlabs GmbH). This detector could measure light signals from DC to 17 MHz (at 0 dB gain). The spectral working range of the detector was 350-1100 nm with a peak wavelength of 970 nm (Fig. 6.4). Optical fibers were coupled to the detector with a FC-connector. A coax cable and a 50 Ω resistor connected the detector output with the ADC input of the Power1401. The detector signals were digitized with 20 kHz. Depending on the setup, the gain was set between 10 and 40 dB. Even at 70dB, input
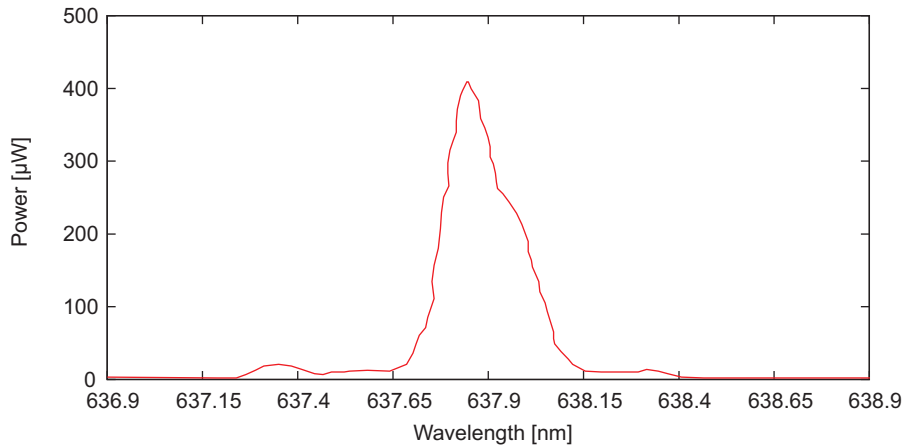
Fig. 6.3: Laser source spectrum. The power of the fiber-coupled laser source is plotted against the wavelength (Data sheet, Thorlabs GmbH).

frequencies up to 12.5 kHz could be used (which was far above the necessary range as the laser was not pulsed). Detector offset depended on the gain and ranged between 6-12 mV for 10 dB amplification and 10-20 mV for 40 dB amplification.
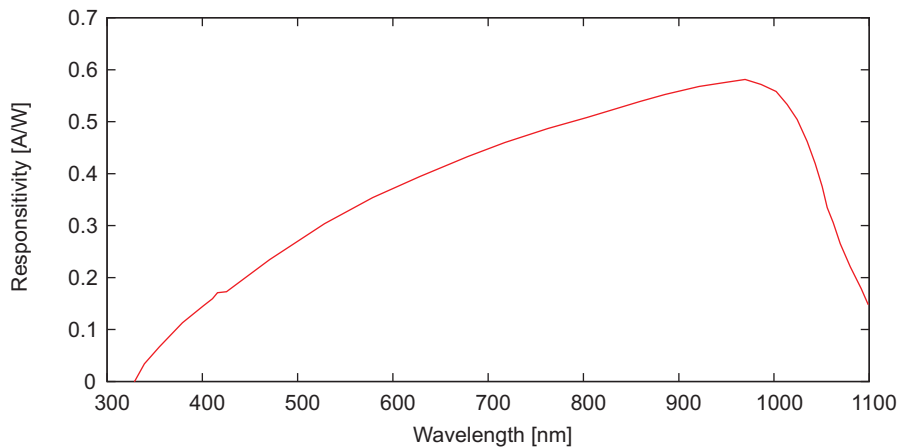

Fig. 6.4: Photodetector spectral responsivity. The spectral responsivity of the amplified silicon photodetector detector is shown (Data sheet, Thorlabs GmbH).

6.2.3 Single mode patch cables

Single mode patch cables with FC connectors either at both ends or only at one end were applied (P1-630A-FC-2, Thorlabs GmbH). The optical fibers were suitable for the applied wavelengths of 630-640 nm. The fibers were equipped with a protective jacking

of 3 mm diameter, their cladding diameter was 125 μm. Typical return loss of these fibers was 50 dB (40 dB min, 50 dB equals a fiber optic junction that reflects 0.001 % of the incident power). Their numerical aperture had an average value of 0.12 (all data provided in the data sheet, Thorlabs GmbH).

Some fibers were used to measure the amount of reflected or transmitted light. In these fibers, the protective coatings were removed around the end that was positioned at the transducer unit. Therefore, only bare fibers were used in the transducers (125 μm diameter). The bare ends (without connector) were cleaved at an angle of 0°, perpendicular to the fiber longitudinal axis[2].

6.2.4 2x2 Fiber optic coupler (50/50-coupler)

The employed 2x2 single mode fiber optic coupler had a split ratio of approx. 50%/50% (FC632-50B-FC, Thorlabs GmbH). A coupler consists of two combined fibers and therefore has 4 fiber ends, two on each side. If light is transmitted into one of the fibers, the intensity of the light is split equally between the two fibers of the opposite side. The coupler was equipped with FC-connectors.

6.2.5 Preliminary tests

Several preliminary experiments were conducted. Fig. 6.5 illustrates two important tests which established the overall suitability of the setups. Two fibers (emitting and receiving) could be coupled and if an obstacle was moved in between these two fibers, the intensity of the transmitted light was modulated (Fig. 6.5A). Deflection of a fiber that was positioned close to a reflecting surface (mirror) also led to intensity modulation of the light that was reflected back into the fiber (Fig. 6.5B). These two exemplary tests proved that the basic principles were applicable in the intended transducers.

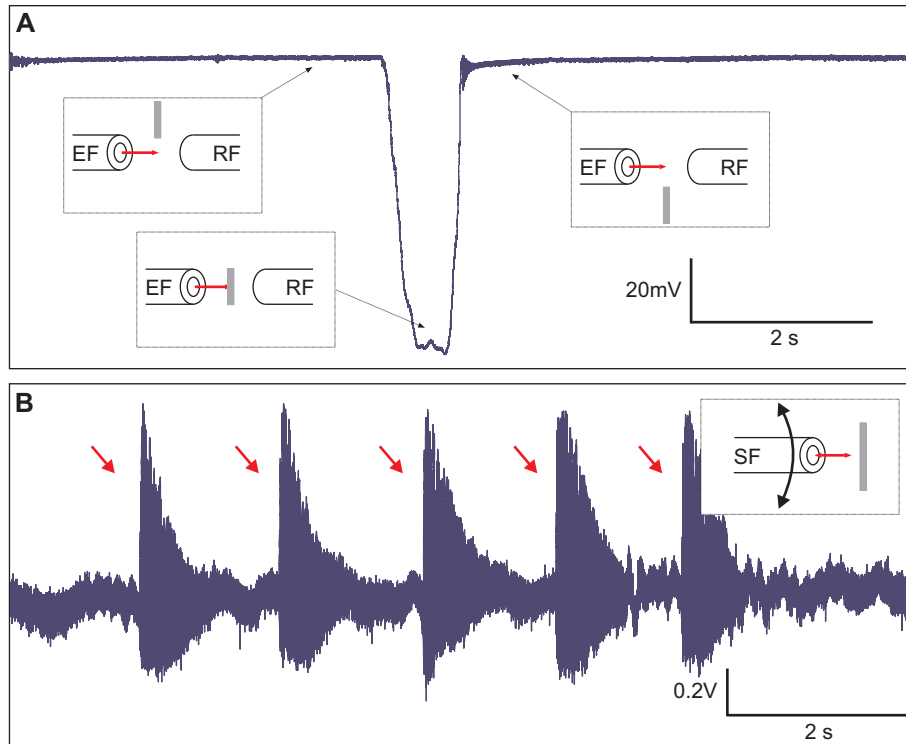2 The cleaving was conducted in the laboratory of Prof. Meschede.

Fig. 6.5: Preliminary tests of the mechano-opto-electrical transducers. **A** Transmissive config-
uration. In this test, a tungsten wire (50 μm diameter) was moved between two optical fibers
(emitting *EF* and receiving fiber *RF*). The test showed, that the amount of transmitted light
depended on the position of the wire. Furthermore, the amount of transmitted light did not
directly go to zero but instead declined if the wire was moved in between and increased again as
the wire left the area between the two fibers. **B** Reflective configuration. A fiber (sensing fiber
SF) was positioned to a mirror that reflected light back into the fiber. At a length of about 2-3
cm, the end of the fiber was not fixed and therefore oscillated if weak air currents were applied
(red arrows). This test showed, that the amount of reflected light was modulated by changing
the angle of the optical fiber in reference to the mirror surface.

6.3 Complete assembly of the sensors

The promising preliminary experiments, especially with utilization of reflective measurements, resulted in the complete sensor design illustrated in Fig. 6.6. In close imitation of the biological example, the sensing fiber was coupled to the hair shaft with the same silicone rubber that was also used to create the socket. Light emitted by the fiber was reflected by the copper plate (the pinhole material was copper). This is in close resemblance to the dendritic compressions that can be observed in arthropod sensory hairs. So far, the preliminary results indicated that the basic concept was valid. However, it was not clear whether the designs would allow the sensors to reliably measure deflections of the hairshafts and result in useful response characteristics.
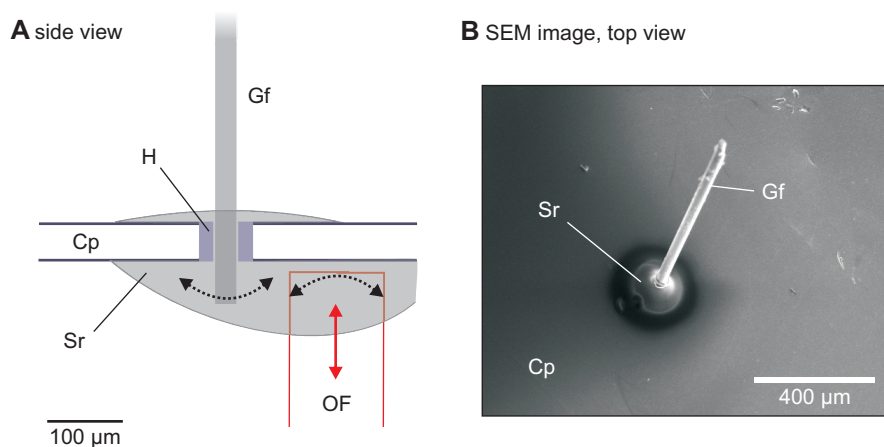

Fig. 6.6: Complete sensor assembly. **A** A schematic side view of the overall sensor design is illustrated. A hairshaft, e.g. a glass fiber *Gf* with a diameter of 30 μm was inserted into the hole *H* with a diameter of 70 μm within the copper sheet *Cp* that had a thickness of 50 μm. The whole structure was suspended in silicone rubber *Sr*. On the inside of the copper sheet, an optical fiber with a diameter of 125 μm was also embedded in the silicone rubber. Deflections of the hair shaft led to elastic deformations within the rubber and therefore to deflections of the optical fiber *OF*. This resulted in changed angles between the optical fiber and the copper sheet and therefore led to modulations of the reflected light intensities. **B** The SEM image illustrates the outside of a sensor. The hairshaft (glass fiber *Gf*), the silicone rubber socket *Sr* and the copper sheet *Cp* can be seen.

Fig. 6.7 illustrates a preliminary experiment that was used to test the overall sensor design. This test showed, that the sensor design using the reflective configuration was capable to measure hair deflections of a few degrees. During deflections, the photodetector output decreased. This indicated that the angle between the optical fiber and the copper plate changed in a way that less light was reflected back into the fiber. As this setup was very promising, it was analyzed in detail (see chapter 7).
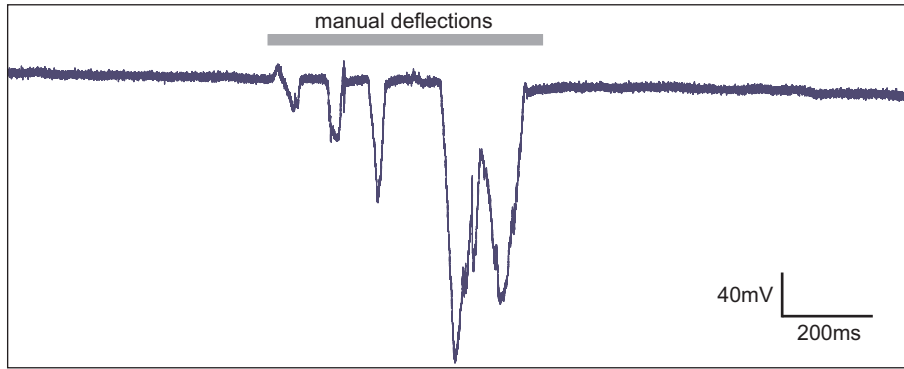
Fig. 6.7: Preliminary test of the complete sensor design. This test showed that the sensor design was capable to measure deflections of the hairshaft. In the presented example, the hairshaft was manually deflected by a few degrees. During deflection, the photodetector output decreased, indicating angular changes of the optical fiber.

6.4 Mechanical stimulation and analysis of detector output

The setup for recording and mechanical stimulation was identical to the setup used for the electrophysiological experiments (see chapter 3). Instead of recording electrophysiological data, the photodetector output was digitized (20 kHz) and recorded with the Power1401/Spike2.

Analysis

The same software that was used to analyze and visualize the neurobiological and morphological experiments was also applied for this study. Data was exported as Tab-separated values from Spike2 for further analysis using a custom written script. This script exported relative amplitudes of the data at manually set points (in relation to the detector output without deflection, detector offset).

Root-mean-square (RMS) smoothing: As the photodetector output was only amplified and not filtered, it was sometimes necessary to smooth the data prior to the analysis. For a time range P surrounding a data point x_{rms}, all data points $x_1 - x_n$ within the time range P were used to calculate a mean value as follows:

$$x_{rms} = \sqrt{\left(\frac{1}{n} \sum_{i=1}^{n} x_i^2 \right)} \tag{6.1}$$

Chapter 7

Results

This chapter describes the main results of the modeling studies. It begins with the description of the constructed artificial and hybrid sensors, including their response characteristics. Finally, electronic circuits for possible further processing of the sensor output are described.

7.1 The constructed artificial and hybrid tactile sensors

20 biomimetic sensilla were constructed using the procedures described in chapter 6. Both transduction designs were applied, with 15 sensilla utilizing the reflection method and 5 sensilla the transmission method (see chapter 6.2).The results present the data of 6 artificial sensilla (glass fibers as hairshafts) and 5 hybrid sensilla (PHS as hairshafts). Artificial sensilla had hairshaft lengths of 440-1580 μm and hybrid sensilla had hairshaft lengths of 350-770 μm. Approximately 4h were required for the assembly of a sensor (including transducer).

7.2 Response characteristics of the constructed sensors

The response characteristics of the constructed sensors were analyzed by deflecting the hairshafts with a mechanical stimulator and measuring the output of the photodetector (setup similar to the measurements on the PHS). All following results are based on the reflective transduction method (see chapter 6.2), except specifically declared otherwise.

7.2.1 Basic characteristics

Fig. 7.1 shows the basic response characteristics of the sensors. The examples illustrate the responses of an artificial sensor. The constructed sensors were capable to measure

the deflections of the hairshafts with great accuracy as photodetector output closely followed the mechanical input. Fig. 7.1A shows the photodetector output to slow ramp stimuli of 7.9° deflection amplitude (DA). The sensor was able to measure the deflection within the required working range (1°-20°). Fig. 7.1B illustrates that the sensor even followed stimuli with higher frequencies of 100 Hz. Not shown are the offset values of the photodetector output.
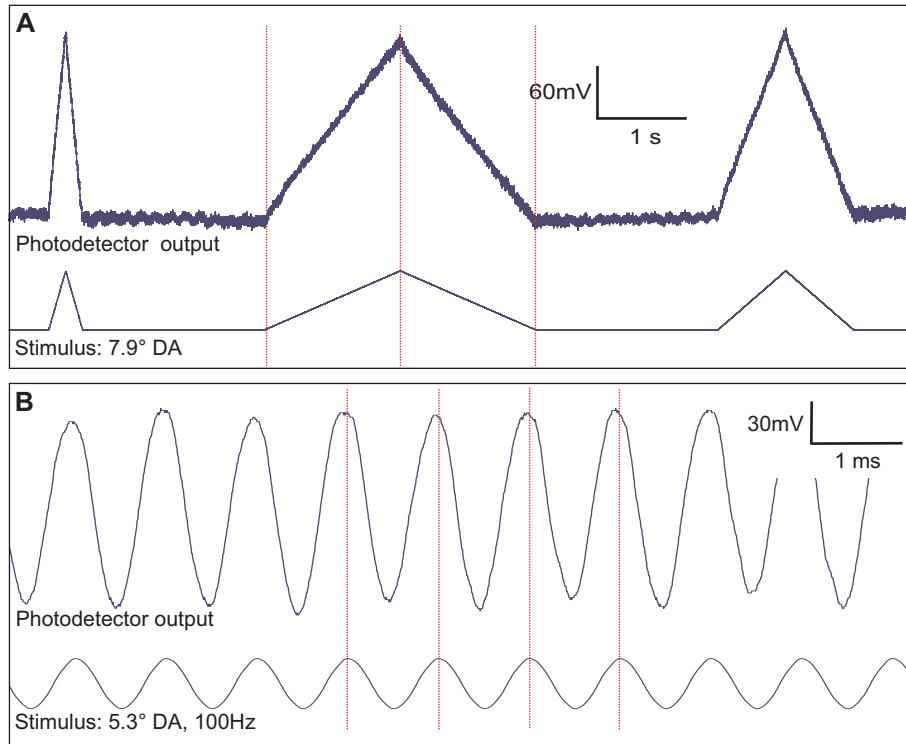

Fig. 7.1: Basic sensor response characteristics. The sensor was capable to reproduce stimulus patterns in the same range that was applied in the experiments with biological sensilla. **A** shows that the photodetector output corresponded to very slow ramp stimuli. **B** shows that the sensor output corresponded to 100 Hz sinusoidal stimulations. Photodetector output was smoothed with an RMS-smoothing (time range $5 \cdot 10^{-4}s$).

Not all constructed sensors precisely measured the deflection of the hairshafts. Fig. 7.2 illustrates two response properties that could diminish the quality of the sensors, hysteresis and drift. Hysteresis especially occurred if the stimulus direction was changed. Then, the sensor did not return to its initial position after the stimulus. This could lead to errors of 10-20 % of signal size (Fig. 7.2A). A few times, the baseline of the photodetector output varied over time without the application of mechanical stimuli. This could consist of unidirectional drift or oscillations in the range of minutes (Fig. 7.2B). If these drifts were larger than changes induced by stimulation, the sensors were not evaluated any further.
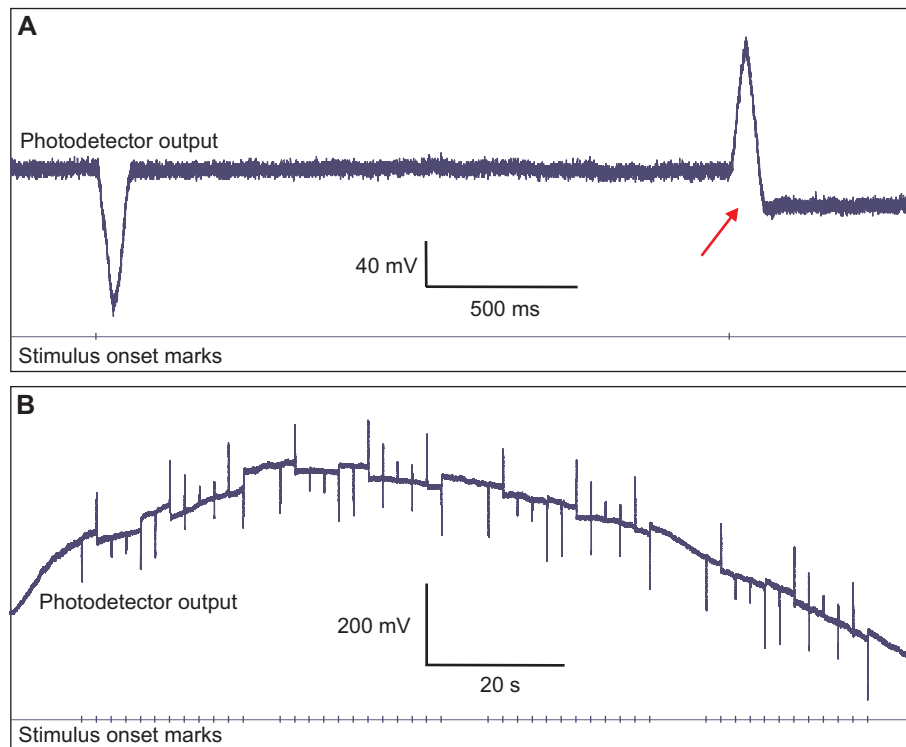
Fig. 7.2: Further sensor response characteristics – Hysteresis and drift. **A** Hysteresis. Especially if stimulus direction was changed, the transducer did not return to its initial position. This error could be as large as 10-20 % of signal size. **B** Drift. Either slow oscillations (in the range of minutes) or unidirectional drift sometimes occured. These could even by larger than output changes induced by deflections of the hairshafts. Photodetector output was smoothed with an RMS-smoothing (time range $1 \cdot 10^{-4}$).

Fig. 7.3 shows the response of the sensors to sustained deflections (step deflections). This illustrates another example where the sensors did not precisely follow the stimuli. The sensor shown in Fig. 7.3B was able to follow the sustained deflection but showed fast oscillations at stimulus onset and offset. Fig. 7.3A shows an example where the sensor returned to its initial position prior to stimulus offset. Furthermore, a sensor could also show a damped response to stimulus onset (not shown).

Another property of the sensors was that deflections could exceed the working range of a sensor (Fig. 7.4). In these cases, increasing stimulus amplitudes led to decreasing photodetector outputs.

7.2.2 Amplitude response characteristics

The working ranges of the constructed sensors were tested by varying the stimulus amplitudes of step stimuli which were delivered in the preferred directions of the according sensors. Fig. 7.5 shows the working ranges of 2 artificial (A,B) and 2 hybrid (C,D) sensors. The results indicate that the constructed sensors had average deflection thresholds
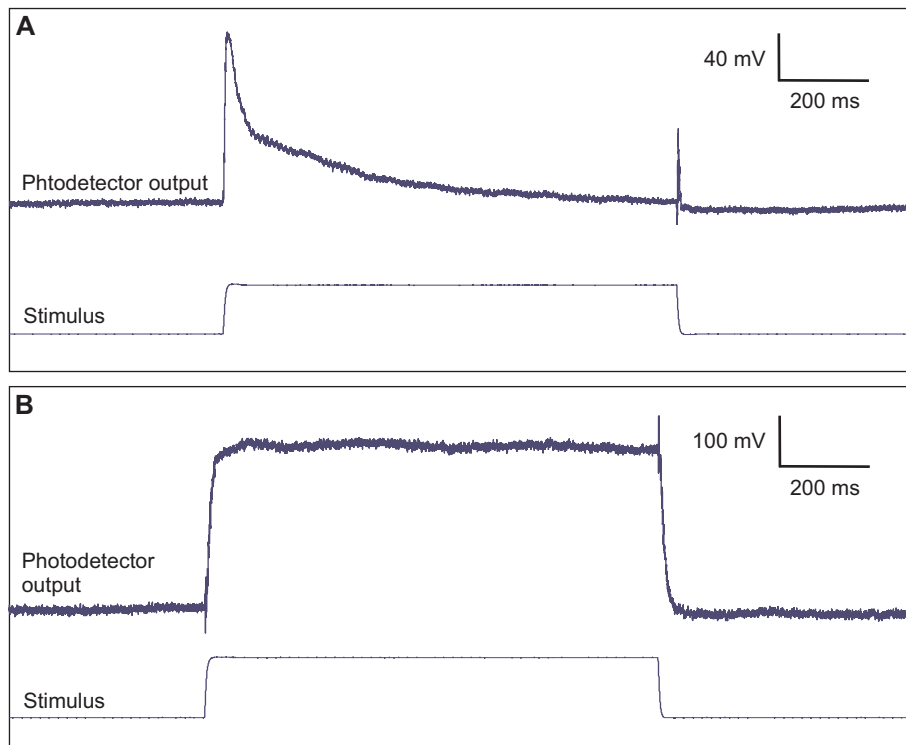
Fig. 7.3: Further sensor response characteristics – Damping. **A** In some sensors, deflection of the hairshaft was not represented linearly by the sensor as it returned to its initial state prior to the end of the stimulus. **B** The sensor reflected the stimulus rather linearly with fast oscillations occurring at stimulus onset and offset.
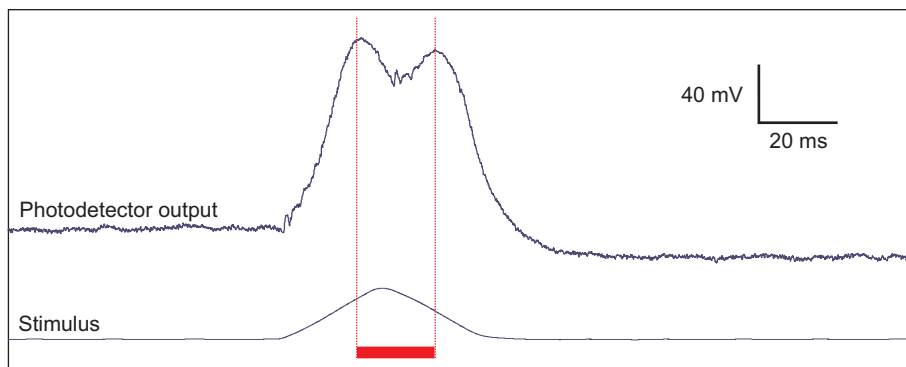

Fig. 7.4: Further sensor response characteristics – Working range exceedance. In a few sensors, the working range was exceeded at larger stimuli. This was due to the fact that the angle between the optical fiber and the reflecting copper surface at first improved reflection but exceeded the optimal point and therefore the output of the sensor decreased at the tip of the stimulus (indicated by the red bar).

of approx. 1°. The maximum values of the working ranges were not determined for all sensors as their lengths and the attachment of the mechanical stimulator did not enable the coverage of the whole working ranges. However, the results indicate that saturation

occurred at deflection amplitudes of 10°-14°. The amplitude response curves differed between the sensors. While some sensors showed rather linear response curves (e.g. Fig. 7.5B,C), other sensors showed sigmoid response curves (e.g. 7.5A).

Fig. 7.5D compares the photodetector output for laser powers of 1mW and 2.5mW. This test showed that it is basically possible to apply low-cost laserdiodes with a maximum output power of 1mW for the construction of the sensors.
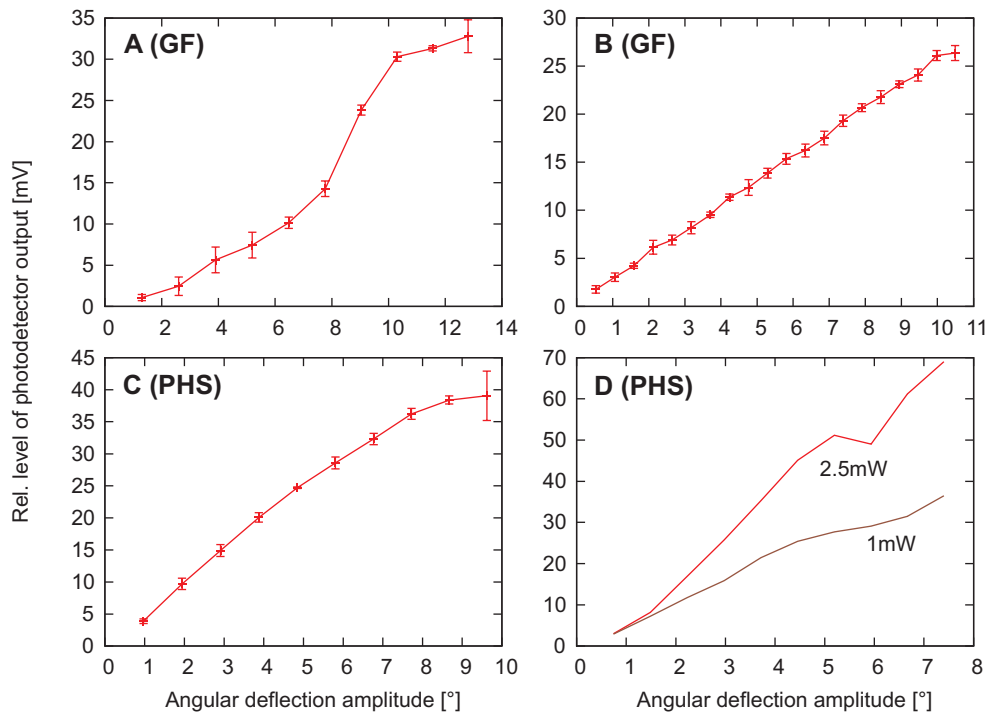

Fig. 7.5: Amplitude response characteristics of the constructed sensors. **A-D** show 4 examples of amplitude response characteristics where the relative level of photodetector output (normed to detector offset) is plotted against deflection amplitude. Each sensor was deflected by step-stimuli in the preferred direction. Mean values (± standard deviation) represent 5 repeats per amplitude. *GF*: artificial sensilla using glass fibers as hairshafts, *PHS*: hybrid sensilla using torn out pectinal hair sensilla as hairshafts. **D** additionally compares photodetector output for laser-powers of 2.5 mW and 1 mW.

7.2.3 Directional characteristics

Directional characteristics were tested at the beginning of each experiment to determine the preferred direction of the according sensor. Two examples of these measurements are shown in Fig. 7.6. The artificial and hybrid sensors showed broad directional tuning and the amplitudes of the responses in each direction depended on the according stimulus

amplitudes. Since some directions led to an increase of the response while others led to a decrease, the output of the sensor could be rectified to obtain bidirectional cardioid response characteristics.
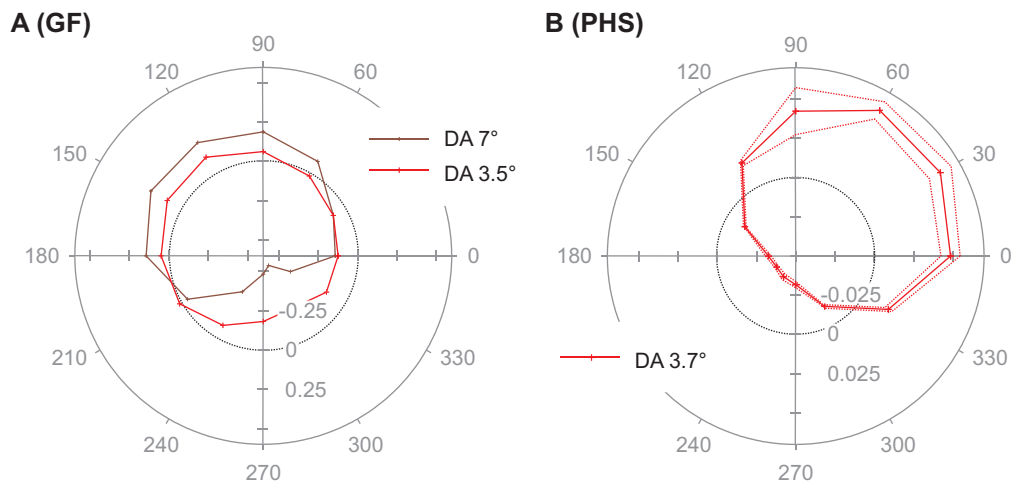

Fig. 7.6: Directional sensitivity of the constructed sensors. The black circles indicate the normed offset level (zero) that was used as a reference for sensor output. **A** shows an example of an artificial sensillum (glass fiber, *GF*) which was deflected in different directions. Two different deflection amplitudes are illustrated. Higher deflection amplitude led to larger responses in all directions (either positive or negative, depending on the stimulus angle). **B** shows an example of a hybrid sensor (*PHS*) which was deflected in different directions. In addition to the mean value of photodetector output, the standard deviations are shown (dotted lines). The data points represent mean values of 5 repeats per deflection direction (30° steps) and deflection amplitude.

Fig. 7.7 shows the amplitude response characteristics of a single artificial sensor for different deflection directions (deflection angles). It can be observed that all directions are dependent on stimulus amplitude. In this case, the dependency seemed to be more pronounced for decreases in photodetector output (and therefore the according directions).

7.2.4 Response characteristics using the transmissive configuration

This is an exemplary measurement where the transduction of the sensillum applied the transmissive configuration of the optical fibers with the hairshaft representing an obstacle between the two optical fibers. In comparison to the previously described results, similar working ranges and amplitude response curves can be obtained. This indicates that both transduction methods could be applied for the construction of the sensilla (although the transmissive configuration was not extensively tested).
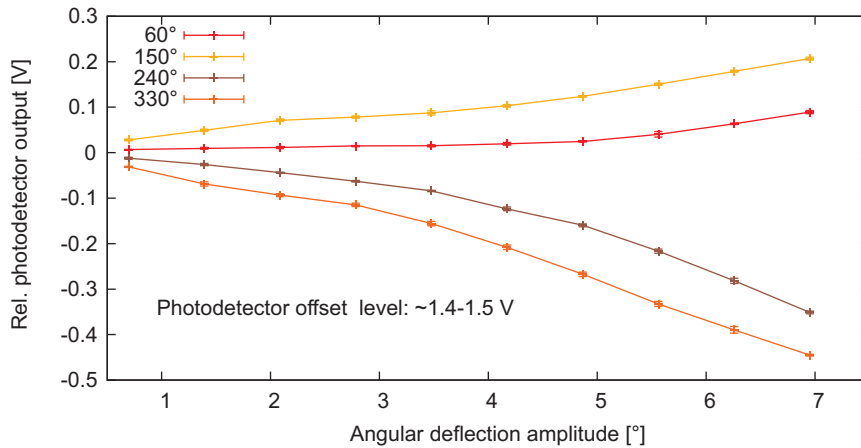
Fig. 7.7: Amplitude and directional response characteristics of one artificial sensor. Relative photodetector output (normed to detector offset) is plotted against deflection amplitude for different deflection directions (mean values of 5 repeats per amplitude). All directions show a dependency on amplitude, but the dependency seemed to be more pronounced for decreases in photodetector output (and therefore the according directions).
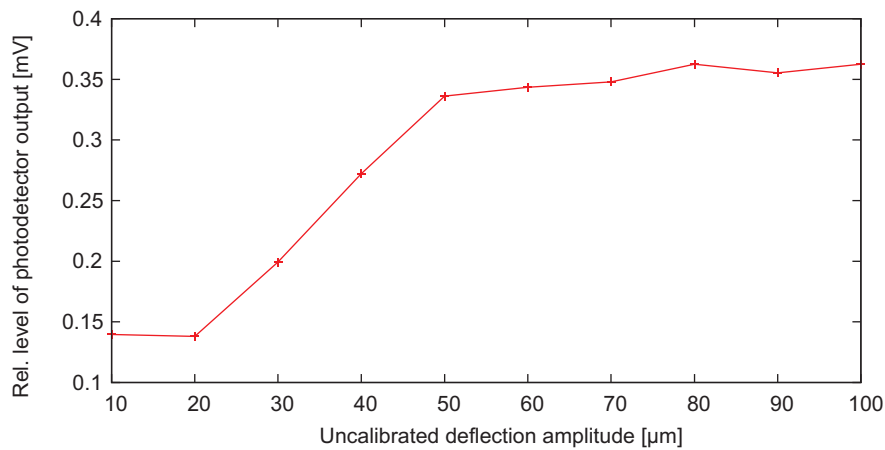

Fig. 7.8: Amplitude response curve of a sensor using the transmissive transduction method. Using this transduction method, the hairshafts represent obstacles between two optical fibers. Relative photodetector output (normed to detector offset) is plotted against stimulator deflection amplitude. The amplitude was not calibrated as it was impossible to determine the position of the stimulator along the hairshaft.

7.3 Further processing of sensor output

Sensors extract relevant information from the environment and provide this information
to some processing system. Therefore, an interface between the sensor and the processing
system needs to be described. A common way to process the information is to display
the data on a scale, readable for a human operator (e.g. standard thermometers or car
speed controls). For research applications, the sensor output is usually digitized, either
for display, storage and later processing in a digital device (computer), or for direct
digital processing in a robot. Many industrial standards (e.g. defined by IEEE[1]) and
guidelines for a variety of interfaces exist. For computers, commonly known interfaces
are, for example, SCSI[2] (parallel) or USB[3] (serial). However, in addition to the interface
processing and (later on) digital processing, data is usually preprocessed with analog
electronics (e.g. amplification, filtering). For application of sensors in biorobotics, several
requirements make analog preprocessing preferable, e.g. fast (real time) processing or
small sizes of integrated circuits.

For the construction of a biomimetic mechanical sensor, this preprocessing can be
used to mimic the response properties of arthropod mechanoreceptors. This work will
present a few simple means of such preprocessing that – at least roughly – can mimic
certain properties of sensory hairs[4].

7.3.1 Possible components of processing electronics

In the following, some simple circuits are described that can mimic certain properties of a
biological sensor. These components are subsequently integrated into a complete circuit
and the input-output characteristics of this circuit are described. For the construction of
the circuits, low-cost components were used (purchased at Conrad Electronics, Hirschau
and Bürklin OHG, Munich). No attention was paid to the power consumption, voltage
requirements or dimensions of the components. However, this would be necessary to
construct integrated circuitry within a sensor.

Rectifier

Fig. 7.9 shows the circuitry and input/output characteristics of a simple rectifier circuit.
This circuit is capable to change negative amplitudes of a signal into positive ones. For
example, this can be used to mimic the behavior of a biological sensillum that depolarizes
by deflections in any direction. Furthermore, this circuit allows attenuation of either the
positive or negative amplitude (or both). The circuit was constructed to work with input
voltages between -5V and 5V and output voltages of 0-5V.

---

1   Institute of Electrical and Electronics Engineers
2   Small Computer System Interface
3   Universal Serial Bus
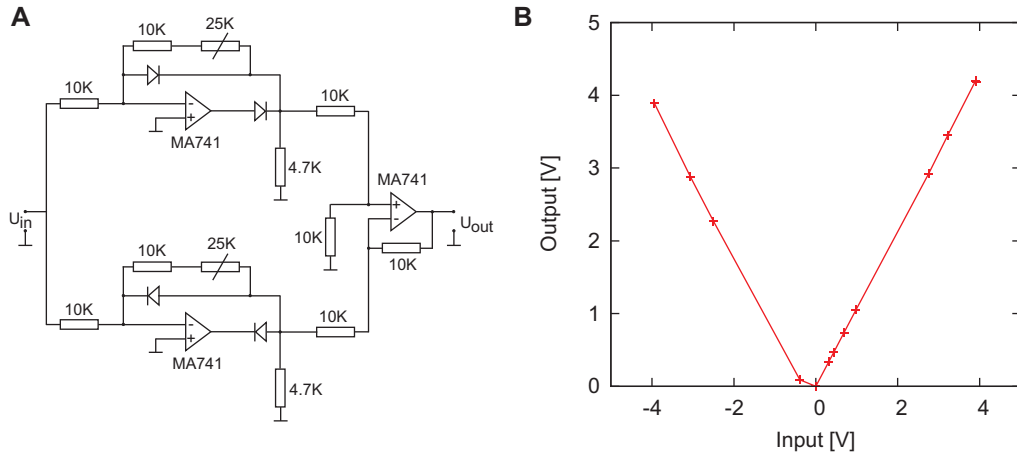4   The design and construction of the circuits was supported by Dipl. Ing. Oliver Rast.

Fig. 7.9: Rectifier circuit. **A** Circuit diagram. **B** Input-output characteristics. The circuit was constructed to work with input voltages between -5V and 5V and output voltages of 0-5V.

Logarithmic amplifier

A nonlinear amplifier can be used to modify the transfer functions of a sensor. For example, the logarithmic circuit described in Fig. 7.10 can be used to enhance amplification of small input amplitudes in comparison to higher input amplitudes. The circuit was designed to work with input and output voltages of 0-5V. This could mimic nonlinear response properties.
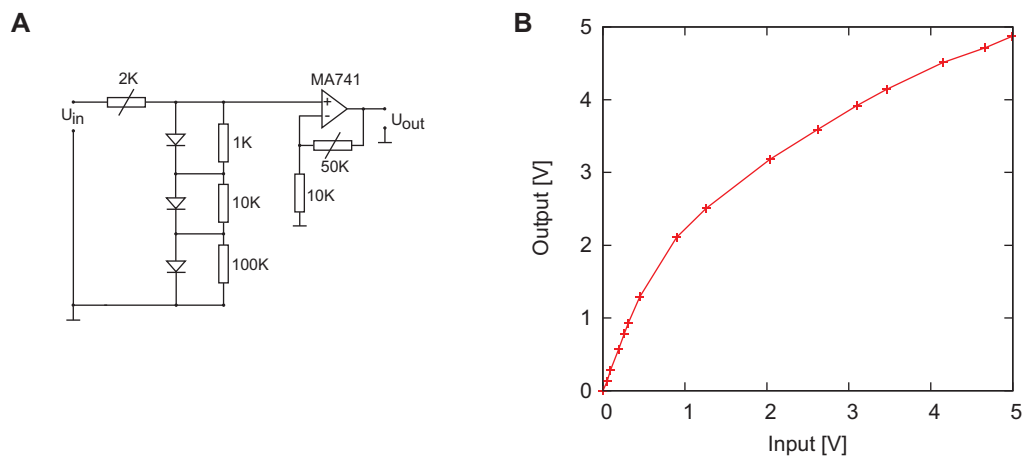

Fig. 7.10: Logarithmic amplifier. **A** Circuit diagram. **B** Input-output characteristics. The circuit was designed to work with input and output voltages of 0-5V.

Other components

In addition to the two described components, especially the application of bandpass filters is useful. These allow removal of slow drift and high-frequency noise. Furthermore, this mimics intrinsic behaviors of mechanosensors which are always tuned to specific input frequencies. Simple circuits such as RC-elements can be used to design filters with variable time constants.

Voltage-frequency converter

A variety of analog-digital converters are available with all kinds of specifications. In this example, a low-cost voltage-to-frequency converter (AD654, Analog Devices Inc., Norwood, Massachusetts) was applied. The converter was used with an input voltage of 0-5V and a frequency output range of 0-1kHz. The converter produced squarewave output with a frequency that depended upon the input voltage.
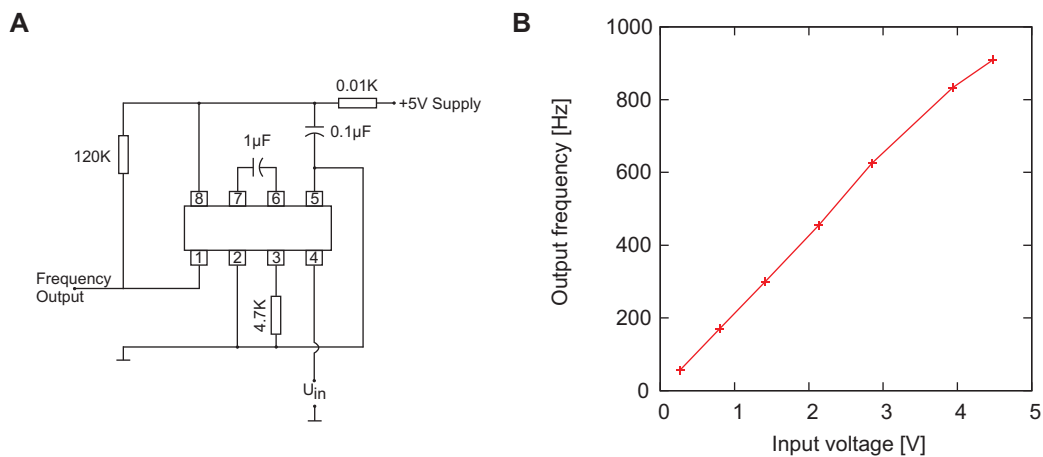
Fig. 7.11: Voltage-to-frequency converter. **A** Circuit diagram. This circuit diagram was adapted from the manual of the AD654. **B** Input-output characteristics. The converter was used with an input voltage of 0-5V and an output frequency of 0-1kHz.

7.3.2 Example of an overall processing circuitry

After testing single circuit components, they were combined into an overall circuitry to show that the processing is capable to mimic behavior of biological sensilla and that it can be used to preprocess data obtained from the previously described sensors. The overall circuitry is illustrated in Fig. 7.12A. The rectifier, logarithmic amplifier, highpass filter (time constant 0.2s) and the voltage-frequency converter were applied. The response of the circuit to step deflections of 0.5 s duration and different stimulus amplitudes is shown in Fig. 7.12B. Higher stimulus amplitudes led to higher output frequencies. All frequencies decline over time (a result of the highpass filter).
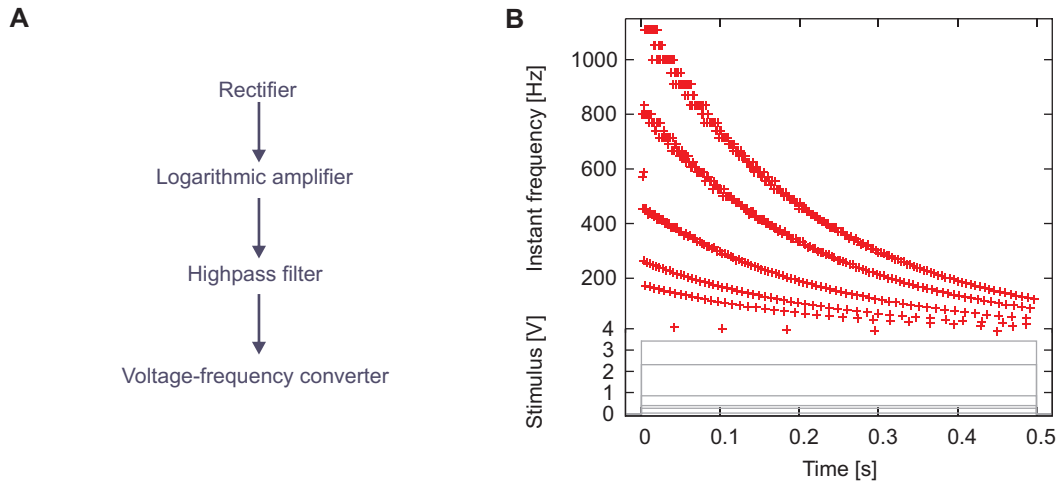
A

Rectifier

↓

Logarithmic amplifier

↓

Highpass filter

↓

Voltage-frequency converter

B

Fig. 7.12: Overall processing circuitry. **A** Combination of different circuits. **B** Input-output characteristics. Higher input amplitudes lead to higher output frequencies. Furthermore, output frequencies decline over time.

Fig. 7.13 illustrates the dependency of the maximum frequency on the input voltage. Higher input voltages lead to higher frequencies with maximum frequencies of about 1100 Hz. Due to the logarithmic amplifier, the response curve is logarithmic.
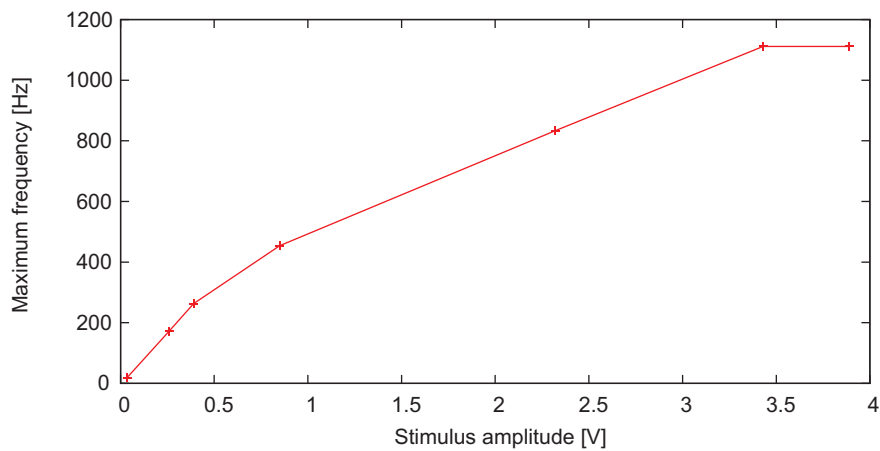
Fig. 7.13: Stimulus-frequency plot of processing electronics. Maximum frequency output of the circuit is plotted against input voltage. Higher input voltages lead to higher frequencies with maximum frequencies of about 1100 Hz. The response curve is logarithmic.

In summary, these circuits have shown that it is possible to apply simple electronics to preprocess sensor outputs in a way that can increase the biomimetic properties of the whole sensor.

Part III

Discussion

Chapter 8

Conclusions and Outlook

8.1 Review of the main objectives

In the general introduction, two major objectives were described. The aim was to perform a neurobiological analysis of cuticular hair sensilla of scorpions, which were supposed to represent a 'simple' type of touch receptor, and use these neurobiological results to develop a biomimetic, physical model of the hairs. To place emphasis on particular backgrounds, problems and methodology of the two different aspects of studying arthropod mechanoreception, these topics were presented as separate parts.

The first part provided a detailed analysis of the morphology, innervation and electrophysiological characteristics of the pectinal hair sensilla. Furthermore, a detailed description of the outer morphology of the pectines was given and the response characteristics with regard to a possible function as obstacle detectors were investigated.

The second part described the construction and the characteristics of biomimetic models of mechanoreceptive hair sensilla. Furthermore, a description of possible processing electronics was given.

8.2 The neurobiology of hair sensilla on the pectines of scorpions

8.2.1 Assessment of the methods

The neurobiological examinations required the modification and development of several methods to obtain valid results. Among these were suitable animal dissections and extracellular recording methods, the development of a mechanical stimulator and the modification of staining methods for the examination of sensilla innervation. As these methods were developed in the course of this work, their advantages and disadvantages will be discussed in the following.

Recording methods

The first task for the analysis of the response properties of the PHS was the establishment of suitable recording methods and animal dissections. At first, simple extracellular measurements were performed, where tungsten electrodes were placed in the base of a pectine (method 1, chapter 3.3.2). With this method, one class of action potentials was recorded. As a few experiments indicated that there were probably more than one class of action potentials associated with one PHS, other recording methods were tested with special regard to the number of recorded AP-classes. Improved methods, especially recordings from the pectine nerve in isolated pectines (method 3) and animal preparations (method 4), constantly revealed 3 electrophysiologically active units. As all possible recording sites were examined (directly beneath a hair and at different positions along the pectine nerve up to the cephalothoracic nervous mass) and different electrode types were tested, it can be assumed that best possible extracellular pectine nerve recordings were obtained.

Mechanical stimulator

Another method that was developed for the electrophysiological experiments was a setup for mechanical stimulation of single hairs (chapter 3.4). For the construction of a stimulator, piezoceramics were chosen as they exhibit several advantageous properties. Their small size, low weight, easy handling and precision in the submicrometer range made these devices excellent choices for the application in this context. It was possible to construct a mechanical stimulator that enabled the delivery of arbitrary stimuli within a plane. This eliminated the need to reposition the stimulator each time the stimulus direction was changed. The closed-loop control allowed high precisions of the deflections, although some precision was lost due to the mechanical arrangements (see chapter 3.4). However, there were also disadvantages. The frequency response characteristics of the stimulator showed that from frequencies of about 20 Hz, the resulting amplitude decreased. Therefore, even rather low frequencies of 50-100 Hz had to be compensated to produce equal stimuli between 0.1 and 100 Hz. Furthermore, stimulus frequencies above 100 Hz were not possible. This made it difficult to test the whole velocity and frequency working ranges of the sensilla.

Computer control of the experiments

The mechanical stimulator and the recordings were controlled by a custom-written script within the Spike2 software. This setup proved to be very useful: the electrophysiological setup was automated, the places and names of data files were automatically generated and different types of stimuli could be generated by using a few dialog boxes (with reasonable, preset values). Thus, full concentration on other experimental details was possible. Furthermore, the preliminary online analysis was a useful tool for fast, rough assessment of response properties. However, this also bears the risk that experiments

are discarded if unexpected response characteristics occur. It had to be taken care of to record all sensilla, regardless of expected or unexpected responses.

Nerve stainings

Different staining methods using cobalt-chloride, nickel-chloride and cobalt-lysine were tested. The most successful stainings were achieved with cobalt-lysine (chapter 3.2.3). Although it was possible to repeatedly stain the sensory cells associated with the PHS, these stainings showed variations in the number of well-stained cells. Further improvements of the methods will be necessary to elucidate the exact number of sensory cells per sensillum. This will require more investigations of suitable timings of the procedures, concentrations of solutions and application of the stains (e.g. staining from the base of a hair could possibly improve the results).

Analysis of maximum deflections of the hairs

The analysis of the maximum deflections of the hairshafts within their sockets without bending was only preliminary (see chapter 4.2.2). The experiments were performed using a dissection microscope with 125fold maximum magnification. This magnification was not sufficient to exactly discern contact of the hairshafts or detect small bending of the hairshafts close to the sockets. Therefore, these studies will have to be carried out using a microscope with higher magnification. The application of dynamometers for the deflections of the hairshafts could further improve these measurements (as contact of a hair with its socket would be detected).

8.2.2 Morphology of the pectines

The pectines of *P. cavimanus* show no differences from the general pectine scheme available in literature. They consist of a spine and teeth. Three types of cuticular sensilla are found on the pectines: chemosensory peg sensilla, probably chemosensory, short, curved hairs and long hair sensilla (PHS).

A detailed analysis of pectine outer morphology revealed that the ventral side of the spine exhibited three marginal lamellae and the dorsal side additionally three median lamellae. The interlamellar membranes were more pronounced on the dorsal side. Overall, the pectines are flattened, elongated structures (Fig. 4.2).

An analysis of the number of teeth per pectine revealed that males tend to possess one more tooth than females (m/f: 27.89 ± 1.73 / 25.82 ± 1.85, Fig. 4.3). However, this is only of little use for sexual discrimination as the number of teeth often also varied between the left and right pectine of one animal. This variation of up to 2 teeth difference showed no preference for either side or sex. These results indicate that *P. cavimanus* is representative for the Scorpionidae, where sexual dimorphism in the number of teeth can only be found if extensive data are compared (Tab.4.1). A comparison with the

pectines of other species revealed that concerning the number of teeth, size or density of hair sensilla, *P. cavimanus* has average pectines (chapter 4.1.2).

8.2.3 Morphology and innervation of the pectinal hair sensilla

The morphology of the PHS reveals that these sensilla are thick and robust hairs, especially in comparison with trichobothria (Fig. 4.8). They have lengths between 300 μm and 1400 μm (Fig. 4.7) and diameters of 30 μm at the base tapering to below 10 μm at the tip (Fig. 4.8). They possess low rimmed sockets which allow a wide range of deflections of the hairshafts (certainly 20°-30°, see chapter 4.2.2). The hairshafts protrude from the sockets at angles of 90°-75°, relative to the surface of the pectine cuticle.

Similar morphological features are found in the long hair sensilla (LHS) that have been studied in *Heterometrus fulvipes*. In this species, metasomal LHS are 750-3000 μm long and have a diameter of 50 μm at the base to 10 μm at the tip (Babu and Jacobdoss, 1994). Measurements on the mLHS of *P. cavimanus* showed similar lengths. Coxal LHS are 2100-3000 μm long and show diameters of 40-50 μm at the base to 10 μm at the tip. These coxal hairs also have a socket which allows a wide range of hair movements and the hairs are inserted into the cuticle either straight or at an angle (Babu et al., 1993). As the length distribution of the LHS depends on their location on the scorpion body, the PHS could possibly belong to the same type of cuticular receptors as the LHS.

In scorpions, almost all mechanoreceptors which have been studied so far show multiple innervation (Kasaiah et al., 1989). Therefore, the innervation pattern of the PHS observed in this thesis confirms this common scheme. The cobalt-lysine stains revealed that there are probably 4-6 bipolar sensory neurons associated with one PHS. The good filled preparations showed consistently stainings with a minimum of four sensory cells associated with one PHS. An innervation with seven sensory cells was never observed.

In comparison, the LHS of *H. fulvipes* were found to be innervated by seven bipolar neurons (Kasaiah et al., 1989), the same number of sensory cells was found for long straight mechanoreceptive hairs on the tarsi and basitarsi of *A. australis*, *E. italicus* and *Buthus occitanus* (Foelix and Schabronath, 1983a). As all comparable mechanoreceptive sensilla in scorpions are innervated by seven bipolar neurons, it is not clear whether the results of this work are specific for the PHS or species-specific for *P. cavimanus*. If the assumption that the PHS belong to the same type of receptors as the LHS is true, it will be important to examine the innervation pattern of the mLHS in *P. cavimanus*.

8.2.4 Response characteristics

The present electrophysiological examination provides a detailed analysis of the response properties of the PHS, in particular of two sensory units. This includes their temporal, spatial, velocity and frequency response characteristics. Three units could be identified

repeatedly, and two units could be characterized extensively. The units could be distinguished by the criteria spike size and shape, conduction velocity and response dynamics (Fig. 4.11).

Basic response properties

During all experiments, the sensory hairs never showed spontaneous activity. Of the three different units, the largest unit (L-unit) is extremely phasic and codes the angular velocity as well as the duration of the dynamic part of a stimulus (Figs. 4.13,4.15). The medium-sized unit (M-unit) shows phasic-tonic response properties and thus codes the duration as well as the amplitude of a stimulus (Fig. 4.14). The smallest unit (S-unit) also codes the velocity of a stimulus but is probably less phasic than the L-unit (Figs. 4.13,4.15). All units had a deflection threshold of approximately 1°. The responses of the M- and L-units started to saturate at deflection angles of 8°-14° (Figs. 4.16,4.18). While the L-unit responded to large stimuli with only 6-8 spikes per stimulus, the M-unit responded with up to 100 spikes for a stimulus of 5 s duration. An analysis of the mean frequencies during a stimulus indicate that the phasic component of the M-unit follows a power function (Fig. 4.17). Estimations of L-unit response times revealed that latencies can be estimated to be approx. 1-2 ms or even less (Fig. 4.19).

In comparison, electrophysiological experiments with LHS in *H. fulvipes* revealed the discharges of 4 or 5 units after mechanical stimulation. Of these units, especially one large phasic unit, an intermediate tonic unit and a small phasic unit could be discriminated, with the intermediate tonic unit probably representing several sensory neurons (Sanjeeva-Reddy, 1971). A threshold of approx. 1° and maximum discharges at deflections of 20°-25° was reported for metasomal LHS of *H. fulvipes* (Babu and Jacobdoss, 1994). Thresholds of 1° and two electrophysiologically active units (fast and slow) were also reported for touch receptors on the tarsi and metatarsi of the spider *Cupiennius salei* (Albert et al., 2001). In comparison, these thresholds are much larger than thresholds reported for trichobothria (Barth, 2002) or campaniform sensilla (Heinzel, 1978).

Velocity and frequency response properties

The velocity response curves showed that the M-unit respond best to angular velocities between 2 °/s and 500 °/s while the L-unit respond best to velocities between 50-2500 °/s (Figs. 4.21,4.22). These values were confirmed by the frequency response curves. The M-unit showed a threshold below 0.1 Hz and its response declined sharply between 10 and 50 Hz while the L-unit responded in a range between 1 Hz and >100 Hz (Fig. 4.23).

Directional characteristics

The directional sensitivity of the L-unit was investigated in more than 50 hairs and the results for the M-unit are based on 15 hairs (Figs. 4.25,4.26). Both units showed similar

responses to variations of the stimulus directions. A detailed comparison revealed, that the response patterns resemble a broad cardioid. This was investigated by fitting a cosine to the normalized data of 40 L-unit samples. The directional sensitivity was independent on stimulus amplitude, only the overall response increased.

Directional sensitivities are found in many hairlike mechanoreceptors. For example, tactile bristles of *A. mellifera* (Gaffal et al., 1975) or filiform hairs on the crayfish tailfan (Douglass and Wilkens, 1998) show distinct directional sensitivities. An explanation of the cardioid shape is given by Thurm (1963), assuming that an excentrical position of the receptive structures leads to the directional sensitivity.

Number of electrophysiologically active units

Once, it was possible to record four different units during an experiment (Fig. 4.20). Two medium-sized units exhibited response characteristics like the M-unit in this experiment. Taken together with the fact that the M-unit showed much variability in its response behavior, for instance with regard to temporal characteristics, it is possible that more than one unit with similar response properties are hidden in the present characterization of the M-unit.

Functional significance of multiple innervation

Multiple innervation of mechanoreceptors has been reported by a number of other studies investigating scorpions (e.g. Kasaiah et al., 1989; Sanjeeva-Reddy, 1971; Messlinger, 1987; Foelix and Schabronath, 1983a) or spiders (e.g. Albert et al., 2001; Eckweiler and Seyfarth, 1988). If multiple innervation is found, its functional significance has to be examined. The response properties of the PHS indicate, that the different sensory cells code different properties of a stimulus. In addition to these different response properties, the sensory cells can also have different effects in the central nervous system. Although central nervous processing was not investigated in this thesis, the different conduction velocities of the units could be a suggestion that the cells have different effects. It could be speculated that the phasic, large unit, showing the highest conduction velocities, could be responsible for eliciting reflex behaviors, while the other units convey more information about the stimulus, e.g. object or surface structure. However, these remain speculations as no studies about central nervous processing of pectine sensory information exist.

8.2.5 Conclusions and possible behavioral functions

In summary, both, morphological parameters and electrophysiological response characteristics, indicate that the PHS are tactile mechanoreceptors, responsible for detecting substrate structure and obstacles along the walking path. These data as well as their innervation patterns further indicate that the PHS are pectinal LHS. Nevertheless, the question remains to be answered whether five sensory cells per sensillum are the common

scheme for *P. cavimanus* or whether this result is an artifact of the staining method, seven cells being the common scheme. A possible, differential behavioral relevance of the five identified sensory cells which are associated with one PHS, and of the three or four physiologically identified response units remains unclear. Intriguingly, a discrepancy between the number of sensory cells in morphological counts and electrophysiological experiments was also found in studies of the LHS (Kasaiah et al., 1989) or, for instance, in studies of the multiply innervated touch receptors of *Cupiennius salei* (Albert et al., 2001).

As stimulation of single PHS in restrained animals is able to elicit movements of the animal, and also considering the timing between stimulus, sensory discharge and motor activity, it can be concluded that single PHS are able to elicit reflex behaviors (Fig. 4.27). To further examine whether the working ranges of the PHS match behavioral relevant stimuli, walking speeds of scorpions can be considered. A study on *P. cavimanus* reported average walking speeds of 0.67 cm/s in darkness and 1.19 cm/s in daylight (Kowalski, 2006). This study further shows that scorpions meander during walking and walk in bouts, short periods of walking, interrupted by periods of inactivity. Other studies report similar walking speeds, for example the study of Köpke (2001) on *Hadogenes bicolor* reported walking speeds of 0.5-15 cm/s, Abushama (1964) conducted studies on *L. quinquestriatus* and found average walking speeds of 2.4-3.9 cm/s and Shaffer and Formanowicz (2000) reported sprint speeds up to 0.5 m/s. With the simplification of orthogonal contact of a sensillum with an object at the tip of the hair, a sensillum length of 1000 μm and a walking speed of 1 cm/s, the resulting angular deflection velocity would be in the range of 550 °/s. This is further evidence, that these hairs can function as obstacle detectors.

Previous studies on the LHS of *H. fulvipes* have shown (1) that their ablation leads to general floppiness and the absence of withdrawal responses, at the same time deflection of LHS on the legs immediately leads to turning responses mediated by plurisegmental pathways (Babu et al., 1993), (2) that the input from a single hair is adequate to trigger interneuron discharges (Sanjeeva-Reddy and Rao, 1970), and (3) that ipsilateral monosynaptic junctions exist between sensory fibers and giant motor neurons with conduction velocities of 6-7 m/s (Yellamma et al., 1980).

These previous findings indicate a role of the PHS – as a subgroup of the LHS – that is responsible for reflexive withdrawal behavior of the pectines. This is of importance since the pectines are a major source for chemosensory information (see chapter 2, e.g. Gaffin and Brownell, 1997a,b). Therefore, a function of the PHS for obstacle detection and height-control to protect and to position the chemosensitive peg sensilla adequately with regard to substrate structures is suggested.

8.3 Modeling arthropod mechanoreceptors

8.3.1 Properties of the biomimetic sensors

This study presents working prototypes of biomimetic models of arthropod mechanoreceptive sensilla. These sensors consisted of a hairshaft (length <1-2 mm), which was embedded in a socket of silicone rubber (diameter 70 μm) (chapter 6.1). Deflections of the hairshaft were measured with a fiber optic transducer (chapter 6.2). An analysis of the response properties revealed that the sensor outputs corresponded the hair deflections with great accuracy up to maximum tested stimulus frequencies of 100 Hz. The sensors had deflection thresholds of about 1°, linear, logarithmic or sigmoid amplitude response curves with responses up to 15° and broad cardioid directional characteristics (chapter 7.2). Furthermore, it was possible to use variable hairshaft lengths and hairshaft materials. Including their fast assembly, these sensors are well suited for rapid prototyping and use in biological contexts.

However, several limitations of the model sensors need to be discussed.

The construction process:
Arrangement of sensor components: The manual construction process which applied micromanipulators to arrange the hairshafts, sockets and optical fibers reached the limits of the available methods. With the maximum 125fold magnification of the dissection microscope used, an accuracy of ±5 μm could be achieved. Although this was sufficient to position the elements of the sensors, small inaccuracies occurred. In the case of hairshaft positioning, this was favorable to increase equivalence with the PHS (which protrude at angles of 90°-75° from their sockets). In the case of optical fiber positioning, this inaccuracy had advantages and disadvantages. The main advantage was that different deflection directions could result in increases or decreases of the sensor outputs. If optimal positioning would have been achieved, only decreases of optical fiber output would have been possible. The main disadvantage was unpredictable sensor output, i.e. each sensor had to be tested whether output increased or decreased.
The silicone rubber socket: The inaccuracies during the construction of the fibers were mainly caused by the construction of the rubber sockets. It was not possible to exactly determine the amount of silicone rubber that was applied. Even the application of the rubber under inspection of the drop-sizes that formed at the tip of a glass fiber yielded disappointing results. Furthermore, the uncured rubber crept along the optical fiber and the hairshaft. Although this was necessary to ensure firm embedding of the components, it also resulted in an unpredictable shape of the cured rubber. Thus, it was impossible to design sensors with intended socket elasticities.
Hairshafts: All kinds of hairshafts could be used, even torn out PHS were possible. Especially the use of biological structures is an interesting possibility which could be

exploited in future studies to investigate the performance of biological structures.

Transducer designs:

Two different approaches were investigated for the design of the transducers. The first approach was a reflective measurement, where changes in angle between the optical fiber and the copper sheet modulated the intensity of light that was reflected back into the fiber (Fig. 6.2A). This approach was thoroughly tested. The second approach consisted of two opposite optical fibers with the hairshaft in between (Fig. 6.2B). Depending on the deflection of the hairshaft, the intensity of light reaching the receiving optical fiber was modulated. Overall, the methods were very successful but several improvements of the transducer designs seem reasonable. In this study, the bare fibers were cleaved but not modified further and therefore had diameters of 125 μm. While this was not of importance in this study, smaller fiber diameters would be necessary to decrease the size of the transducers below the hair sockets and set these in better relation to the dimensions of the hairshafts and sockets. Thus, the application of different fiber shapes and diameters seems to be one of the next steps to improve overall sensor design.

Response characteristics:

The sensors could measure hairshaft deflections with great accuracy, up to stimulus frequencies of 100 Hz (Fig. 7.1). Their deflection threshold was about 1° and their responses saturated at deflection angles of 10°-14° (chapter 7.2.2). The directional characteristics showed broad unidirectional cardioids (Fig. 7.6). Furthermore, if the sensor outputs would be rectified, the directional characteristics would resemble a bidirectional cardioid.

The largely uncontrolled elastic properties of the sockets resulted in sensors with different damping properties (Fig. 7.3). While some sensor outputs linearly represented the stimuli, other sensors showed fast adaptation. Latter behavior resembles Pacinian corpuscles which are rapidly adapting receptors in the (human) skin (Kandel et al., 2000).

Despite the sensor qualities described so far, some sensors showed response properties diminishing their quality. Among these properties were hysteresis (Fig. 7.2), drift (Fig. 7.2) and working range exceedance (Fig. 7.4). Most of these effects were probably caused by insufficiencies of the construction process described above, especially the lack of control over the elasticity of the socket.

Further restrictions:

The experimental design required other restrictions. To enable the reuse of the optical fibers, the sensors were not firmly encased and transportable. Thus, they had to remain attached to the micromanipulators. However, the sensors were designed in a way that it would have been possible to embed a whole sensor in a casing.

Further processing of sensor output

Simple circuits can be applied to preprocess sensor output and increase the equivalence with a biological hair sensillum (see chapter 7.3). For example, sensors with a linear amplitude response curve could apply nonlinear amplifiers to achieve a logarithmic response curve. Especially the use of bandpass filters seems reasonable as they can mimic different adaptational processes and can remove small, slow drifts and high frequency noise.

For application in a sensor, a redesign of the circuits including appropriate amplification and offset-removal of the sensor output would be necessary. Furthermore, the components should be integrated to be as small as possible, including the light source and the photodetector.

8.3.2 Comparison of the biomimetic sensors and pectinal hair sensilla

For the comparison of the biomimetic models with their biological counterparts, parameters of the classification scheme provided by Webb (2001, see also chapter 5), together with other schemes for the classification of technical sensors (e.g. Russell, 1990; López-Higuera, 2002) are applied.

1. **Performance match:** If the response characteristics of the sensors are compared with the PHS, several similarities are obvious: the thresholds, working ranges and the directional characteristics of some sensors matched the response characteristics of the PHS rather well. If further processing is included in the comparison, the sensors would be capable to mimic nonlinear properties or more complex adaptations of the PHS.

2. **Abstraction level:** The main objective to construct sensors which represent the functional biomechanics of the PHS was successful. The sensors showed similar dimensions of the sockets as well as the hairshafts. A comparison of further biomechanical parameters was impossible as the parameters were unknown for the PHS and the sensors as well (e.g. socket elasticity).

3. **Robustness:** In comparison to the PHS, the biomimetic sensors were very sensitive to excess forces. Especially stimuli from above the sensors pushed their hairshafts into the sockets and destroyed the sensors. Hybrid sensors showed slightly improved characteristics as the hairshafts did not break, but also resulted in the destruction of the sockets. Further investigations will be necessary to find materials that are more resistant to overloads, especially elastic materials which can be used to construct the sockets. One possible solution to increase the robustness would be the application of a second copper sheet, encasing the socket. This would

provide stability to the hairshaft (it could not be pushed into the socket) and could further lead to a better control of socket elasticity.

4. **Integrativeness:** The nature of the sensor construction process limits their use as prototypes. Light source and photodetector, as well as preprocessing electronics were not included in the sensor. Furthermore, only single sensors were constructed, disabling the integration of a large number of sensors. However, a single sensor could be assembled within one day.

5. **Biological relevance:** So far, this study has shown that it was possible to design sensors which equal their biological counterparts in some crucial aspects. However, the usefulness of these sensors in biological research is still limited. Manipulations of the socket and hairshaft elasticities could provide some insight into the biomechanics of the sensilla, especially if biological parts are integrated (e.g. hairshafts, pieces of cuticle with embedded glass fibers, ...).

8.3.3 Comparison with other biomimetic sensors

Only a few studies present comparable biomimetic sensor designs. For example, Chapman (2001) describes analog and digital designs for the construction of biomimetic sensors resembling filiform hairs and employs the digital design in a cricket-robot. However, these sensors have lengths in the centimeter range and are therefore better compared to small antenna and whisker designs.

Several studies using MEMS[1] technology to construct hairlike sensors show sensor properties that closely mimic the biological targets. One of these studies is conducted as part of the CICADA[2] project (e.g. van Baar et al., 2003; Krijnen et al., 2006). This study constructs hairlike structures resembling filiform hairs in dimensions and function, where rotations of the hairshafts are measured by capacitative measurement techniques. Furthermore, highly integrated arrays of numerous hairs of different sizes are presented. The techniques applied in this study allow high control over individual mechanical parameters. MEMS technology is also applied in several other studies constructing artificial hair sensors inspired by filiform hairs (e.g. Chen et al., 2003a,b; Ozaki et al., 2000) or the lateral line of fish (e.g. Fan et al., 2002).

Especially the MEMS sensors show an efficiency that can not be reached with the manual design of a sensor. Using further processing electronics, these sensors can equal the response properties and dimensions of their biological targets. Although the application of MEMS technology seems to be most promising for the construction of devices that – someday – can be purchased at low cost and included in a technical model for the

---

1 Microelectromechanical Systems.
2 Cricket Inspired PerCeption & Autonomous Decision Automata, EU research project which concentrates on air current perception and escape responses elicited by filiform hairs of crickets.

study of biological systems, these technologies are not useful for fast, rapid prototyping in biology. Chen et al. (2003b) provides an example where 20M dollar, a 20-member research team and 3 years were needed for the development of a MEMS prototype gyroscope and furthermore describes that these stunning costs in money, manpower and time apply to the development of every MEMS sensor. Even a tenth of the costs would probably exceed the benefits for most pure biological studies. Until these technologies are more commonly available, prototyping as performed in this study will be necessary.

8.4 General conclusions for arthropod mechanoreception

8.4.1 Pectinal hair sensilla – simple arthropod 'touch' receptors?

The results of this thesis indicate that even presumably 'simple' mechanoreceptors are complex structures. The amount of information that can be obtained from a single sensor proposes a function beyond simple obstacle-detection (time and place of contact). This complexity is further increased if the multiple innervation of the PHS is considered. Indeed, all multiple innervated touch sensors investigated so far show that the different associated sensory cells have different response properties.

In summary, the PHS, belonging to a group of hair sensilla distributed all over the scorpion body, are complex structures that are possibly not only used for the detection of time and place of a contact – at least if their response characteristics are considered.

8.4.2 The biomimetic models and their implications for biology

The biomimetic sensors are working prototypes of touch sensors resembling arthropod cuticular hairs in some crucial aspects. However, this does not necessarily result in a biological relevance. As soon as it is possible to control further parameters of the sensors, such as the elasticity of the sockets, they could be applied to address specific biological questions. For example, one such study could investigate the detection of complex surface structures. Furthermore, several sensors could be combined to address questions of further processing.

Overall, these sensilla are the first step toward a universal model of arthropod hairs, where single biomechanical parameters can be varied and used as a tool for the generation of biological hypotheses (e.g. sensor application in biorobotics).

8.5 Possible future work

This study provided a detailed analysis of the morphology and response characteristics of the pectinal hair sensilla. However, some aspects need to be investigated further. Concerning the hair sensilla, their innervation needs to be studied more closely to elucidate the exact number of sensory cells associated with one sensillum. Furthermore, their biomechanical properties need to be analyzed as they are important characteristics of contact mechanosensors (Barth and Dechant, 2003). This will include studies of the socket elasticity, but also hairshaft properties. The processing of the hairs needs to be examined, especially with regard to the multiple innervation. The most important question will be whether the different units have different effects in the central nervous system. Finally, studies on the metasomal long hair sensilla of *P. cavimanus* need to be performed to determine whether the PHS are indeed a subgroup of these ubiquitously distributed sensilla.

The behavioral context of PHS function has to be analyzed, too. So far, there exists only one study that gives details concerning the actual movements of the pectines and the different types of movement patterns they can show (Gaffin and Walvoord, 2004). Further analysis of the pectinal movement repertoire and stimulation of single PHS in free-walking scorpions while recording from the pectine base and body muscles will be necessary to learn more about the behavioral role of the PHS.

Further modeling of the hair sensilla will inevitably require a more theoretical approach. It seems necessary to provide a theoretical framework that helps to improve the sensor designs. This mathematical model would not only enable better understanding of the elastic deformations within the sockets of the sensors, but would also provide a useful tool for the analysis of the pectinal hair sensilla. Sensor design itself will have to be improved in a way that further miniaturization can be achieved. This includes the light source, the photodetector and the optical fibers.

The results of this thesis suggest that more theoretical and experimental analysis of sensory-motor systems is necessary and that new techniques and concepts have to be applied and developed to establish scientific frameworks that explain the underlying processes.

Abbreviations

ADC Analog-digital converter

AP Action potential

CNS Central nervous system

CTM Cephalothoracic mass

DAC Digital-analog converter

DA Deflection amplitude = stimulus amplitude

LHS Long hair sensilla

PCA Piezoceramic actuator

PHS Pectinal hair sensillum/sensilla

SD Standard deviation

SEM Scanning electron microscopy

SNR Signal-to-noise ratio

List of Figures

List of Tables

Bibliography

Abushama, F. (1964). On the behaviour and sensory physiology of the scorpion *Leiurus quinquestriatus*. *Animal Behaviour*, 12:140–153.

Albert, J. T., Friedrich, O. C., Dechant, H.-E., and Barth, F. G. (2001). Arthropod touch reception: spider hair sensilla as rapid touch detectors. *J. Comp. Physiol. A*, 187:303–312.

Altman, J. and Tyrer, N. (1980). *Neuroanatomical techniques*, chapter 19, pages 373–402. Springer-Verlag, New-York.

Babu, K. (1965). Anatomy of the central nervous system of arachnids. *Zool. Jb. Anat.*, 82:1–154.

Babu, K. and Jacobdoss, P. (1994). Central afferent pathways of long hair sensilla in the ventral nerve cord of the indian black scorpion, *Heterometrus fulvipes* koch. *J. Comp. Physiol. A*, 174:495–505.

Babu, K. and Sanjeeva Reddy, P. (1967). Unit-hair receptor activity from the telson of the scorpion *Heterometrus fulvipes. Current Science*, 26:599–600.

Babu, K., Sreenivasulu, K., and Sekhar, V. (1993). Sensory projections of identified coxal hair sensilla of the scorpion *Heterometrus fulvipes* (Scorpionidae). *J. Biosci.*, 18:247–259.

Barth, F. (2000). How to catch the wind: Spider hairs specialized for sensing the movement of air. *Naturwissenschaften*, 87:51–58. Review Article.

Barth, F. (2002). Spider senses - technical perfection and biology. *Zoology*, 105:271–285. lecture presented at the DZG meeting 05/22/2002.

Barth, F. (2003). Sensors and sensing: A biologist's view. In Barth, F. G., Humphrey, J., and Secomb, T., editors, *Sensors and Sensing in Biology and Engineering*. Springer Verlag Wien, New York.

Barth, F. and Dechant, H.-E. (2003). Arthropod cuticular hairs: Tactile sensors and the refinement of stimulus transformation. In *Sensors and Sensing in Biology and Engineering*, pages 159–171. Springer, New York.

Barth, F. and Wadepfuhl, M. (1975). Slit sense organs on the scorpion leg (*Androctonus australis* L., Buthidae). *J. Morph.*, 145:209–228.

Barth, F., Wastl, U., Humphrey, J., and Devarakonda, R. (1993). Dynamics of arthropod filiform hairs. II. mechanical properties of spider trichobothria (*Cupiennius salei* keys.). *Phil. Trans. R. Soc. Lond. B*, 340:445–461.

Barth, F. G., Nemeth, S. S., and Friedrich, O. C. (2004). Arthropod touch reception: structure and mechanics of the basal part of a spider tactile hair. *J. Comp. Physiol. A*.

Batschelet, E. (1981). *Circular Statistics in Biology*. Academic Press, London, New York.

Birukow, G. (1958). Zur Funktion der Antennen beim Mistkäfer (*Geotrupes silvaticus* panz.). *Z. f. Tierpsychologie*, 15(3):265–276.

Bowerman, R. (1976). Ion concentrations and pH of the hemolymph of the scorpions *Hadrurus arizonensis* and *Paruroctonus mesaensis*. *Comp. Biochem. Physiol.*, 54A:331–333.

Brown, C. (1997). Growth rates in the scorpion *Pseudouroctonus reddelli* (SCORPIONIDA, VAEJOVIDAE). *J. Arachn.*, 25:288–294.

Brownell, F. and Farley, R. (1979a). Orientation to vibrations in sand by the nocturnal scorpion *Paruroctonus mesaensis*: Mechanism of target localization. *J. Comp. Physiol. A*, 131:31–38.

Brownell, P. (1988). Properties and function of the pectine chemosensory system of scorpions. *Chemical Senses*, 13:677.

Brownell, P. (1989). Neuronal organization and function of the pectinal sensory system in scorpions. *Soc. Neurosci. Abstr.*, 15:1289.

Brownell, P. and Farley, R. (1979b). Detection of vibrations in sand by tarsal sense organs of the nocturnal scorpion, paruroctonus mesaensis. *J. Comp. Physiol.*, 131:23–30.

Caldwell, W. and Hatcher, J. (1972). A linear motion generator for physiological research. *Journal of Applied Physiology*, 33(4):532–535.

Carthy, J. (1966). Fine structure and function of the sensory pegs on the scorpion pectines. *Experientia*, 22:89–91.

Carthy, J. (1968). The pectines of scorpions. *Symp. zool. Soc. Lond.*, 23:251–261.

Chang, C. (2001). Biorobotics researcher: To be or not to be? Open peer commentary to the article of Barbara Webb (2001) Can robots make good models of biological behaviour? Behavioral and brain sciences 24:1033-1050.

Chapman, T. (2001). Morphological and neural modelling of the orthopteran escape response. PhD Thesis, University of Stirling.

Chen, J., Engel, J., and Liu, C. (2003a). Development of polymer-based artificial haircell using surface micromachining and 3d assembly. In *12th International Conference on Solid State Sensors, Actuators and Microsystems*.

Chen, J., Fan, Z., Engel, J., and Liu, C. (2003b). Towards modular integrated sensors: The development of artificial haircell sensors using efficient fabrication methods. In *Proc. of the IEEE/RSJ Intl. Conference on Intelligent Robots and Systems*.

Chiel, H. and Beer, R. (1997). The brain has a body: adaptive behavior emerges from interactions of nervous system, body and environment. *TINS*, 20:553–557.

Cloudsley-Thompson, J. (1955). On the function of the pectines of scorpions. *Annals and Magazine of Natural History*, 12,8:556–60.

De Rossi, D., Domenici, C., and Chiarelli, P. (1988). *NATO ASI Series, Sensors and Sensory Systems for Advanced Robots*, chapter Analogs of biological tissues for mechanoelectrical transduction: tactile sensors and muscle-like actuators, pages 189–199. Springer-Verlag, Berlin.

Dechant, H.-E., Rammerstorfer, F. G., and Barth, F. G. (2001). Arthropod touch reception: stimulus transformation and finite element model of spider tactile hairs. *J. Comp. Physiol. A*, 187:313–322.

Delcomyn, F. (2001). Biorobotic models can contribute to neurobiology. Open peer commentary to the article of Barbara Webb (2001) Can robots make good models of biological behaviour? Behavioral and brain sciences 24:1033-1050.

Douglass, J. and Wilkens, L. (1998). Directional selectivities of near-field filiform hair mechanoreceptors on the crayfish tailfan (Crustacea:Decapoda). *J. Comp. Physiol. A*, 183:23–34.

Eckweiler, W. and Seyfarth, E.-A. (1988). Tactile hairs and the adjustment of body height in wandering spiders: behavior, leg reflexes, and afferent projections in the leg ganglia. *J. Comp. Physiol. A*, 162:611–621.

Fan, Z., Chen, J., Zou, J., Bullen, D., Liu, C., and Delcomyn, F. (2002). Design and fabrication of artificial lateral line flow sensors. *J. Micromech. Microeng.*, 12:655–661.

Farley, R. (2001). Development of segments and appendages in embryos of the desert scorpion *Paruroctonus mesaensis* (Scorpiones: Vaejovidae). *Journal of Morphology*, 250:70–88.

Fet, V., Sissom, W., Lowe, G., and Braunwalder, M. (2000). *Catalog of the scorpions of the world (1758-1998)*. The New York Entomological Society.

Foelix, R. and Schabronath, J. (1983a). The fine structure of scorpion sensory organs. I. Tarsal sensilla. *Bull. Br. arachnol. Soc.*, 6(2):53–67.

Foelix, R. and Schabronath, J. (1983b). The fine structure of scorpion sensory organs. II. Pecten sensilla. *Bull. Br. arachnol. Soc.*, 6(2):68–74.

Frigg, R. and Hartmann, S. (Spring 2006). Models in science. In Zalta, E. N., editor, *The Stanford Encyclopedia of Philosophy*, URL: *http://plato.stanford.edu/archives/spr2006/entries/models-science/*.

Gaffal, K., Tichy, H., Theiss, J., and Seelinger, G. (1975). Structural polarities in mechanosensitive sensilla and their influence on stimulus transmission. *Zoomorphologie*, 82:79–103.

Gaffin, D. (2002). Electrophysiological analysis of synaptic interactions within peg sensilla of scorpion pectines. *Microscopy Research and Technique*, 58:325–334.

Gaffin, D. and Brownell, P. (1992). Evidence of chemical signaling in the sand scorpion *Paruroctonus mesaensis* (Scorpionida: Vaejovida). *Ethology*, 91:59–69.

Gaffin, D. and Brownell, P. (1997a). Electrophysiological evidence of synaptic interactions within chemosensory sensilla of scorpion pectines. *J. Comp. Physiol. A*, 181:301–307.

Gaffin, D. and Brownell, P. (1997b). Response properties of chemosensory peg sensilla on the pectines of scorpions. *J. Comp. Physiol. A*, 181:291–300.

Gaffin, D. and Brownell, P. (2001). Chemosensory behavior and physiology. In Brownell, P. and Polis, G., editors, *Scorpion Biology and Research*. Oxford University Press.

Gaffin, D. and Walvoord, M. (2004). Scorpion peg sensilla: are they the same or are they different? *Euscorpius*, (17):7–15.

García, A. and Cuenca, J. (2002). Transduction techniques based on intensity modulation of light (chapter 11). In López-Higuera, J., editor, *Handbook of optical fibre sensing technology*, pages 211–226. Wiley&Sons, LTD, West Sussex, England.

Hadley, N. (1990). Environmental physiology. In Polis, G. A., editor, *The Biology of Scorpions*, pages 247–293. Stanford University Press, Palo Alto, CA.

Haradon, R. (1985). New groups and species belonging to the nominate subgenus *Paruroctonus* (Scorpiones, Vaejovidae). *J. Arachnol.*, 13:19–42.

Heinzel, H.-G. (1978). Aerodynamische, mechanische und elektrophysiologische Untersuchung der Heuschreckenantenne als Luftströmungs-Sinnesorgan. Dissertation, Universität Düsseldorf.

Hjelle, J. T. (1990). Anatomy and morphology. In Polis, G. A., editor, *The Biology of Scorpions*, pages 9–63. Stanford University Press, Palo Alto, CA.

Hodgkin, A. and Huxley, A. (1952). A quantitative description of membrane current and its application to conduction and excitation in nerve. *J. Physiol.*, 117:500–544.

Hoffmann, C. (1964). Zur Funktion der kammförmigen Organe von Skorpionen. *Die Naturwissenschaften*, page 172.

Hoffmann, C. (1967). Bau und Funktion der Trichobothrien von *Euscorpius carpathicus* l. *Zeitschrift für vergleichende Physiologie 54*, pages 290–352.

Horn, A. and Achaval, M. (2002). The gross anatomy of the nervous system of *Bothriurus bonariensis* (L.C.KOCH, 1842) (Scorpiones, Bothriuridae). *Braz. J. Biol.*, 62(2):253–262.

Horsman, U., Heinzel, H.-G., and Wendler, G. (1983). The phasic influence of self-generated air current modulations on the locust flight motor. *J. Comp. Physiol. A*, 150:427–438.

Kandel, E., Schwartz, J., and Jessell, T., editors (2000). *Principles of Neural Science, 4th ed.* McGraw-Hill, New York.

Kasaiah, A., Sekhar, V., Rajarami Reddy, G., and Babu, K. (1989). Distribution and innervation of cuticular sense organs in the scorpion, *Heterometrus fulvipes*. In *Neurobiology of sensory systems*, International Conference on Neurobiology of Sensory Systems. Singh, Ram N.

Kim, D. and Möller, R. (2005). Object exploration using whisker sensors. In *Proceedings of Int. Symposium on Adaptive Motion in Animals*.

Kladt, N. (2003). Mechanoreception by cuticular sensillae on the pectines of the scorpion *Pandinus cavimanus*. Diploma thesis. Institute for Zoology, University of Bonn.

Kowalski, K. (2006). Hindernisdetektion mit Hilfe von aktivem Tastverhalten der Pecten beim Skorpion *Pandinus cavimanus*. Diploma thesis. Institute for Zoology, University of Bonn.

Köpke, I. (2001). Das Laufverhalten des Skorpions *Hadogenes bicolor* in schwierigem Gelände, mit dem Schwerpunkt des Laufens im Sand. Diploma thesis. Institute for Zoology, University of Bonn.

Krapf, D. (1986). *Verhaltensphysiologische Untersuchungen zum Beutefang von Skorpionen mit besonderer Berücksichtigung der Trichobothrien*. PhD thesis, University of Würzburg.

Krijnen, G., Dijkstra, M., van Baar, J., Shankar, S., Kuipers, W., de Boer, R., Altpeter, D., Lammerink, T., and Wiegerink, R. (2006). MEMS based hair flow-sensors as model systems for acoustic perception studies. *Nanotechnology*, 17:S84–S89.

Lee, M. and Nicholls, H. (1999). Tactile sensing for mechatronics - a state of the art survey. *Mechatronics*, 9:1–31.

Linsenmair, K. (1968). Anemomenotaktische Orientierung bei Skorpionen. *Zeitschrift für vergleichende Physiologie*, 60:445–449.

Lourenco, W. and Cloudsley-Thompson, J. (1996). Recognition and distribution of the scorpions of the genus pandinus thorell, 1876 accorded protection by the washington convention. *Biogeographica*, 72(3):133–143.

López-Higuera, J. (2002). Introduction to fibre optic sensing technology (chapter 1). In López-Higuera, J., editor, *Handbook of optical fibre sensing technology*, pages 211–226. Wiley&Sons, LTD, West Sussex, England.

Mahsberg, D., Lippe, R., and Kallas, S. (1999). *Skorpione*. Natur- und Tier- Verlag, Münster.

McCormick, S. and Polis, G. (1990). Prey, predators, and parasites. In Polis, G. A., editor, *The Biology of Scorpions*, pages 247–293. Stanford University Press, Palo Alto, CA.
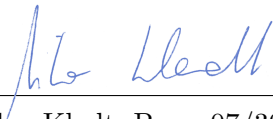
Meeting of the Nomenclature Committee, N. D. . (2003). Taxonomy and Distribution of Pandinus Species listed by CITES. *Convention on international trade in endangered species of wild fauna and flora*.

Mesce, K., Amos, T., and Clough, S. (1993). A light insensitive method for contrast enhancement of insect neurons filled with a cobalt-lysine complex. *Biotechnic & Histochemistry*, 68(4):222–228.

Messlinger, K. (1987). Fine structure of scorpion trichobothria (Arachnida, Scorpiones). *Zoomorphology*, 107(1):49–57.

Middelhoek, S. and Hoogerwerf, A. (1986). Classifying solid-state sensors - the 'sensor effect cube'. *Sensors and Actuators*, 10:1–8.

Middelhoek, S. and Hoogerwerf, A. (1988). *NATO ASI Series, Sensors and Sensory Systems for Advanced Robots*, chapter Basic tranduction mechanisms and techniques, pages 189–199. Springer-Verlag, Berlin.

Mineo, M. and Claro, K. (2006). Mechanoreceptive function of pectines in the brazilian yellow scorpion *Tityus serrulatus*: perception of substrate-borne vibrations and prey detection. *Acta Ethologica*, 9(2):79–85.

Niebur, E., Elhilali, M., Obeid, I., Werfel, J., Blanchard, M., Frasca, M., Ghose, K., Hofstoetter, C., Indiveri, G., and Tilden, M. (2001). Research, robots, and reality: A statement on current trends in biorobotics. Open peer commentary to the article of Barbara Webb (2001) Can robots make good models of biological behaviour? Behavioral and brain sciences 24:1033-1050.

Ochoa, J. and Acosta, L. (2002). Two new andean species of Brachistosternus Pocock (Scorpiones: Bothriuridae). *Euscorpius*, (2):1–15.

Ozaki, Y., Ohyama, T., Yasuda, T., and Shimoyama, I. (2000). An air flow sensor modeled on wind receptor hairs of insects. *Proc. MEMS (Miyazaki, Japan)*, pages 531–537.

Polis, G. and Sissom, W. (1990). Life history. In Polis, G. A., editor, *The Biology of Scorpions*, pages 247–293. Stanford University Press, Palo Alto, CA.

Polis, G. A. (1990a). Ecology. In Polis, G. A., editor, *The Biology of Scorpions*, pages 247–293. Stanford University Press, Palo Alto, CA.

Polis, G. A. (1990b). Introduction. In Polis, G. A., editor, *The Biology of Scorpions*, pages 1–8. Stanford University Press, Palo Alto, CA.

Root, T. (1990). Neurobiology. In Polis, G. A., editor, *The Biology of Scorpions*, pages 341–413. Stanford University Press, Palo Alto, CA.

Russell, R. (1990). *Robot tactile sensing.* Prentice Hall, Australia.

Sanjeeva-Reddy, P. (1971). Function of the supernumerary sense cells and the relationship between modality of adequate stimulus and innervation pattern of the scorpion hair sensillum. *J. Exp. Biol.*, 54:233–238.

Sanjeeva-Reddy, P. and Rao, K. (1970). The central course of the hair afferents and the pattern of contralateral activation in the central nervous system of the scorpion, *Heterometrus fulvipes. J. Exp. Biol.*, 53:165–169.

Schneider, W. (2002). Untersuchungen zum Einfluss der taktilen Sensorik auf das Laufverhalten von Skorpionen. Diploma thesis. Institute for Zoology, University of Bonn.

Selverston, A. (2001). Biomimetic robots and biology. Open peer commentary to the article of Barbara Webb (2001) Can robots make good models of biological behaviour? Behavioral and brain sciences 24:1033-1050.

Shaffer, L. and Formanowicz, D. (2000). Sprint speeds of juvenile scorpions: Among family differences and parent offspring correlations. *Journal of Insect Behaviour*, 13:45–54.

Simard, J. and Watt, D. (1990). Venoms and toxins. In Polis, G. A., editor, *The Biology of Scorpions*, pages 247–293. Stanford University Press, Palo Alto, CA.

Tauber, E. and Eberl, D. (2003). Acoustic communication in *Drosophila. Behav. Processes*, 64:197–210.

Tegin, J. and Wikander, J. (2005). Tactile sensing in intelligent robotic manipulation - a review. *Industrial Robot: An International Journal*, 32:64–70.

Thurm, U. (1963). Die Beziehungen zwischen mechanischen Reizgrößen und stationären Erregungszuständen bei Borstenfeld-Sensillen von Bienen. *Zeitschrift für vergleichende Physiologie*, 46:351–382.

van Baar, J. J., Dijkstra, M., Wiegerink, R., Lammerink, T., and Krijnen, G. (2003). Fabrication of arrays of artificial hairs for complex flow pattern recognition. In *Proceedings of the IEEE Sensors Conference, Toronto.*

Webb, B. (2001). Can robots make good models of biological behaviour? *Behavioral and Brain Sciences*, 24:1033–1050.

Wehner, R. (1987). 'matched filters' - neural models of the external world. *J. Comp. Physiol. A*, 161:511–531.

Wettels, N., Popovic, D., and Loeb, G. (2007). Biomimetic tactile sensor. In *Proceedings of BioMed2007, 2nd Frontiers in Biomedical Devices Conference.*

Wijaya, J. and Russell, R. (2002). Object exploration using whisker sensors. In *Proc. Australasian Conference on Robotics and Automation.*

Wolf, H. (2007). The pectine organs of the scorpion, *Vaejovis spinigerus*: Structure and (glomerular) central projections. *Arthropod Structure and Development*, page doi: 10.1016/j.asd.2007.05.003.

Wolf, H. and Pearson, K. (1989). Comparison of motor patterns in the intact and deafferented flight system of the locust. iii. patterns of interneuronal activity. *J. Comp. Physiol. A*, 165:61–74.

Yahia, N. and Sissom, W. (1996). Studies on the systematics and distribution of the scorpion *Vaejovis bilineatus* POCOCK (Vaejovidae). *J. Arachn.*, 24:81–88.

Yellamma, K., Murali Mohan, P., and Babu, K. (1980). Morphology and physiology of giant fibres in the seventh abdominal ganglion of the scorpion *Heterometrus fulvipes*. *Proc. Indian. Acad. Sci.*, 89(1):29–38.

Declaration

Hiermit erkläre ich an Eides statt, dass ich für meine Promotion keine anderen als die angegebenen Hilfsmittel benutzt habe, und dass die inhaltlich und wörtlich aus anderen Werken entnommenen Stellen und Zitate als solche gekennzeichnet sind.

Nikolay Kladt, Bonn 07/30/2007